



**Studies on the influence of mutations in the  
*Myh9* gene on platelet function**

**\*\*\***

**Studien zum Einfluss von Mutationen im  
*Myh9* Gen auf die Thrombozytenfunktion**

Doctoral thesis for a doctoral degree  
at the Graduate School of Life Sciences,  
Julius-Maximilians-Universität Würzburg,  
Section: Biomedicine

submitted by  
**Juliane Baumann**  
from Arnstein, Germany

- Würzburg, 2022 -

Submitted on:

---

Office stamp

Members of the *Promotionskomitee*:

Chairperson: Prof. Dr. Manfred Gessler

Primary Supervisor: Prof. Dr. Markus Bender

Supervisor (Second): Prof. Dr. Thomas Dandekar

Supervisor (Third): Prof. Dr. Andreas Greinacher

Supervisor (Fourth): \_\_\_\_\_ (if applicable)

Date of Public Defense: \_\_\_\_\_

Date of Receipt of Certificates: \_\_\_\_\_

There are no such things as limits to growth,  
because there are no limits to the human capacity for  
intelligence, imagination, and wonder.

-Ronald Reagan-

## Summary

The platelet cytoskeleton ensures normal size and discoid shape under resting conditions and undergoes immediate reorganization in response to changes in the extracellular environment through integrin-based adhesion sites, resulting in actomyosin-mediated contractile forces. Mutations in the contractile protein non-muscle myosin heavy chain IIA display, among others, macrothrombocytopenia and a mild to moderate bleeding tendency in human patients. It is insufficiently understood which factors contribute to the hemostatic defect found in *MYH9*-related disease patients. Therefore, a better understanding of the underlying biophysical mechanisms in thrombus formation and stabilization is warranted.

This thesis demonstrates that an amino acid exchange at the positions 702, 1424 and 1841 in the heavy chain of the contractile protein non-muscle myosin IIA, caused by heterozygous point mutations in the gene, resulted in macrothrombocytopenia and increased bleeding in mice, reflecting the clinical hallmark of the *MYH9*-related disease in human patients. Basic characterization of biological functions of *Myh9* mutant platelets revealed overall normal surface glycoprotein expression and agonist-induced activation when compared to wildtype platelets. However, myosin light chain phosphorylation after thrombin-activation was reduced in mutant platelets, resulting in less contractile forces and a defect in clot retraction. Altered biophysical characteristics with lower adhesion and interaction forces of *Myh9* mutant platelets led to reduced thrombus formation and stability. Platelets from patients with the respective mutations recapitulated the findings obtained with murine platelets, such as impaired thrombus formation and stiffness.

Besides biological and biophysical characterization of mutant platelets from mice and men, treatment options were investigated to prevent increased bleeding caused by reduced platelet forces. The antifibrinolytic agent tranexamic acid was applied to stabilize less compact thrombi, which are presumably more vulnerable to fibrinolysis. The hemostatic function in *Myh9* mutant mice was improved by interfering with the fibrinolytic system. These results show the beneficial effect of fibrin stabilization to reduce bleeding in *MYH9*-related disease.

## Zusammenfassung

Das thrombozytäre Zytoskelett gewährleistet eine normale Zellgröße und diskoide Form unter ruhenden Bedingungen. Als Reaktion auf Veränderungen in der extrazellulären Umgebung wird das Zytoskelett durch Integrin-basierte Adhäsionsstellen reorganisiert, was zu Aktomyosin-vermittelten kontraktile Kräfte führt. Mutationen in der schweren Kette des kontraktile nicht-muskulären Proteins Myosin IIA führen bei Patienten u. a. zu einer Makrothrombozytopenie und einer leichten bis mittelschweren Blutungsneigung. Es ist unzureichend geklärt, welche Faktoren zum hämostatischen Defekt bei Patienten mit *MYH9*-bedingter Erkrankung beitragen. Daher ist ein besseres Verständnis der zugrunde liegenden biophysikalischen Mechanismen bei der Thrombusbildung und -stabilisierung erforderlich.

In dieser Arbeit konnte gezeigt werden, dass der Austausch von einzelnen Aminosäuren an den Positionen 702, 1424 und 1841 im kontraktile Protein Myosin IIA, hervorgerufen durch Punktmutationen im kodierenden Gen, zu einer Makrothrombozytopenie und zu einer verlängerten Blutungszeit in Mäusen führt. Dies spiegelt die klinischen Merkmale der *MYH9*-assoziierte Erkrankungen bei Patienten wider. Die basale Charakterisierung der biologischen Funktionen von *Myh9*-mutierten Thrombozyten im Vergleich zu Wildtyp-Thrombozyten ergab eine insgesamt normale Oberflächenglykoproteinexpression und Agonisten-induzierte Aktivierung. Interessanterweise war die Phosphorylierung der leichten Myosinkette in den mutierten Thrombozyten nach Aktivierung reduziert, was zu einer geringeren Kontraktionskraft und damit zu einem Defekt beim Zusammenziehen des Gerinnsels führte. Mit Hilfe von biophysikalischen Untersuchungen konnte gezeigt werden, dass geringere Adhäsions- und Interaktionskräfte von Thrombozyten mit Punktmutationen im *Myh9* Gen zu einer verminderten Thrombusbildung und -stabilität führen. Thrombozyten von Patienten mit den entsprechenden Mutationen rekapitulierten die mit murinen Thrombozyten erhaltenen Ergebnisse, wie z. B. eine beeinträchtigte Thrombusbildung und -steifigkeit.

Neben der biologischen und biophysikalischen Charakterisierung der Thrombozyten von Mäusen und Menschen mit den Punktmutationen wurden Behandlungsmöglichkeiten untersucht, um die erhöhte Blutungsneigung aufgrund der

verminderten Thrombozytenkräfte zu verhindern. Das Antifibrinolytikum Tranexamsäure wurde eingesetzt, um weniger kompakte Thromben zu stabilisieren, die vermutlich anfälliger für Fibrinolyse sind. Die hämostatische Funktion von Mäusen mit *Myh9*-Mutationen konnte durch die Gabe von Tranexamsäure verbessert werden. Diese Ergebnisse zeigen die positive Wirkung der Fibrinstabilisierung zur Verringerung von Blutungsneigungen bei *MYH9*-assoziierte Erkrankungen.

# Contents

Summary .....	I
Zusammenfassung .....	II
1 Introduction .....	1
1.1 Megakaryocytes and platelet biogenesis.....	1
1.2 Platelets.....	3
1.2.1 Platelet morphology .....	3
1.2.2 Platelet function .....	4
1.3 Platelet cytoskeleton.....	6
1.3.1 Platelet cytoskeleton components.....	6
1.3.2 The actin cytoskeleton .....	7
1.3.3 The motor protein myosin IIA.....	10
1.4 <i>MYH9</i> - related disease .....	17
1.4.1 Clinical presentation of <i>MYH9</i> -RD patients.....	17
1.4.2 Treatment of <i>MYH9</i> -RD patients.....	19
1.4.3 Mouse models to study myosin IIA .....	20
2 Aim of the study .....	24
3 Materials .....	25
3.1 Human blood samples.....	25
3.2 Animals.....	25
3.3 Antibodies.....	27
3.4 Material.....	28
3.5 Chemicals and reagents.....	30
3.6 Buffer.....	34
3.7 Devices.....	39
4 Methods .....	41
4.1 Molecular biological analyses .....	41
4.1.1 Isolation of murine DNA .....	41
4.1.2 Polymerase chain reaction.....	41
4.1.3 Agarose gel electrophoresis.....	44
4.1.4 Real-time PCR .....	44
4.1.5 Blood parameters.....	45

4.2	Platelet function analyses .....	45
4.2.1	Platelet preparation .....	45
4.2.2	Aggregometry .....	46
4.2.3	Platelet spreading .....	47
4.2.4	Platelet adhesion and thrombus formation under flow conditions .....	47
4.2.5	Bleeding time .....	48
4.2.6	Clot retraction.....	49
4.2.7	Migration .....	49
4.2.8	Thromboelastometry .....	50
4.3	Flow cytometric analysis of platelet function.....	50
4.3.1	Glycoprotein expression .....	50
4.3.2	Activation .....	50
4.3.3	F-actin content and assembly .....	51
4.4	Biochemical analyses .....	51
4.4.1	Immunoblotting with SDS-PAGE.....	51
4.4.2	Immunoblotting with ProteinSimple Jess .....	52
4.4.3	Actin sedimentation.....	53
4.5	Imaging.....	53
4.5.1	Immunostaining of platelets .....	53
4.5.2	Transmission electron microscopy of platelet ultrastructure .....	54
4.5.3	Platinum replica electron microscopy of platelet cytoskeleton .....	54
4.5.4	Cryo sectioning and staining .....	55
4.5.5	Image processing and analysis.....	55
4.6	Biophysical analyses .....	55
4.6.1	Real-time fluorescence deformability cytometry.....	55
4.6.2	Single platelet force spectroscopy .....	56
4.6.3	Colloidal probe spectroscopy.....	57
4.6.4	Micropost assay .....	58
4.6.5	Scanning ion conductance microscopy .....	59
4.7	Data analysis .....	60
5	Results .....	61
5.1	Characterization of <i>Myh9</i> mutant mice .....	61
5.1.1	Unaltered protein expression of the RhoA-ROCK-myosin IIA pathway. 61	61



5.1.2	<i>Myh9</i> mutant mice display macrothrombocytopenia .....	62
5.1.3	Comparable activation and aggregation of <i>Myh9</i> mutant platelets.....	66
5.1.4	Increased stiffness and F-actin content in <i>Myh9</i> mutant platelets.....	70
5.1.5	<i>Myh9</i> mutant platelets adhere and fully spread on fibrinogen .....	77
5.1.6	Decreased myosin light chain phosphorylation and contractile forces of <i>Myh9</i> mutant platelets .....	84
5.1.7	Reduced adhesion and interaction forces and decreased thrombus formation of <i>Myh9</i> mutant platelets .....	89
5.1.8	Impaired hemostasis in <i>Myh9</i> mutant mice .....	92
5.2	Analyses of samples from <i>MYH9</i> -RD patients.....	93
5.2.1	Platelets of <i>MYH9</i> -RD patients are stiffer under resting conditions.....	93
5.2.2	Faster adhesion of <i>MYH9</i> -RD patient platelets on fibrinogen .....	94
5.2.3	Impaired thrombus formation of platelets from <i>MYH9</i> -RD patients .....	97
5.3	Treatment with TXA and magnesium supplementation .....	100
5.3.1	TXA improves clot retraction and stabilizes plasminogen-induced fibrinolysis of <i>Myh9</i> mutant platelets .....	100
5.3.2	Supplementation of magnesium has no effect on thrombocytopenia in <i>Myh9</i> mutant mice.....	108
6	Discussion.....	109
6.1	Genotype-phenotype relationship.....	110
6.2	Correlation of men and mice .....	111
6.3	Impact of myosin IIA mutations on hemostasis and thrombosis .....	113
6.4	Myosin IIA-mediated contraction forces in <i>Myh9</i> mutant platelets.....	115
6.5	The fibrinolytic system .....	118
6.6	Proplatelet formation .....	119
7	Concluding Remarks.....	121
8	Outlook.....	122
9	References.....	125
10	Appendix.....	133
10.1	Abbreviations .....	133
10.2	Acknowledgment.....	138
10.3	Publications.....	139
10.3.1	Original Article .....	139
10.3.2	Oral Presentation.....	139

10.3.3	Poster .....	139
10.4	Curriculum vitae .....	141
10.5	Affidavit .....	142

## Introduction

### 1 Introduction

#### 1.1 Megakaryocytes and platelet biogenesis

During embryonic development, hematopoietic stem cells (HSCs) are derived from hemogenic endothelial cells in placenta and aorta-gonad-mesonephros and migrate to the fetal liver, thymus, spleen, and finally to the bone marrow (BM). HSCs differentiate over more committed progenitor cells to terminally mature cells, like megakaryocytes (MKs). MK differentiation is regulated amongst others by different cytokines, predominantly by thrombopoietin (TPO). The ligand TPO together with its receptor the cellular myeloproliferative leukemia protein (c-Mpl) promotes development and maturation of MKs from HSC precursors by activation of a number of downstream signaling pathways.<sup>1</sup>

Besides of the spleen, MKs are mainly located in the BM of adult mice. During MK development the cell size increases, MKs become fully equipped with granules and expand their cytoplasmic content.<sup>2</sup> Through the process of endomitosis which includes several cycles of deoxyribonucleic acid (DNA) replication without cell division, MKs become polyploid up to 128N.<sup>3,4</sup> Granules are derived from the trans-Golgi network through budding of small vesicles containing granule cargo (Figure 1A, B). Granules are indispensable in MKs and platelets through their key roles in hemostasis and thrombosis.<sup>5</sup> During maturation, MKs develop an invaginated membrane system called demarcation membrane system (DMS), which serves as membrane reservoir for platelet biogenesis (Figure 1C).<sup>6,7</sup>

The BM is the main site of platelet biogenesis.<sup>8</sup> In the BM microenvironment mature MKs extend long, cytoplasmic protrusions, called proplatelets, into the lumen of sinusoidal blood vessels.<sup>8</sup> Microtubule cytoskeleton undergoes rearrangement during proplatelet production and drives elongation of protrusions (Figure 1D).<sup>8,9</sup> In addition, granule transport into the proplatelet tips along the shafts is dependent on microtubules<sup>5</sup> in which  $\beta$ 1-tubulin is the main isoform of tubulin in MKs.<sup>10,11</sup> The tips of elongated protrusions then separate from the MKs and are released into the blood stream. The released barbell-shaped proplatelets can reversibly convert into large platelets, called preplatelets.<sup>12</sup> Barbell-shaped proplatelets have bulbous tips at the ends already containing organelles, granules and cytoskeletal components. Bidirectional polymerization of microtubules at each end of the barbell-shaped

## Introduction

proplatelet forms two microtubule coils and splits the proplatelet into two individual platelets (Figure 1E).<sup>12</sup> This, together with the high shear rates caused by the bloodstream and actin dynamics, leads to the formation of the terminal platelets.<sup>12,13</sup>

To amplify protrusion ends during proplatelet branching, the cytoskeletal protein, filamentous actin (F-actin), is required.<sup>14,15</sup> Fewer and shorter proplatelets with less branching are caused by mutations in the *MYH9* gene, encoding for the actin motor protein myosin IIA.<sup>16</sup> These observations suggest efficient proplatelet formation is also dependent on precise regulation of the cytoskeleton.

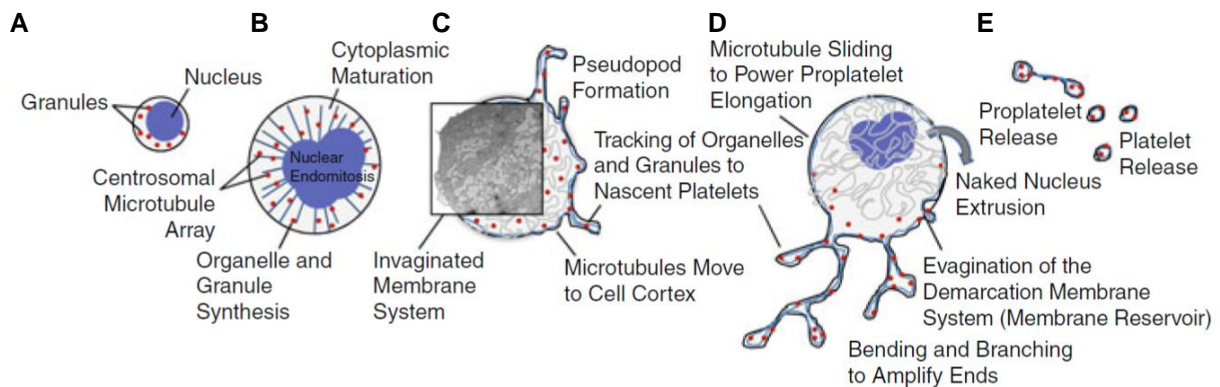


**Figure 1. *In vitro* model of MK maturation and (pro-)platelet release.** (A) Immature MKs (B) undergo endomitosis to replicate DNA for organelle synthesis, cytoplasmic maturation and expansion. (C) To produce pseudopods microtubules move to cell cortex and the invaginated membrane system is formed. (D) Elongation of proplatelet shafts is induced by microtubule sliding and amplification of proplatelet ends induced by F-actin and myosin IIA. After converting the whole mass of MK cytoplasm into proplatelets, the naked nucleus of the MK is extruded. (E) Proplatelets are released into circulation in a barbell shape and with granules and organelles for two individual platelets, separating from each other through microtubule reorganization. Figure adapted from <sup>8</sup>.

## Introduction

### 1.2 Platelets

#### 1.2.1 Platelet morphology

Continuous production of platelets by MKs is required to compensate clearing of aged platelets by macrophages in the liver and spleen. The normal physiological platelet concentration in peripheral blood of humans lies between  $1.5$  and  $4.5 \times 10^5$  platelets per microliter, whereas the platelet counts in mice are physiologically higher ranging from  $1$  to  $1.5 \times 10^6$  platelets per microliter blood. Compared to other blood cells, platelet life span is rather short with 8-12 days for human platelets and 3-4 days for mouse platelets, respectively. Platelets are the smallest cells in the blood with a diameter of 1-2  $\mu\text{m}$  in humans and 0.5  $\mu\text{m}$  in mice, respectively. Platelets exhibit a discoid shape under resting conditions (Figure 2) and contain numerous structural organelles, including  $\alpha$ -granules, dense-granules, peroxisomes, lysosomes, and mitochondria received from MKs during platelet production.<sup>8,17,18</sup> The cytoskeleton of platelets consists of a densely packed actin cytoskeletal network and a peripheral band of microtubules. Microtubule coils, composed of polymers of  $\alpha$ - and  $\beta$ -tubulin, are located beneath the plasma membrane forming a microtubule ring.<sup>8</sup> Like MKs, the surface membrane of platelets is invaginated and forms the open canalicular system, which serves as the main pathway to transport substances into the cell and discharge  $\alpha$ -granules content out of the cell.<sup>19</sup> The dense tubular system (DTS), which is a smooth endoplasmic reticulum, initiates and modulates platelet activation (Figure 2). The DTS serves as internal calcium store and harbors a series of endoplasmic reticulum enzymes supporting the platelet function in hemostasis and thrombosis.<sup>20-22</sup>

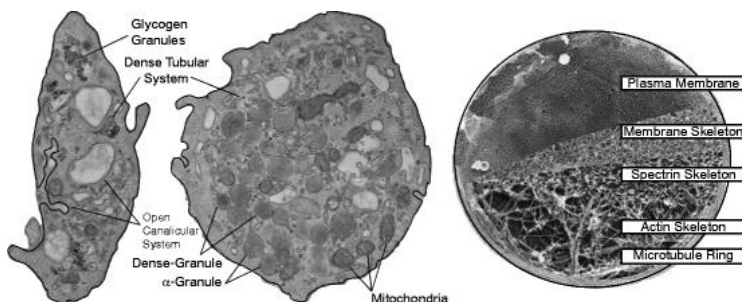


**Figure 2. Morphology and structural elements of resting platelets.** Ultrastructural components of platelets and their cytoskeletal elements. Image by <sup>8</sup>.

Upon activation of platelets by various stimuli, the platelet cytoskeleton undergoes rapid reorganization resulting in shape change. First, actin filaments are fragmented followed by shape changes of the platelets from discoid (Figure 3A) to spherical (Figure 3B, C). Second, actin filaments assemble, resulting in protrusions of the cell membrane called filopodia. Phosphorylation of the myosin light chain (MLC) facilitates binding of

## Introduction

myosin to actin filaments, generating contractile forces on the framework of F-actin. Thus, phosphorylation of MLC directly induces shape change of platelets.<sup>23,24</sup> In *in vitro* spreading assays, mouse platelets adhere to fibrinogen in the presence of thrombin, change their shape forming filopodia (Figure 3B, C) and finally lamellipodia (Figure 3D), that grow from short actin filament templates at the platelets' periphery.<sup>25</sup> It has been shown that platelets lacking the ability to form lamellipodia can form stable thrombi on collagen *ex vivo* and *in vivo*, providing evidence that platelet lamellipodia formation is not required for stable thrombus formation.<sup>26</sup> In contrast, inhibition of actin polymerization resulted in the loss of leading edge lamellipodia and abrogation of platelet migration, indicating that migration of platelets is dependent on branched lamellipodial actin networks.<sup>27</sup>

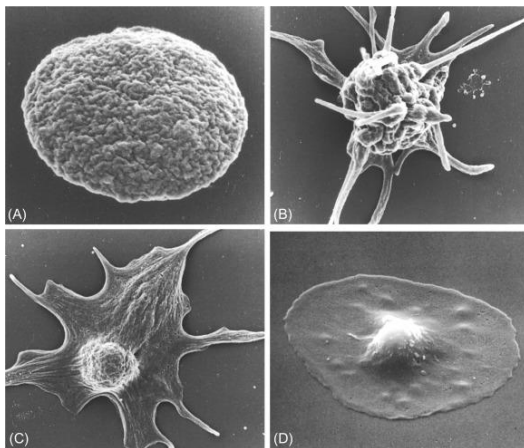


**Figure 3. Platelet shape changes.** (A) Resting platelets exhibit a discoid shape. (B) Upon platelet activation, cytoskeletal reorganization results in shape change. Platelets form filopodia through remodeling of actin filaments. (C) Upon further activation, platelet shape changes to spherical. (D) Fully spread platelets appear in a “fried-egg” like shape with the formation of lamellipodia at the periphery of the cell. Image from <sup>28</sup>.

### 1.2.2 Platelet function

Platelets circulating in the blood stream play a major role in hemostasis and thrombosis. Upon vessel wall damage, platelets get activated and aggregate to limit blood loss and maintain hemostasis. Uncontrolled and excessive platelet activation and aggregation can lead to pathological occlusive thrombus formation.<sup>29</sup> To minimize unwanted platelet activation, mainly endothelial cells contribute to regulate this mechanism. To prevent platelet activation in healthy vessels, endothelial cells release prostaglandin and nitric oxide to keep platelets in a resting state. Additionally, platelet agonists, such as ADP and thromboxane A<sub>2</sub>, are metabolized by endothelial cells into non-activating products.<sup>30</sup>

## Introduction

After platelet activation, granules are released into the platelet surrounding to amplify activation and facilitate adhesion of further platelets. Three major types of granules have been described in platelets:  $\alpha$ -granules,  $\delta$ -granules, and lysosomes. The  $\alpha$ -granules contain over 300 proteins, including membrane-associated receptors such as P-selectin and  $\alpha\text{IIb}\beta\text{3}$  integrin, and soluble cargos such as platelet factor 4 (PF4), fibrinogen and the von Willebrand factor (vWF). The  $\delta$ -granules (or dense granules) contain amines (e.g., serotonin, histamine), adenosine diphosphate (ADP) and high concentrations of cations, most notably calcium. Proteolytic enzymes contributing to thrombus remodeling can be found in lysosomes (or  $\lambda$ -granules).<sup>31,32</sup>

Upon vessel wall injury extracellular matrix (ECM) proteins are exposed to blood cells, causing platelets to adhere rapidly and form a hemostatic plug to prevent blood loss.<sup>30</sup> A multi-step process of thrombus formation is initiated, involving numerous platelet receptors and platelet ligands. Binding of platelets to ECM proteins is mediated by interactions of the platelet glycoprotein (GP) Ib-V-IX complex with immobilized vWF on exposed subendothelial collagen. This interaction called platelet tethering allows platelets to slow down in the flowing blood stream (Figure 4: Unstable adhesion). Binding of GPVI to collagen is then enabled by the platelet tethering. Cellular activation is initiated, including inside-out upregulation of integrin affinity, which leads to firm adhesion (Figure 4: stable adhesion). Release of ADP from dense granules and synthesis of thromboxane A<sub>2</sub> mediates thrombus growth by activating recruited platelets (Figure 4: Aggregation).<sup>33</sup> A further step of the hemostatic response is the coagulation pathway, which generates thrombin, a platelet agonist. Factors of the extrinsic pathway of coagulation, factor VIIa and the exposed tissue factor, and factors from the intrinsic coagulation pathway (finally factor IXa) lead to the common activation of factor X and finally to the generation of thrombin (factor IIa) (Figure 4: Thrombin generation). Thrombus growth is accompanied by the binding of integrin  $\alpha\text{IIb}\beta\text{3}$  to fibrinogen. Fibrinogen embedded in the growing clot is converted to fibrin via thrombin, resulting in the formation of a stable clot. The increase of intracellular  $\text{Ca}^{2+}$  and the procoagulant activity of activated platelets leads to activation amplification, clot stabilization and blood vessel constriction (Figure 4: Contraction/clotting).<sup>33,34</sup>

## Introduction

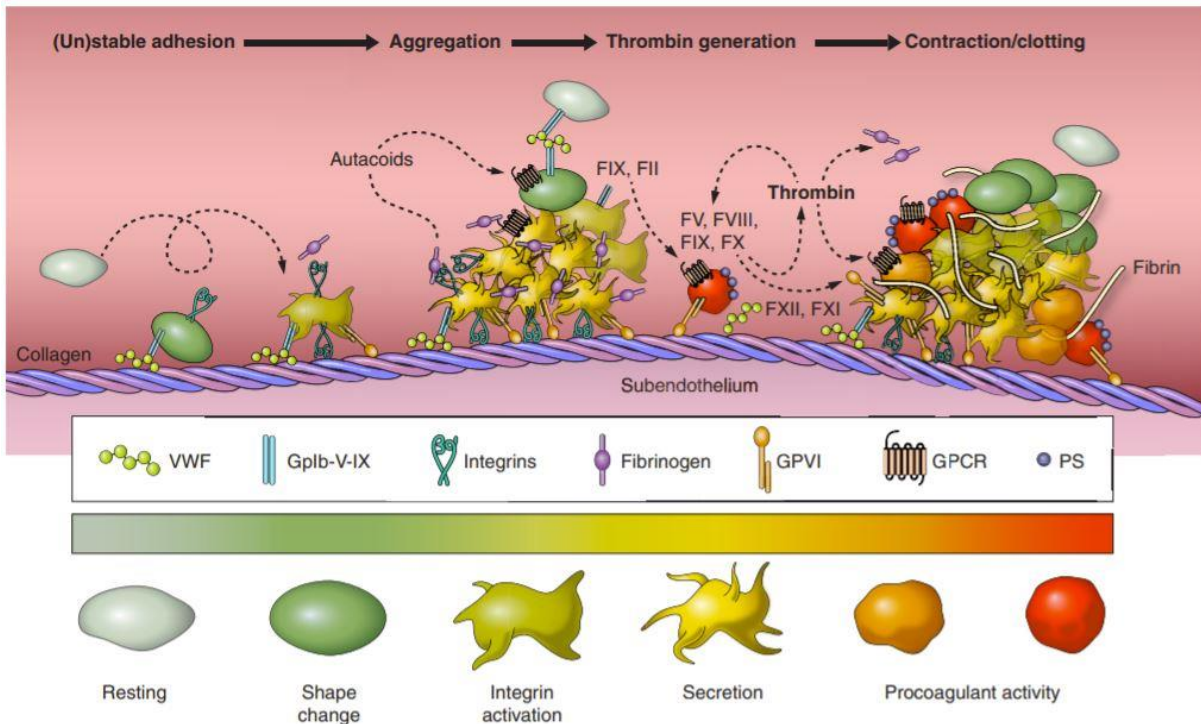


**Figure 4. Multi-step process of platelet activation and thrombus formation.** Resting platelets adhere via GPIb-V-IX complex to exposed vWF on the injured vessel wall, resulting in tethering of platelets including start of shape change. Stable adhesion is mediated through binding of GPVI to collagen and activation of integrins. Granule release and cellular activation leads to recruitment of additional platelets and thrombus growth. Generation of thrombin through coagulation cascade induces fibrin production. A stable contracted clot is formed where platelets expose their procoagulant activity. Heat map indicates the increase in intracellular Ca<sup>2+</sup>, which shows the highest concentration in a stable clot (green: low Ca<sup>2+</sup>; red: high Ca<sup>2+</sup>). Platelet morphology and shape change are shown over time. Image taken from <sup>34</sup>.

### 1.3 Platelet cytoskeleton

#### 1.3.1 Platelet cytoskeleton components

Cytoskeletal structures are highly interconnected to maintain cell shape, mechanics, dynamics, and resistance to mechanical forces. Therefore, the cytoskeleton is a highly adaptive and dynamic network of cytoskeletal components in a constant change of assembly and disassembly. Three major polymer types of the cytoskeleton can be distinguished: microtubules, intermediate filaments and actin filaments (Figure 5A).<sup>35,36</sup>

Microtubules play key roles in cellular processes, such as cell division, motility and differentiation, and are responsible for the maintenance of the discoid shape of resting blood platelets.<sup>35,36</sup> Polarized structures of heterodimer subunits of  $\alpha$ - and  $\beta$ -tubulin assemble to linear protofilaments. A cylindrical and hollow microtubule of 24 nm wide



## Introduction

in mammals is formed by 13 protofilaments. Microtubules are polarized with  $\beta$ -tubulin at the faster-growing (+) end and  $\alpha$ -tubulin at the slower-growing (-) end.<sup>37</sup> In resting platelets microtubules of mixed polarity form the marginal band (Figure 5B).<sup>35,36</sup>

In comparison to microtubules and actin filaments, which are composed of conserved globular proteins with nucleotide-binding and hydrolytic activity site, intermediate filaments are assembled by filamentous proteins sharing conserved structures. Intermediate filaments have a diameter of 10 nm and show no enzymatic activity.<sup>38</sup> Although association of intermediate filaments with actin in human platelets was reported, the cytoskeletal crosstalk of intermediate filaments has been little investigated.<sup>39</sup>

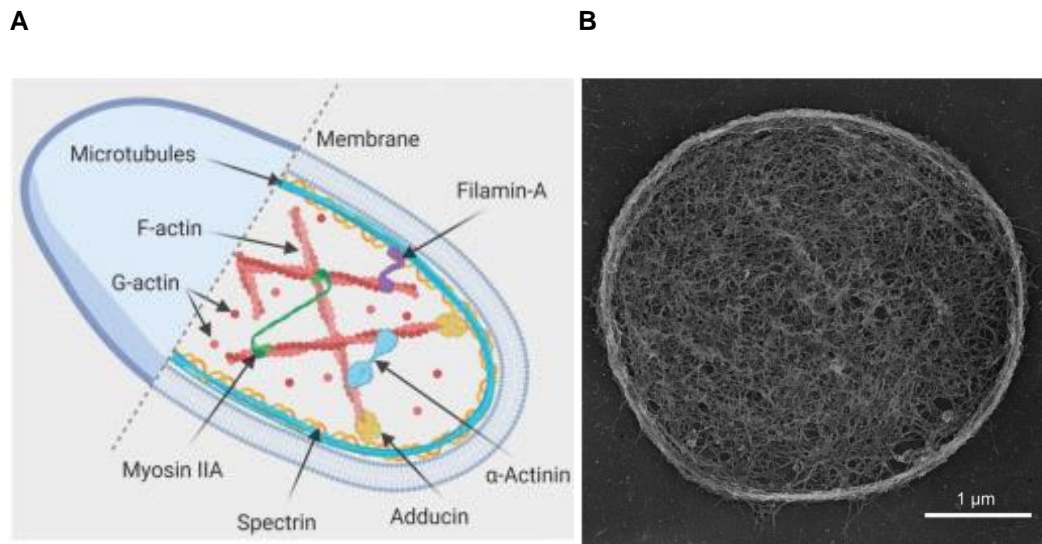


**Figure 5. The platelet cytoskeleton.** (A) Scheme of a resting platelet with cytoskeletal components. (B) Ultrastructure of a resting mouse platelet on poly-L-lysine performed with platinum replica electron microscopy (scale bar 1  $\mu$ m). Adapted from <sup>40</sup>.

### 1.3.2 The actin cytoskeleton

In many cells including platelets, one of the most abundant proteins is actin with more than 15 to 20% of the total protein content.<sup>41</sup> As a key component, actin participates in a large variety of cellular processes, such as cell polarization and migration, as well as phago- and exocytosis and cytokinesis. Actin is a highly conserved protein in evolution and is not only found in eukaryotes, but also in bacteria and archaea.<sup>42</sup> In mammals, three actin isoforms have been identified:  $\alpha$ -actin for the muscles,  $\beta$ -actin for non-

## Introduction

muscle cells and  $\gamma$ -actin in smooth muscles and non-muscle cells.<sup>43</sup> Actin has a molecular weight of roughly 42 kDa and a filament diameter of 8 to 10 nm.<sup>44</sup>

The actin cytoskeleton exhibits a very dynamic behavior of depolymerization and polymerization, enabling cellular processes. Monomeric globular actin (G-actin) gets polymerized to F-actin and depolymerized back to actin monomers.<sup>44</sup> Actin monomers assemble in a first step called nucleation phase to form polarized actin filaments. Filaments consist of two ends, an around 10 times faster-growing barbed end (+) and a slower-growing pointed end (-). In platelets over two million actin molecules are present in monomer-polymer dynamics. The instability of actin dimers and trimers is responsible for the rate-limiting step of nucleation. Elongation of F-actin proceeds rapidly upon a steady state phase.<sup>45</sup> When polymerized, F-actin forms a right-handed helix achieved by a  $166^\circ$  rotation of two parallel strands. An adenosine-triphosphate (ATP) nucleotide-binding cleft enables the binding of ATP to G-actin monomers, which boosts the spontaneous polymerization in the presence of  $K^+$  and  $Mg^{2+}$  *in vitro*. After incorporation of ATP-G-actin into actin filaments, ATP is hydrolyzed randomly to ADP and phosphate ( $P_i$ ). At the same time simultaneous depolymerization is caused by the disassociation of ADP-G-actin from the pointed end and dissociation of  $P_i$  from F-actin (Figure 6). Steady state phase is reached when the rate of ATP-G-actin addition is equal to the rate of ADP-G-actin disassociation.<sup>41,46</sup> Many actin-binding proteins are identified during the polymerization process, being responsible for nucleating (Actin related protein 2/3 complex), elongating (formins), bundling (fascin, actinin) and crosslinking (filamin) of actin filaments. Furthermore, several proteins responsible for actin depolymerization, like sequestering (profilin, thymosin beta-4) and severing (cofilin, twinfilin) proteins, are known. Other known actin-binding proteins are responsible for actin-based motility and contractility (myosin) or crosslink actin to other cytoskeletal components like microtubules (spectraplakins).<sup>45</sup>

## Introduction

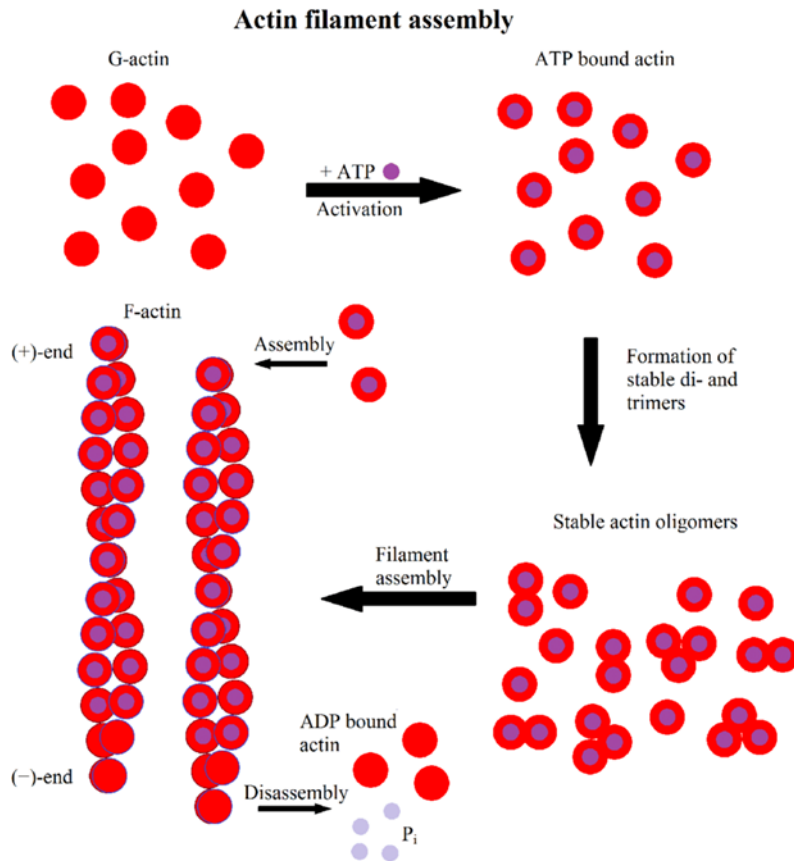


**Figure 6. Actin filament formation.** Monomeric G-actin binds ATP and forms di- and trimers, from which only stable oligomers can be assembled to a filament. Filaments elongate by addition of ATP-G-actin oligomers to barbed ends (+). Hydrolysis of ATP to ADP and  $P_i$  leads to disassembly of ADP-bound G-actin from filaments at the pointed end (-). G-actin is free and available for binding ATP. Image from <sup>47</sup>.

In resting platelets around 40 to 50% of the total actin monomers (around two million molecules) are present in the filamentous form and constitute 2000 to 5000 actin filaments.<sup>48</sup> The remaining 50-60% of monomeric actin is stored in complexes with actin sequestering proteins. Upon platelet activation the amount of F-actin quickly increases (e.g., 20 seconds after stimulation with thrombin) up to 70%,<sup>49,50</sup> enabling actin reorganization into different F-actin rich structures, such as filopodia, lamellipodia, and stress fiber-like structures during platelet spreading. Filopodia are thin, long, finger-like membrane protrusions, formed by parallel bundles of F-actin filaments. Lamellipodia are broad and thin, and define the sites where branched network of F-actin filaments protrude from the membrane.<sup>25</sup> Stress fiber-like structures are bundles of F-actin filaments, crosslinked by proteins (e.g.  $\alpha$ -actinin). These higher order structures in non-muscle cells play a key role in cellular contraction through interaction with myosin II and are comparable to the structures seen in highly ordered actomyosin arrays, typically seen in muscle cells.<sup>51</sup> Stress fibers are connected to integrin-based structures, called focal adhesions (FAs). These interactions provide dynamic links between ECM and the actin cytoskeleton,<sup>52</sup> and contractile forces are

## Introduction

exerted through them (Figure 7). Contractile forces mediated by FA proteins in interaction with stress fiber-like structures have been shown to play a role in compacting the blood clot, as the absence of stress fiber-like structures weakens its integrity.<sup>53</sup>

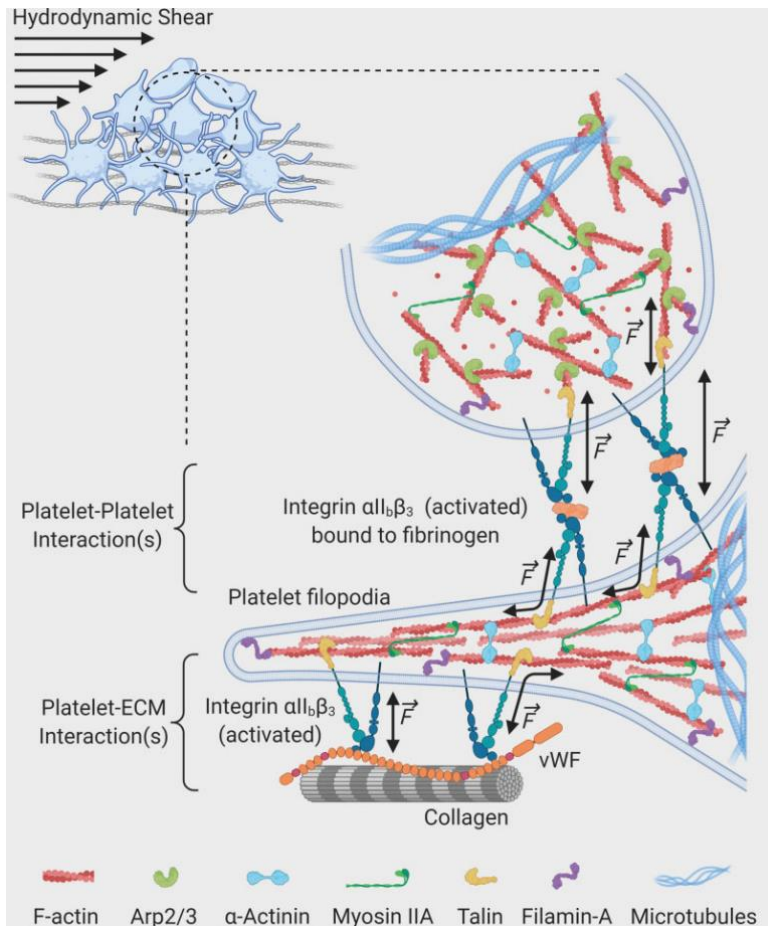


**Figure 7. Schematic of a dynamic platelet to ECM and platelet to platelet interaction in thrombus biomechanics.** Exposed ECMs, like collagen initiates platelet activation and thrombus formation. Shape change of activated platelets is mediated through F-actin to form filopodial extensions. Bundled F-actin filaments reach into filopodia together with motor protein myosin IIA. Through second wave mediators integrin activation is amplified and interaction of focal adhesion sites and F-actin is provided to exert contractile forces. Through multiple receptor - ligand interactions platelets are arrested to drive thrombus growth and clot compaction. Image from <sup>40</sup>.

### 1.3.3 The motor protein myosin IIA

Motor proteins of microtubules or actin filaments power directed movements through kinesin and dynein motors on microtubules and myosin motors on actin filaments, respectively. Energy from ATP is converted into force and movement of motor domains on either actin or microtubule tracks and thereby powers cellular functions such as contraction, cytokinesis, chromosomal as well as organelle movements, membrane trafficking and cellular migration.<sup>54</sup>

Myosins power muscle contraction in interaction with actin filaments in all eukaryotic cells. All known superfamily members of myosin follow the same structure: the myosin

## Introduction

head, neck, and tail domain (Figure 8A). The N-terminal head domain or globular motor domain includes a catalytic site for ATP hydrolysis (MgATPase) as well as an actin binding site. The neck domain is composed of the “lever arm”, which is a converter subdomain attached to an extended helix, consisting of a variable number of calmodulins and calmodulin-like light chains. Movements from myosin motor domain are amplified by the lever arm, which additionally serves as a binding site for light chains. The tail domain is responsible for dimerization of the heavy chains (HC) and formation of functional filaments of myosin II.<sup>54</sup> A small C-terminal helical tailpiece is crucial for the proper filament size and determines the myosin II filament structure in an isoform-specific manner, thus it is accounting for the main difference in the myosin II isoforms (Figure 8A).<sup>55</sup>

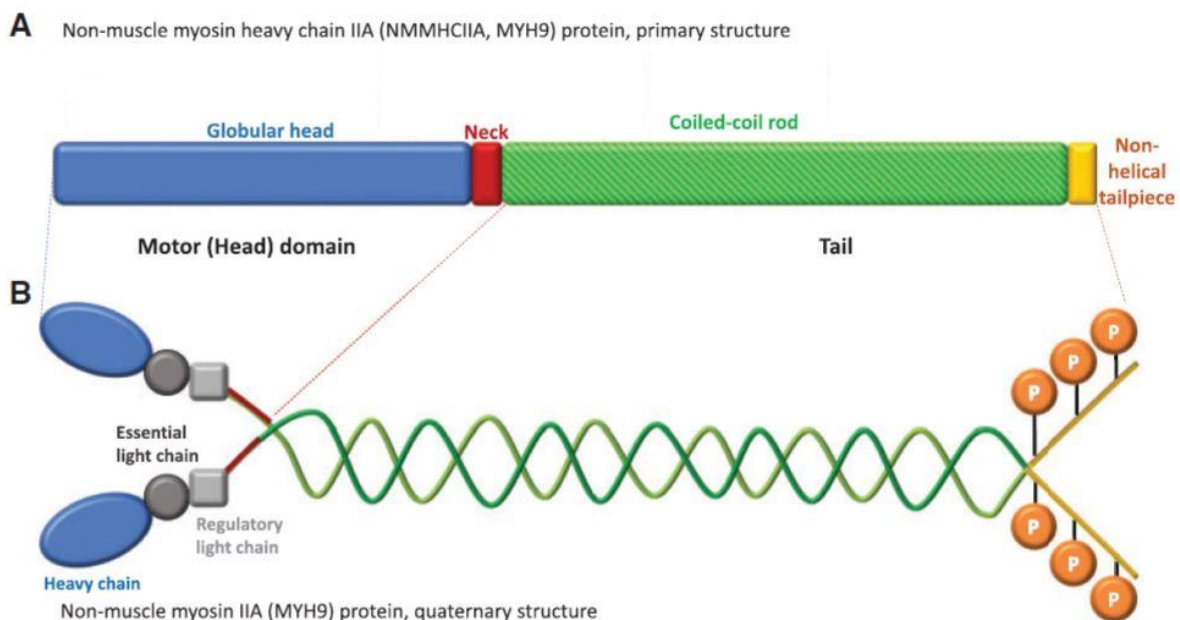


**Figure 8. Primary structure of non-muscle myosin heavy chain IIA (NMMHCIIA) encoded by *MYH9* and quaternary structure of non-muscle myosin IIA protein.** (A) The gene *MYH9* encodes the HC of non-muscle myosin IIA. The structure of myosin is subdivided into a globular head, a neck and a coiled-coil rod domain. A small C-terminal tailpiece is non-helical. (B) The quaternary structure of myosin IIA is composed of two HCs, a pair of essential light chains and a pair of regulatory light chains. Adapted from <sup>56</sup>.

In platelets and MKs only non-muscle myosin IIA (further referred to as myosin IIA) is expressed, while many other non-muscular cells, such as eosinophilic granulocytes, express also non-muscle myosin IIB or the third isoform IIC in many tissues during embryonic development. Thus, myosin IIA can be compensated by other isoforms in other non-muscle cells.<sup>57,58</sup> Myosins of class II consist of six subdomains, a pair of HCs

## Introduction

with a molecular weight of 230 kDa and two pairs of light chains (Figure 8B). The pair of regulatory light chains (RLCs) (20 kDa) control the myosin activity and two essential light chains (17 kDa) stabilize the HC structure. Each HC recapitulates the general structure of the myosin superfamily. The myosin IIA HCs are encoded by the gene *MYH9*, which is localized on chromosome 22q12.3 in humans and composed of 41 exons, whereby the open reading frame reaches from exon 2 to exon 41.<sup>59</sup> The region of exon 2 to exon 19 encodes the motor domain, exon 20 the neck, and exons 21 until 40 encode the tail domain of myosin IIA. Exon 41 encodes for a non-helical tailpiece consisting of 34 amino acids.<sup>59</sup>

The mouse ortholog of myosin IIA is encoded by the *Myh9* gene on chromosome 15.<sup>59</sup> Genomic organization and protein length of mouse and human myosin IIA are identical with an amino acid homology of 97.1%, suggesting the mouse organism as a suitable model to study the function of myosin IIA and the role of *Myh9* in pathogenetic mechanisms.<sup>59</sup>

Myosin IIA in a folded inactive form is inhibited in its most critical biological functions: bipolar filament formation, the ability to hydrolyze MgATP and to slide on actin filaments. Phosphorylation of the RLC (Figure 9) activates myosin IIA, making it available for fulfilling its biological functions.<sup>59,60</sup>

## Introduction

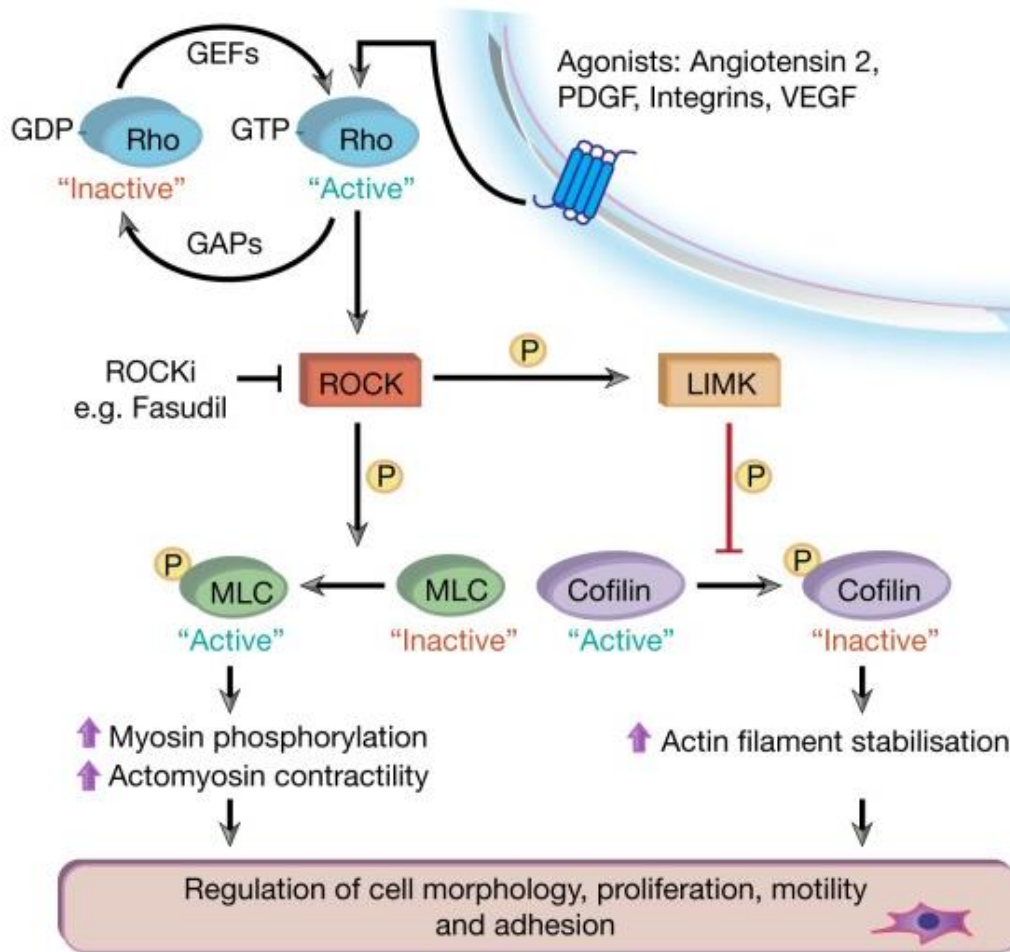


**Figure 9. Key components of the signaling pathway via Rho/ROCK.** Extracellular stimuli bind to cell membrane receptors and regulate the activation of Rho GTPase proteins through guanine-nucleotide-exchange factors (GEFs) and GTPase-activating proteins (GAPs). Once Rho is in its GTP-bound active state, it binds to ROCK to stimulate downstream effectors. ROCK-mediated phosphorylation of MLC promotes actomyosin contractility. Actin filament stabilization is promoted by ROCK-mediated activation of LIMK leading to inactivation of the actin-depolymerizing protein cofilin. Adapted from <sup>60</sup>.

Kinases, most prominent the myosin light chain kinase (MLCK), and the Rho-associated, coiled-coil containing protein kinase (ROCK), can phosphorylate the light chain on serine 19 (S-19) and threonine 18 (T-18) (Figure 10).<sup>59,61</sup> Functional filaments composed of two HCs self-associate to form bipolar filaments, which can bind to actin at specific actin-binding sites, located at head domains, and move on actin filaments in an anti-parallel manner.<sup>59</sup> Although several kinases capable of phosphorylating myosin IIA are known, only one phosphatase dephosphorylating the RLC to inhibit myosin IIA activity could be identified, called the myosin phosphatase 1 (MYPT1).<sup>59</sup>

Other kinases (such as protein kinase C (PKC)) phosphorylating the light chain are responsible for decreasing myosin IIA activity by rendering myosin IIA into a poorer

## Introduction

substrate for MLCK. PKC phosphorylates the light chain at serine 1 and 2, and threonine 9 (Figure 10).<sup>59</sup>

Phosphorylation and dephosphorylation of the myosin IIA HC play an important role in assembly (non-phosphorylated HC) and disassembly (phosphorylated HC) of myosin filaments. Phosphorylation sites of the HC are in the carboxyl-terminal end of the molecule. Kinases, like PKC, casein kinase II (CKII) and transient receptor potential melastatin 7 (TRPM7) phosphorylate the HC to dissociate myosin filaments or prevent filament formation (Figure 10).<sup>59</sup>

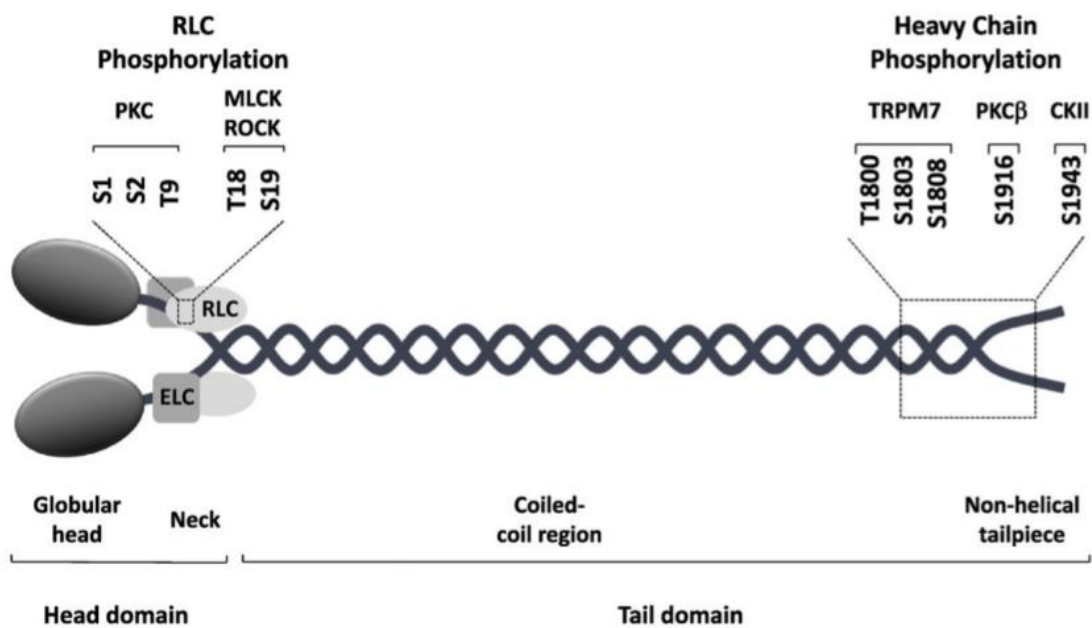


**Figure 10. Phosphorylation sites of myosin IIA.** Schematic representation of myosin IIA including phosphorylation sites at RLC and HC. Specific kinases are indicated: PKC; MLCK and ROCK; TRPM7; PKCβ and CKII (adapted from <sup>59</sup>).

The myosin motor mechanism is dependent on the binding of ATP to myosin IIA. The hydrolysis of ATP occurs rapidly in the absence of actin (Figure 11: step 2). The release of  $P_i$  and ADP requires the interaction of myosin with an actin filament. Myosin binds actin via actin-binding sites at the head domain. The resulting structure is called pre-power stroke. Weak binding of the pre-power stroke triggers  $P_i$  release (Figure 11: step 3), resulting in conformational changes of the lever arm, which is involved in the formation of a higher-affinity binding to actin (Figure 11: step 4). Furthermore, the  $P_i$  release drives the reaction towards a large movement of the lever arm. Further isomerization of the motor destroys  $Mg^{2+}$  binding and movement of the lever arm



## Introduction

(Figure 11: step 5). This process greatly weakens ADP affinity which results in ADP release completing the myosin power stroke on actin (Figure 11: step 6). The binding of ATP to myosin IIA terminates the power stroke by causing the dissociation of myosin from actin (Figure 11: step 1). Myosin motor cycle starts again with the post rigor (PR) state. Dissociation from actin in the PR state induces repriming of the lever arm, known as the recovery stroke.<sup>62</sup>

Blebbistatin is a small molecule inhibitor, selective to muscle and non-muscle myosin II.<sup>63</sup> Binding of blebbistatin to myosin-ADP-P<sub>i</sub> complex interferes with phosphate release, keeps myosin in an actin-detached state and prevents actomyosin interaction.<sup>64,65</sup> The advantage of blebbistatin blocking the myosin II heads in a state with low affinity to actin is to have no adverse effects arising from rigid actomyosin cross-links.<sup>64</sup> Therefore, blebbistatin is a useful compound to investigate all aspects of myosin II motor activity by blocking myosin-mediated mechanisms, like muscle contraction, cytokinesis, and cortical tension maintenance.<sup>64</sup> Contraction of blood clots to enhance wound healing and restore blood flow is a highly actomyosin-driven mechanism and is abrogated by blebbistatin.<sup>66</sup>

## Introduction

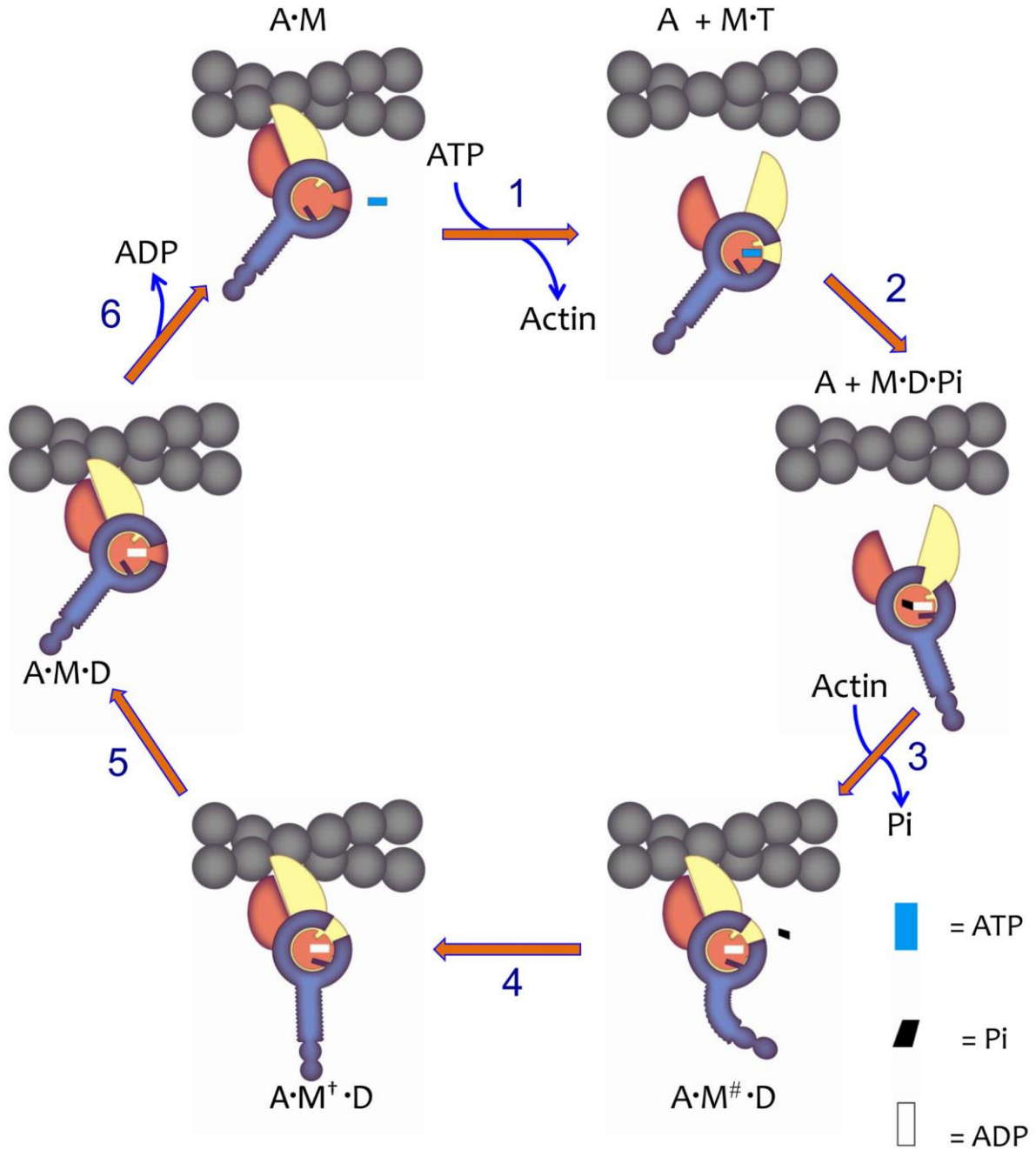


**Figure 11. The ATP driven actin-myosin motor mechanism.** Myosin head is shown in red (lower 50k domain) and yellow (upper 50k domain) with the major cleft that splits the actin binding site. A dark blue ring represents ATP-binding site of myosin IIA. The lever arm is projected from the ring in dark blue. ATP is shown in blue, phosphate in black and ADP in white. (1) Postrigor state: myosin (M) dissociates from actin (A) and binds ATP (T) at ATP-binding site at the head domain. (2) Recovery stroke: Repriming of the lever arm and hydrolysis of ATP to ADP (D) and Pi. (3) Pre-power stroke: weak binding of myosin to actin induces Pi release. (4) Conformational changes of the lever arm leads to higher affinity to actin. (5) Power stroke: further isomerization leads to greater movement of the lever arm. (6) Weakening of ADP affinity terminates power stroke and release of ADP. Adapted from <sup>67</sup>.

## Introduction

### 1.4 *MYH9* - related disease

#### 1.4.1 Clinical presentation of *MYH9*-RD patients

In the 20<sup>th</sup> century several scientists described patients with syndromes characterized by giant platelets, minor bleeding symptoms and situationally accompanied by granulocyte inclusion bodies, hearing loss, nephritis and cataracts.<sup>68</sup> The four syndromes described (1) May-Hegglin anomaly, (2) Epstein syndrome, (3) Fechtner syndrome and (4) Sebastian platelet syndrome were identified with the same underlying cause: mutations in the gene *MYH9* encoding for myosin IIA (Figure 12). Those syndromes are described now as *MYH9*-related disease (*MYH9*-RD), an autosomal-dominant disorder always affecting platelet formation.<sup>68</sup>

	May-Hegglin anomaly	Epstein syndrome	Fechtner syndrome	Sebastian platelet syndrome
macrothrombocytopenia	+	+	+	+
inclusion bodies	+	-	+	+
sensorineural hearing loss	-	+	+	(+)
nephritis	-	+	+	-
cataract	-	-	+	(+)

**Figure 12. The four syndromes of *MYH9*-RD.** The hematological and non-hematological manifestations in *MYH9*-related platelet disorders are shown for the four described syndromes (- absent; + present; (+) possible). Image from <sup>69</sup>.

Patients with *MYH9*-RD present a spectrum of clinical features with macrothrombocytopenia present in all affected individuals. Platelet numbers varying from mild reduction (100 000/ $\mu$ l) to severe thrombocytopenia (30 000/ $\mu$ l). Other features, like the degree of bleeding tendency, renal impairment, and the age of onset of cataracts and hearing loss vary between individuals.<sup>57,63</sup> Bleeding tendency of *MYH9*-RD patients is mild to moderate, but petechiae and major bleeding episodes are rare. More frequent are easy bruising, hematomas and, especially for female patients, menorrhagia. Often macrothrombocytopenia of *MYH9*-RD patients is diagnosed when their iron-deficiency anemia due to menorrhagia prompts a clinical presentation.<sup>57,68</sup> Inclusion bodies found in granulocytes of *MYH9*-RD patients originate from aggregates of abnormally accumulated myosin IIA protein, *MYH9* messenger ribonucleic acid (mRNA) and clusters of ribosomes.<sup>70</sup> The size of inclusion bodies in granulocytes depends on the location of the mutation. Large, spindle-shaped inclusion bodies are caused by mutations in regions coding for the C-terminus. Further

## Introduction

upstream mutations cause smaller myosin IIA inclusion bodies indicated by oval-shaped, small spots.<sup>57</sup> While macrothrombocytopenia of *MYH9*-RD patients is present since birth, other organ manifestations usually develop at higher age (>20 years).<sup>69</sup> Hearing loss is expected to occur in almost all patients over time, kidney damage occurs in 25% of all *MYH9*-RD patients and presenile cataracts affects about 20%.<sup>59</sup>

*MYH9*-RD is a rare disease. Although it is the most frequent form of inherited thrombocytopenia, its prevalence is estimated only around 3:1,000,000.<sup>59</sup> However, mild forms of *MYH9*-RD are often discovered accidentally, or patients are misdiagnosed as having chronic autoimmune thrombocytopenia, expecting the actual prevalence of *MYH9*-RD to be higher.<sup>59,68</sup> Mutations in the *MYH9* gene are responsible for the disease, with missense mutations as the most identified type of mutations. Until now, more than 80 mutations have been found located in 16 different exons.<sup>59</sup> All of the missense mutations are only heterozygous mutations. Homozygous mutations at amino acid position 702 are lethal based on animal experiments.<sup>16,68</sup>

In the German population the most frequent mutation is located at the base triplet coding for amino acid aspartic acid at position 1424 in exon 30. Individuals with mutations in exon 30 seem to have higher risks for developing cataracts and sensorineural hearing loss.<sup>71</sup> Both complications appear at an age of 40 years or later, accompanied with an only mild clinical phenotype, which is typical for patients with mutations in the tail region (as for mutation at position 1841 for glutamic acid), compared to mutations in genes coding for the head region, which are linked to higher risk for bleeding, renal and hearing impairment. Individuals with mutations in exon 16 affecting amino acid arginine at position 702 seem to be the most affected patients. Given that the head domain of myosin IIA is important for interactions with actin and ATP binding, a mutation affecting position 702 impairs the myosin ATPase system with a reduction of MgATPase activity to 25%.<sup>72,73</sup>

In *MYH9*-RD patients macrothrombocytopenia derives from defects in platelet biogenesis, especially regarding the formation of proplatelets from mature MKs.<sup>74,75</sup> MKs of *MYH9*-RD patients develop normally,<sup>74,75</sup> but show defective proplatelet formation.<sup>75</sup> MK protrusions had a significant defect in proplatelet branching and tip formation, which might contribute to the pathogenesis of thrombocytopenia.<sup>75,76</sup> Platelets of *MYH9*-RD patients showed no alteration of platelet aggregation in

## Introduction

response to collagen, but an absence of the typical shape change upon platelet activation.<sup>74,77,78</sup> Further studies on the platelet cytoskeleton of *MYH9*-RD patients indicated increased association of myosin with actin filaments in resting platelets, which was not further increased upon activation with TNF Receptor Associated Protein 1 (TRAP1). These data demonstrate that platelets of *MYH9*-RD patients showed impaired composition and reorganization of the cytoskeleton.<sup>79</sup> Organelle distribution of granules and mitochondria was heterogenous in platelets of *MYH9*-RD patients, resulting in platelets with low or high content of organelles, evoked by abnormal organelle distribution already present in MKs. Based on these results it was concluded that organelle motility in the cytoplasm of MKs is actomyosin-dependent.<sup>80</sup>

### 1.4.2 Treatment of *MYH9*-RD patients

Differential diagnosis of *MYH9*-RD and immune thrombocytopenia (ITP) is a key feature of the correct treatment of *MYH9*-RD patients. Since lot of *MYH9*-RD individuals are misdiagnosed with ITP, they are treated with intravenous immunoglobulin G (IgG), immunosuppressive therapy or splenectomy, which might be more harmful than the *MYH9*-RD itself.<sup>69</sup>

The most important preventive measure for *MYH9*-RD patients is to avoid medications that impair platelet function (e.g., aspirin), as well as to avoid iron deficiency anemia, especially in women at childbearing age. TPO receptor agonists increase the platelet count and reduce bleeding tendency in most *MYH9*-RD patients.<sup>57,59,68,69,81</sup> This medication is a short-term treatment option before a surgery. Given that TPO receptor agonists like eltrombopag increase platelet production, more larger platelets in *MYH9*-RD patients are present in the blood flow, which might influence microcirculation.<sup>57,68,69,81</sup> Since larger cells are known to flow in the middle of the microcirculatory bloodstream (Figure 13, upper), it was suggested that the increase in platelet production of *MYH9*-RD patients might lead to worsened microcirculation (Figure 13, lower).<sup>68</sup>

## Introduction

Major hemorrhage during surgery is rare in *MYH9*-RD patients, making prophylactic platelet transfusions needless. To reduce minor hemorrhage during surgery or to reduce higher bleeding tendency during menstruation administration of tranexamic acid (TXA) or the combination of TXA and desmopressin is recommended,<sup>57,68,69,82</sup> while desmopressin applied alone as nasal spray is only little effective to menorrhagia in *MYH9*-RD.<sup>57,69</sup>

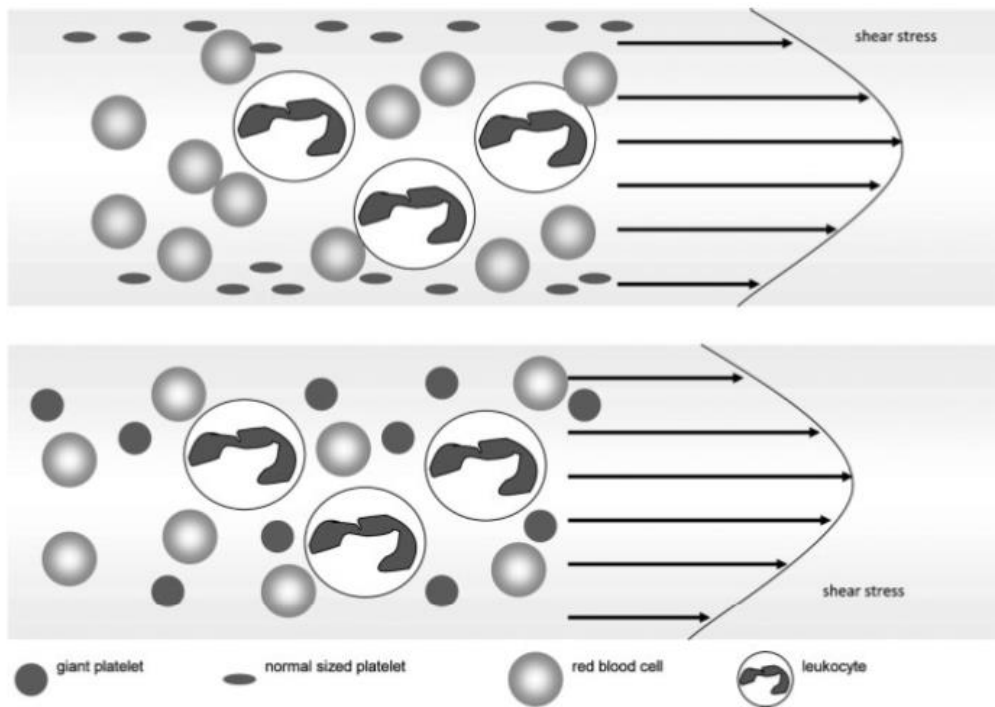


**Figure 13. Microcirculatory blood stream.** Upper part: normal-sized platelets flow close to the vessel wall, whereas red blood cells flow in the middle of the blood stream. Lower part: Reduced red blood cell count or giant platelets of *MYH9*-RD patients impair microcirculation due to platelets flowing more central in the blood flow. Image from <sup>68</sup>.

### 1.4.3 Mouse models to study myosin IIA

Several publications dealing with the role of myosin IIA in mouse platelets and MKs benefit from the high homology (97.1%) between the human and the mouse *Myh9* gene.<sup>59</sup> Existing mouse models either do not express myosin IIA specifically in the megakaryocytic lineage (knockout) or have heterozygous point mutations, which were inserted via homologous recombination into the respective exon representing the mutations found in *MYH9*-RD patients. Other studies are based on the inhibitory effect of blebbistatin on myosin IIA.

## Introduction

Studies on the *Myh9* knockout mouse line (*Myh9*<sup>-/-</sup>) in the megakaryocytic lineage (PF4-cre system) revealed a phenotype that partially resembles *MYH9*-RD in humans, such as thrombocytopenia and giant platelets.<sup>80,83</sup> A dramatic decrease in the number and complexity of proplatelets from BM-derived explants was observed and suggested to be responsible for the thrombocytopenia in those mice.<sup>84</sup> The ultrastructure of *Myh9* knockout platelets was heterogeneous with normal discoid platelets but also platelets with more ovoid morphology, which contained large amounts of rough endoplasmic reticulum, typical for immature cells, reflecting a defect in formation of mature platelets.<sup>80,83</sup> Myosin-deficient platelets appeared with abnormal distribution of organelles, such as  $\alpha$ - and  $\delta$ -granules as well as mitochondria, resulting in “low-content” and “high-content” platelets, originating from abnormal organelle distribution pattern already within MKs.<sup>80</sup> Granule transport from MKs to proplatelets is tubulin-dependent, but interaction of myosin IIA with organelle membranes independently of F-actin might lead to abnormal distribution of organelles in platelets.<sup>80</sup> Knockout mice presented no evidence of spontaneous bleeding, but primary hemostasis function was strongly affected, as shown by infinite bleeding times. Clot retraction of *Myh9*<sup>-/-</sup> platelets was completely abolished, aggregation was overall normal, but shape change was absent in knockout cells.<sup>83</sup> *Myh9*<sup>-/-</sup> platelets were able to adhere and spread on fibrinogen in the presence of thrombin, but were unable to form stress fiber-like structures. Furthermore, F-actin in *Myh9*<sup>-/-</sup> MKs appeared shorter and stress fibers were absent.<sup>80,83</sup> Outside-in signaling in response to thrombin was strongly impaired in myosin knockout cells. Loosely packed thrombi generated by *Myh9*<sup>-/-</sup> platelets under arterial shear *in vitro* and *in vivo* showed large emboli, continuously detaching from the thrombus, indicating instability of the thrombus (Figure 14).<sup>83</sup>

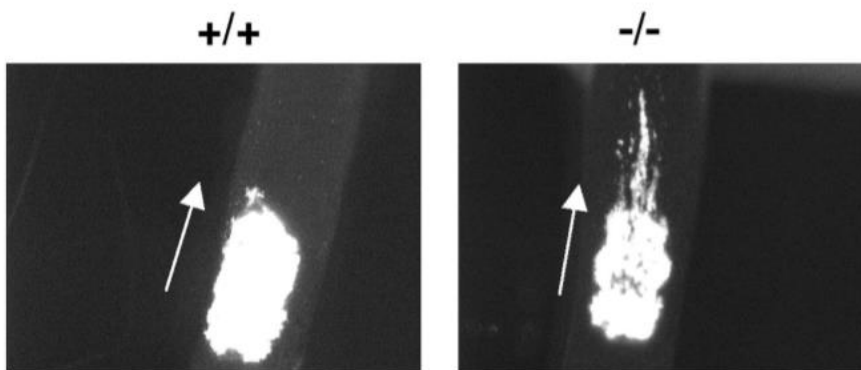


**Figure 14. Defective thrombus formation *in vivo*.** Representative images of carotid FeCl<sub>3</sub>-induced injury from busulfan-treated mice (to reach comparable thrombocytopenia) on the left (+/+) and *Myh9* knockout mice (-/-) on the right. 600 seconds after injury. Adapted from <sup>83</sup>.

## Introduction

Heterozygous point mutations in the *Myh9* gene were generated with homologous recombination at regions coding for amino acid positions 702, 1424 and 1841 with exchange of arginine to cysteine, aspartic acid to asparagine or glutamic acid to lysine, respectively (Figure 15) (further referred to as *Myh9*<sup>R702C/+</sup>, *Myh9*<sup>D1424N/+</sup>, *Myh9*<sup>E1841K/+</sup>).<sup>16</sup> These 3 mutations are the most frequent mutations found in human patients.<sup>85</sup>

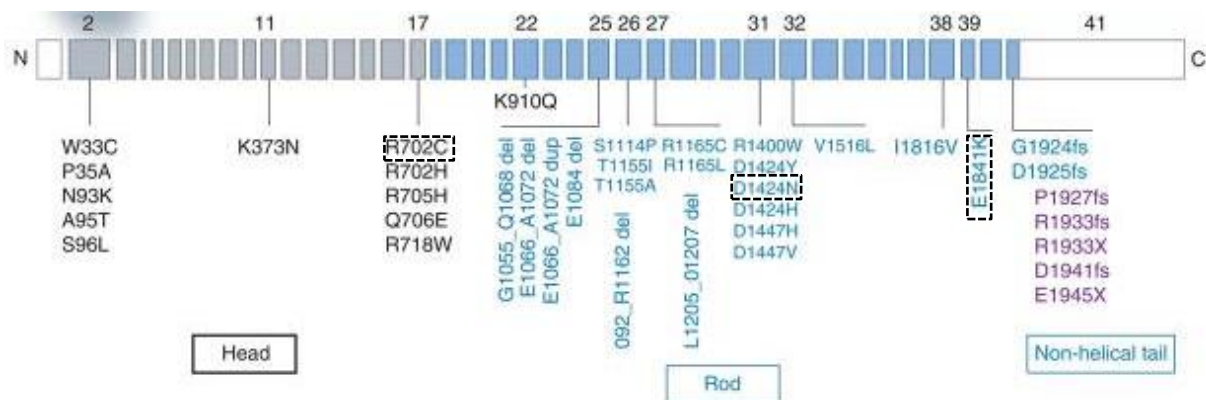


**Figure 15. MYH9 exon structure with autosomal dominant MYH9 mutations.** Non-coding first exon is shown in white, exons encoding the head domain in grey, encoding for rod domain in blue and exon 41 (non-helical tail) is shown in white. Corresponding mutations: 39 variants are shown here, in the same color as the location and mutations in the non-helical tail are shown in purple. Encircled are the three most abundant mutations in humans. Adapted from <sup>86</sup>.

Zhang and colleagues found out that the three mouse lines with these heterozygous point mutations in myosin IIA reveal macrothrombocytopenia and granulocyte inclusion bodies, as found in human patients. Other clinical features of *MYH9*-RD patients were present in the mouse models, including cataracts, hearing loss, and kidney abnormalities. Impaired platelet functions were observed with prolonged bleeding times and partial failure in clot retraction.<sup>16</sup> Mutant platelets were able to spread on a fibrinogen-coated surface in the presence of thrombin with a larger spreading area, but less *Myh9*<sup>D1424N/+</sup> platelets with extending lamellipodia were observed.<sup>76</sup> MKs in BM and spleen were more numerous in mutant mice, which suggests an attempt to compensate for the decrease in platelet production, but their morphology was unaltered. MKs developed fewer proplatelets, which showed shorter and fewer branches and thicker stalks with increased size of proplatelet tips.<sup>16</sup> MKs in the BM of *Myh9* mutant mice were more distant from the sinusoids than wildtype MKs, raising the hypothesis that migration of mutant MKs is impaired towards BM sinusoids. The ploidy



## Introduction

of the heterozygous mutant MKs was unaltered. MKs in BM of mutant *Myh9* mice showed differences in focal adhesion assembly and myosin IIA activity. Phosphorylated RLC was increased in *Myh9<sup>D1424N/+</sup>* MKs, suggesting increased contractility, whereas *Myh9<sup>R702C/+</sup>* MKs showed elevated HC phosphorylation, suggesting impaired filament assembly and stability. In agreement with the increased contractility of *Myh9<sup>D1424N/+</sup>* MKs, stress fiber formation was enhanced in those MKs. Although all mutant variants of myosin IIA were capable to form bipolar filaments, filaments of MKs from mouse line E1841K were more abundant, longer, and wider.<sup>76</sup>

## 2 Aim of the study

Several studies on the role of myosin IIA in platelets and megakaryocytes have been performed until now, including studies using samples from *MYH9*-RD patients, myosin IIA knockout and knock-in mice, as well as using the myosin IIA inhibitor blebbistatin. These studies demonstrated that myosin IIA is a crucial factor in platelet production and organelle distribution. Although the complex of myosin IIA and F-actin is the main machinery to generate forces in a blood clot, little is known about the biophysical features of platelets. It is currently insufficiently understood which factors contribute to the hemostatic defect observed in *MYH9*-RD patients and mutant mice. Therefore, the first aim of this study was to investigate the underlying biophysical mechanisms of clot formation and stabilization in samples of myosin IIA point mutated mice.

We capitalized on three mouse lines with heterozygous point mutations in the *Myh9* gene, resulting in the amino acid exchanges R702C, D1424N or E1841K which were described to reflect the key clinical features of human patients,<sup>16</sup> to investigate whether altered biomechanical properties might be responsible for the increased bleeding phenotype in *MYH9*-RD patients. In cooperation with the Institute for Immunology and Transfusion Medicine at the University of Greifswald, we performed biophysical assays and verified our key findings obtained in mice by analyzing platelets from *MYH9*-RD patients with amino acid exchanges in myosin IIA at the positions D1424N and E1841K.

TXA, a synthetic derivative of the amino acid lysine, possesses antifibrinolytic properties by a reversible blockage of the lysine binding sites on plasminogen molecules.<sup>87</sup> Individuals with *MYH9* disorders are treated with TXA before and after dental surgery as well as during menses to prevent increased bleeding.<sup>57,68,69</sup> Contrarily, Samson *et al.* showed that incomplete proteolysis of fibrin polymers facilitates clot retraction, whereas inhibition of endogenous fibrinolysis with TXA reduced clot retraction.<sup>88</sup> We wondered why inhibition of fibrinolysis is especially beneficial for patients with *MYH9* mutations. Therefore, the second aim of this study was to investigate the underlying mechanisms of the beneficial effect of TXA by preventing bleeding in *MYH9*-RD patients.

## Materials

### 3 Materials

#### 3.1 Human blood samples

The use of blood from healthy adult individuals and *MYH9*-RD patients was approved by the ethics committee of the University Medicine Greifswald, Germany (license number: BB 014/14). All participants gave written informed consent. Each patient with the mutation D1424N or E1841K was invited three times to University Medicine Greifswald. Whole blood of patients was drawn into Acid-Citrate-Dextrose (ACD-A) and shipped in Vacutainer® flasks to Würzburg together with a transport control from a healthy donor. Blood was sent overnight and kept at room temperature (RT).

#### 3.2 Animals

*Myh9* mutant mice<sup>16</sup> were purchased from Mutant Mouse Resource & Research Centers. Stock numbers are 036196-UNC (R702C), 036210-UNC (D1424N), and 036698-MU (E1841K). To generate a myosin IIA knock-in R702C mutant, a targeting vector containing GFP fused to human non-muscle heavy chain myosin IIA cDNA with the R702C mutation and flanking genomic sequence was used for homologous recombination. Consequently, the endogenous gene is not expressed and the introduced human version is expressed under the mouse *Myh9* promoter (Figure 16A).<sup>16</sup> For generation of knock-in D1424N and E1841K mutants, a targeting vector containing exon 31 or exon 39 with the respective mutation were generated, respectively. Constructs including a loxP-flanked Neo cassette were introduced via homologous recombination into the respective sequence (Figure 16B, C).<sup>16</sup>

Wildtype littermates were used as controls for the heterozygous mice from each mutant strain (R702C: Albino – Wildtype strain 129/SV, C57BL/6, and BALB/c; D1424N: Agouti – Wildtype strain 129/SV, C57BL/6, and BALB/c; E1841K: Black – Wildtype strain 129/SV and C57BL/6) because of the different backgrounds. Female and male mice were between 6 and 16 weeks of age. Animal studies were approved by the district government of Lower Franconia, Germany (license number 2-523, 2-944). Mice were kept at a 12-hour light and 12-hour dark cycle with food and water available *ad libitum* in the experimental area of the animal facility.

## Materials

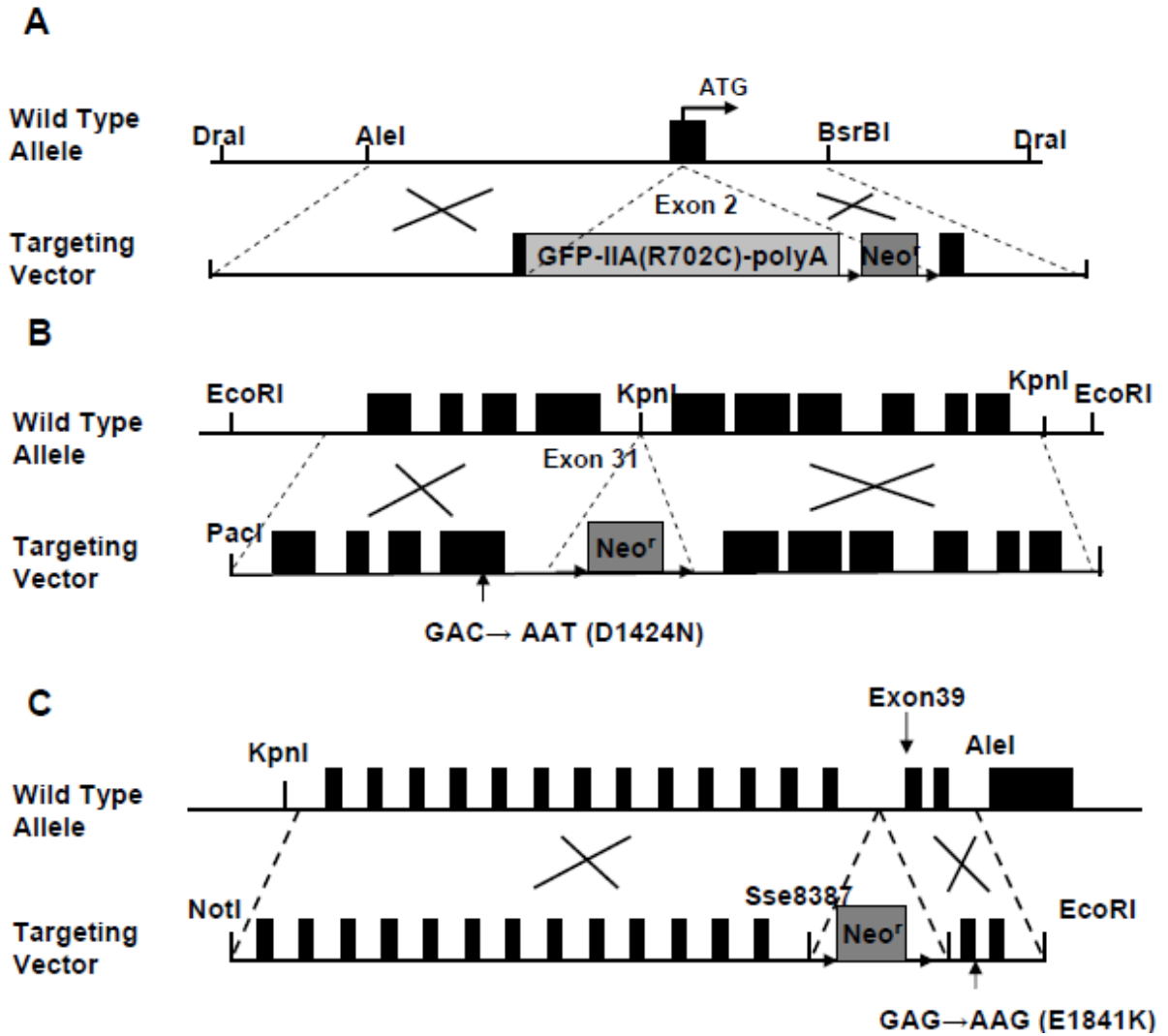


**Figure 16. Generation of myosin IIA knock-in mouse lines by homologous recombination.** (A) Scheme of generating mouse line R702C. Targeting vector containing GFP fused to human myosin IIA cDNA with the R702C mutation was introduced into wildtype allele near exon 2. (B) Generation of mouse line D1424N was performed with targeting vector with respective mutation in exon 31. (C) E1841K mutant mice were generated via homologous recombination of targeting vector with the E1841K mutation in exon 39. Image from reference <sup>16</sup>.

## Materials

### 3.3 Antibodies

#### Commercially purchased antibodies

Antibody	Host	Manufacturer	Catalogue number
Anti-GAPDH	rabbit	Sigma-Aldrich	#G9545
Anti- $\beta$ -actin	rabbit	Sigma-Aldrich	#A2066
Anti-myosin IIA	rabbit	Sigma-Aldrich	#M8064
Anti-ROCK1	rabbit	Abcam	#ab134181
Anti-RhoA	rabbit	Cell Signaling	#67B9
Anti-MLC2	rabbit	Cell Signaling	#3672S
Anti-MLC2-p-S19	mouse	Cell Signaling	#3675S
Anti-MLC2-p-T18/S19	rabbit	Cell Signaling	#3674S
Anti-MYPT1	rabbit	Cell Signaling	#4563T
Anti-vinculin	mouse	Sigma-Aldrich	#V9131

Antibody	Conjugate	Manufacturer	Catalogue number
Anti-CD105	Alexa Fluor 647	eBioscience	#MJ7/18
Anti- $\alpha$ -tubulin	Alexa Fluor 488	Santa Cruz	#sc-23948
Anti- $\alpha$ -tubulin	Alexa Fluor 546	Santa Cruz	#sc-23948
Donkey-anti-rabbit IgG	Cy3	Jackson Immuno	#711-165-153
Donkey-anti-mouse IgG	Alexa Fluor 546	Thermo Fisher Scientific	#10698093
Anti-CD61	FITC	Beckman Coulter	#340715
Anti-CD61	PE	Beckman Coulter	#IM3605
Secondary goat anti-rabbit	HRP	Protein Simple	#042-206
Secondary goat anti-mouse	HRP	Protein Simple	#042-205
Secondary anti-rabbit	near-infrared	Protein Simple	#043-819

## Materials

### Homemade antibodies

Homemade monoclonal antibodies were generated and modified in the Nieswandt laboratory and labeling to fluorescein isothiocyanate (FITC), phycoerythrin (PE) or allophycocyanin (APC) was performed using commercial kits (according to manufacturer's instruction).

Antigen	Antibody	Clone	Isotype	Reference
GPIb $\alpha$	p0p4	15E2	IgG2b	89,90
GPIX	p0p6	56F8	IgG2b	89,90
GPV	DOM2	89H11	IgG2a	89
GPV	DOM2	89F12	IgG2a	89
CD9	ULF1	96H10	IgG2a	unpublished
GPVI	JAQ1	98A3	IgG2a	91,92
$\alpha$ Ib $\beta$ 3	JON6	14A3	IgG2b	unpublished
$\alpha$ Ib $\beta$ 3	JON/A	4H5	IgG2b	93,94
CLEC-2	INU1	11E9	IgG1	95
P-selectin	WUG 1.9	5C8	IgG1	unpublished

### 3.4 Material

Material	Manufacturer
ACD Solution A (Vacutainer®)	BD Biosciences (Heidelberg, Germany)
Adhesive cryo films	Section lab (Hiroshima, Japan)
Borosilicate pipettes	World precision instruments (Friedberg, Germany)
Cantilever (Gold-coated)	NanoAndMore GmbH (Wetzlar, Germany)
Cantilever (Silicon)	MikroMasch (Tallinn, Estonia)
Canula (G)	BD Biosciences (Heidelberg, Germany)
Chamlide	Live Cell Instruments Co. Ltd. (Sunhwagung-ro, Korea)

## Materials

Coverslips #1.5 60x60	Thermo Fisher Scientific (Dreieich, Germany)
Coverslips #1.0 24x24	Thermo Fisher Scientific (Dreieich, Germany)
EDTA tubes Microvette® 500 K3E	Sarstedt (Nürnberg, Germany)
FLic15	Zellmechanik Dresden (Dresden, Germany)
Formvar-carbon-coated grids	Ted Pella Inc. (Redding, US)
Glass bottom trays	Ibidi GmbH (Gräfelfing, Germany)
Glass slide Superfrost Plus	Thermo Fisher Scientific (Dreieich, Germany)
Heparinized capillaries	Hartenstein (Würzburg, Germany)
Ibidi sticky slide VI 0.4	Ibidi GmbH (Gräfelfing, Germany)
Ibidi $\mu$ -Slide VI 0.1	Ibidi GmbH (Gräfelfing, Germany)
Luer Lock Connector Female	Ibidi GmbH (Gräfelfing, Germany)
Luer Lock Connector Male	Ibidi GmbH (Gräfelfing, Germany)
Microcapillaries (50 $\mu$ L)	Hartenstein (Würzburg, Germany)
Sodium-Citrate (Vacutainer®)	BD Biosciences (Heidelberg, Germany)
Polystyrene cell culture dishes	Greiner Bio One (Frickenhausen, Germany)
PVDF membrane	GE Healthcare (Penzberg, Germany)
Silicone Tubing (inner diameter 0.8 mm)	Ibidi GmbH (Gräfelfing, Germany)
Straight channel chip (depth 55 $\mu$ m)	Microfluidic ChipShop (Jena, Germany)
Syringes (1 mL)	Dispomed (Gelnhausen, Germany)

## Materials

### 3.5 Chemicals and reagents

Reagent	Manufacturer
Acetone	Roth (Karlsruhe, Germany)
Adenosine diphosphate (ADP)	Sigma-Aldrich (Schnelldorf, Germany)
Agarose	Roth (Karlsruhe, Germany)
Albumin from human serum	Sigma-Aldrich (Schnelldorf, Germany)
Alexa Fluor 488 NHS ester	Thermo Fisher Scientific (Dreieich, Germany)
Ammonium peroxidsulfate (APS)	Roth (Karlsruhe, Germany)
Apyrase (grade III)	Sigma-Aldrich (Schnelldorf, Germany)
Blue Block	Serva Electrophoresis GmbH (Heidelberg, Germany)
$\beta$ -Mercaptoethanol	Roth (Karlsruhe, Germany)
Bovine serum albumin (BSA)	AppliChem GmbH (Darmstadt, Germany)
Cacodylate	AppliChem GmbH (Darmstadt, Germany)
Calcium-chloride	Roth (Karlsruhe, Germany)
Carbon	Leica (Wetzlar, Germany)
Casein from bovine milk	Sigma-Aldrich (Schnelldorf, Germany)
CellCarrierB	Zellmechanik Dresden (Dresden, Germany)
Citrate	Electron microscopy science (Hatfield, US)
Clarity™ Western ECL Substrate	BIORAD (California, US)
Collagen G	Biochrom (Karlsruhe, Germany)
Collagen-related peptide (CRP)	Cambridge Research Biochemicals (Billingham, UK)
Convulxin (CVX)	Axxora (Lörrach, Germany)
dNTP	Thermo Fisher Scientific (Dreieich, Germany)
DPBS	PAN Biotech GmbH (Aidenbach, Germany)
DreamTaq Polymerase	Thermo Fisher Scientific (Dreieich, Germany)



## Materials

DreamTaq Polymerase 10x green buffer	Thermo Fisher Scientific (Dreieich, Germany)
DyLight 405 NHS ester	Thermo Fisher Scientific (Dreieich, Germany)
Endotoxin-free BSA	Sigma-Aldrich (Schnelldorf, Germany)
Ethylenediaminetetraacetic acid (EDTA)	AppliChem GmbH (Darmstadt, Germany)
Ethylene glycol-bis(2-aminoethylether)- N,N,N',N'-tetraacetic acid (EGTA)	Sigma-Aldrich (Schnelldorf, Germany)
Fentanyl	Rotexmedica GmbH (Trittau, Germany)
Fibrinogen from human plasma	Sigma-Aldrich (Schnelldorf, Germany)
Fibrinogen from human plasma- Alexa Fluor 647	Thermo Fisher Scientific (Dreieich, Germany)
Fibrinogen from human plasma- Alexa Fluor 488	Sigma-Aldrich (Schnelldorf, Germany)
Fluoroshield mounting medium with DAPI	Sigma-Aldrich (Schnelldorf, Germany)
GeneRuler 100bp Plus DNA Ladder	Thermo Fisher Scientific (Dreieich, Germany)
Glutaraldehyde	Electron microscopy science (Hatfield, US)
HALT Protease & Phosphatase Inhibitor Cocktail 2x	Thermo Fisher Scientific (Dreieich, Germany)
Heparin sodium	Ratiopharm (Ulm, Germany)
Hexamethyldisilazane	Sigma-Aldrich (Schnelldorf, Germany)
HORM collagen	NYCOMED (Zürich, Switzerland)
HORM collagen	Takeda (Linz, Austria)
hPDMS	Gelest Inc. (Pennsylvania, US)
IGEPAL CA-630	Roth (Karlsruhe, Germany)
Isofluran CP	cp-pharma (Burgdorf, Germany)
Isopropanol	Roth (Karlsruhe, Germany)

## Materials

iTAQ Universal SYBR Green Supermix	BIORAD (California, US)
Magnesium-rich diet food	Altromin Spezialfutter GmbH & Co. KG (Lage, Germany)
Medetomidine	Zoetis (New Jersey, US)
Midazolam	ROTEXMEDICA GmbH (Trittau, Germany)
Midori Green DNA stain	Nippon Genetics (Düren, Germany)
Sodium-Chloride	B. Braun (Melsungen, Germany)
Nitric acid	Sigma-Aldrich (Schnelldorf, Germany)
PageRuler™ Plus Prestained Protein Ladder	Thermo Fisher Scientific (Dreieich, Germany)
Paraformaldehyde (PFA)	Sigma-Aldrich (Schnelldorf, Germany)
Phalloidin	AppliChem GmbH (Darmstadt, Germany)
Phalloidin-FITC	Enzo Life Science (New York, US)
Phalloidin-Alexa Fluor™ 488	Thermo Fisher Scientific (Dreieich, Germany)
Phalloidin-Alexa Fluor™ 647	Thermo Fisher Scientific (Dreieich, Germany)
Phalloidin-Atto647N	Thermo Fisher Scientific (Dreieich, Germany)
Platinum	Leica (Wetzlar, Germany)
Poly(ethylene glycol)methyl ether thiol (Mn800)	Sigma-Aldrich (Schnelldorf, Germany)
Poly-L-lysine (PLL)	Sigma-Aldrich (Schnelldorf, Germany)
Prostaglandin (PGI <sub>2</sub> )	Sigma-Aldrich (Schnelldorf, Germany)
Protease inhibitor cocktail	Sigma-Aldrich (Schnelldorf, Germany)
Proteinase K	Thermo Fisher Scientific (Dreieich, Germany)
Donkey serum	The Jackson Laboratory (Maine, US)
R ex-TEM	Werfen GmbH (München, Germany)

## Materials

Rhodocytin (RC)	J. Eble (University Hospital Frankfurt, Germany)
Rotiphorese gel 30 acrylamide	Roth (Karlsruhe, Germany)
rtPA	Abcam (Cambridge, UK)
Star-TEM	Werfen GmbH (München, Germany)
Sodium citrate	Merck KGaA (Darmstadt, Germany)
Sodium dodecylsulfate (SDS)	Roth (Karlsruhe, Germany)
Sucrose	Roth (Karlsruhe, Germany)
Super cryo embedding medium	Section lab (Hiroshima, Japan)
Taxol	AppliChem GmbH (Darmstadt, Germany)
Tannic acid	Merck KGaA (Darmstadt, Germany)
Tetramethylethylenediamine (TEMED)	Roth (Karlsruhe, Germany)
Thrombin from human plasma	Roche (Basel, Switzerland)
Tranexamic acid (TXA)	Merck KGaA (Darmstadt, Germany)
Triton X-100	AppliChem GmbH (Darmstadt, Germany)
Tween 20	Roth (Karlsruhe, Germany)
U46619	Enzo Life Science (Lörrach, Germany)
Uranyl acetate	Electron microscopy science (Hatfield, US)

## Materials

### 3.6 Buffer

All buffers were prepared using deionized water obtained from MilliQ Water Purification System (Millipore, Schwalbach, Germany) and pH adjusted, using NaOH and HCl.

- Acid-Citrate-Dextrose (ACD) Buffer, pH 4.5
  - Trisodium citrate dehydrate 85 mM
  - Anhydrous citric acid 65 mM
  - Anhydrous glucose 110 mM
- Gitschierbuffer, 10x, pH 8.8
  - Tris 670 mM
  - Ammonium sulfate 166 mM
  - MgCl<sub>2</sub> 65 mM
  - Triton X-100 0.5% (w/v)
- Lysis Buffer (DNA Lysis)
  - Gitschierbuffer 1x
  - β-Mercaptoethanol 1% (w/v)
  - Proteinase K 0.5 mg/mL
- Miakawa HEPES-Tyrode's buffer
  - NaCl 129 mM
  - NaHCO<sub>3</sub> 8.9 mM
  - KH<sub>2</sub>PO<sub>4</sub> 0.8 mM
  - HEPES 10 mM
  - MgCl<sub>2</sub> 0.8 mM
  - Glucose 5.6 mM
- PFA, 10% in PHEM
  - PHEM Buffer 1x
  - PFA 10% (w/w)

## Materials

- Fixation Buffer
  - PBS 1x
  - PFA 4% (w/w)
- PHEM Buffer, pH 7.0, 10x
  - PIPES 300 mM
  - HEPES 125 mM
  - EGTA 50 mM
  - MgSO<sub>4</sub> x 7H<sub>2</sub>O 20 mM
- Fixation Buffer Cytoskeleton
  - PHEM 1x
  - PFA 4% (w/w)
  - IGEPAL CA-630 0.1% (w/v)
- Phosphate buffered saline (PBS), pH 7.14
  - NaCl 137 mM
  - KCl 2.7 mM
  - KH<sub>2</sub>PO<sub>4</sub> 1.5 mM
  - Na<sub>2</sub>HPO<sub>4</sub> x 2H<sub>2</sub>O 8.0 mM
- Protein lysis buffer, 2x, pH 7.4
  - NaCl 300 mM
  - Tris 20 mM
  - EGTA 2 mM
  - EDTA 2 mM
  - NaF 10 mM
  - Na<sub>3</sub>VO<sub>4</sub> 4 mM
  - IGEPAL CA-630 2% (w/v)
  - 2x HALT Protease & phosphatase inhibitor cocktail 1:100

## Materials

- SDS running buffer
  - Tris HCl 40 mM
  - Glycine 0.95 M
  - SDS 0.5% (w/v)
- SDS Sample Buffer, 4x, pH 6.8
  - Tris HCl (1 M) 20%
  - Glycerol 40%
  - SDS 4%
  - $\beta$ -Mercaptoethanol 20% (w/v)
  - Bromophenol blue 0.04% (w/w)
- Separating Gel Buffer (Western Blot), pH 8.8
  - Tris 1.5 M
- Separating Gel (Western Blot), 10%
  - Separating Gel Buffer -
  - SDS 0.1% (w/v)
  - Acrylamide 10% (w/v)
  - APS 0.1% (w/v)
  - TEMED 0.1% (w/v)
- Separating Gel (Western Blot), 7.5%
  - Separating Gel Buffer 1/4
  - SDS 0.1% (w/v)
  - Acrylamide 7.5% (w/v)
  - APS 0.1% (w/v)
  - TEMED 0.1% (w/v)
- Sodium-Citrate-Buffer, pH 7.0
  - Sodium Citrate 0.129 M

## Materials

- Stacking Gel Buffer (Western Blot), pH 6.8
  - Tris HCl 0.5 M
- Stacking Gel (Western Blot)
  - Stacking Gel Buffer 1/4
  - SDS 0.1% (w/v)
  - Acrylamide 5% (w/v)
  - APS 0.1% (w/v)
  - TEMED 0.1% (w/v)
- Stripping Buffer (Western Blot), pH 2.0
  - PBS 1x
  - Glycine 25 mM
  - SDS 1% (w/v)
- Suspension Buffer (Colloidal probe spectroscopy), pH 7.4
  - NaCl 136 mM
  - Na<sub>2</sub>HPO<sub>4</sub> 0.41 mM
  - KCl 2.65 mM
  - NaHCO<sub>3</sub> 12 mM
  - MgCl<sub>2</sub> 2.13 mM
  - CaCl<sub>2</sub> 2.9 mM
  - D-glucose 5.5 mM
  - BSA 0.35% (w/w)
- Tris-Acetate-EDTA buffer (TAE), 50x, pH 8.0
  - Tris HCl 200 mM
  - Acetic acid 5.7% (w/v)
  - EDTA 50 mM

## Materials

- Tankblot Buffer (Western Blot), 1x
  - NaHCO<sub>3</sub> 1 mM
  - Na<sub>2</sub>CO<sub>3</sub> 0.3 mM
  - Methanol 20% (w/v)
- Tris-Buffered Saline (TBS), pH 7.3
  - NaCl 137 mM
  - Tris HCl 20 mM
- Tyrode's-HEPES buffer without Ca<sup>2+</sup>, pH 7.3
  - NaCl 134 mM
  - KCl 2.9 mM
  - NaHCO<sub>3</sub> 12 mM
  - NaH<sub>2</sub>PO<sub>4</sub> 0.34 mM
  - HEPES 5 mM
  - MgCl<sub>2</sub> 1 mM
  - BSA pH 7.4 0.35% (w/w)
  - Glucose 5 mM
- Tyrode's-HEPES buffer with Ca<sup>2+</sup>, pH 7.3
  - NaCl 134 mM
  - KCl 2.9 mM
  - NaHCO<sub>3</sub> 12 mM
  - NaH<sub>2</sub>PO<sub>4</sub> 0.34 mM
  - HEPES 5 mM
  - MgCl<sub>2</sub> 1 mM
  - BSA pH 7.4 0.35% (w/w)
  - Glucose 5 mM
  - CaCl<sub>2</sub> 2 mM
- Washing Buffer TBS-T (Western Blot)
  - TBS 1x
  - Tween 20® 0.1% (w/v)



## Materials

### 3.7 Devices

Device	Company
AcCellerator	Zellmechanik Dresden (Dresden, Germany)
Amersham Imager 680	GE Healthcare (Penzberg, Germany)
AxioObserver A1	Zeiss (Jena, Germany)
Cryotom CM1900	Leica (Wetzlar, Germany)
Epon 812	Electron microscopy science (Hatfield, US)
Eppendorf centrifuge 5415C	Eppendorf AG (Hamburg, Germany)
Eppendorf centrifuge 5424	Eppendorf AG (Hamburg, Germany)
Eppendorf centrifuge 5427R	Eppendorf AG (Hamburg, Germany)
FACS Calibur	BD Biosciences (Heidelberg, Germany)
FACS Celesta	BD Biosciences (Heidelberg, Germany)
Fibrintimer APACT	LabiTec (Ahrensburg, Germany)
Gene Touch Thermal Cycler	Bioer (Zhejiang, China)
JEM-2100 Electron microscope	JEOL GmbH (Freising, Germany)
Jess	ProteinSimple (California, US)
JPK NanoWizard 3	Bruker (Massachusetts, US)
Herolab	Herolab (Wiesloch, Germany)
Leica CTR 6000	Leica (Wetzlar, Germany)
Leica DMI 6000B	Leica (Wetzlar, Germany)
Leica EL 6000	Leica (Wetzlar, Germany)
Leica EM ACE600	Leica (Wetzlar, Germany)
Leica EM CPD300	Leica (Wetzlar, Germany)
Leica Thunder Imaging System	Leica (Wetzlar, Germany)
Olympus IX8	Olympus (Shinjuku, Japan)

## Materials

Optima™ L-80 XP Ultracentrifuge	Beckman Coulter (Krefeld, Germany)
Scil Vet abc Plus +	Scil Vet (Viernheim, Germany)
Spin coater SCI-20	Schaefer Technologie GmbH (Langen, Germany)
Sysmex KX 21N	Sysmex GmbH (Norderstedt, Germany)
Sysmex Hemato Analyzer poCH-100i	Sysmex GmbH (Norderstedt, Germany)
ROTEM	Pentapharm GmbH (Basel, Switzerland)
TCS SP5 CLSM	Leica (Wetzlar, Germany)
TCS SP8 CLSM	Leica (Wetzlar, Germany)
UV cleaner	Bioforce Nanosciences (Virginia, US)
VWR MEGA STAR 1.6R	VWR part of avantor (Darmstadt, Germany)
Zeiss EM 900	Zeiss (Jena, Germany)
Zeiss incubation microscope	Zeiss (Jena, Germany)
7500 Fast Real-Time PCR System	Applied Biosystems (Massachusetts, US)

### 4 Methods

#### 4.1 Molecular biological analyses

##### 4.1.1 Isolation of murine DNA

A small piece (5 mm<sup>2</sup>) of mouse ear was incubated overnight in 100 µL lysis buffer supplemented with proteinase K under constant shaking at 1,200 rpm and 56°C. Samples were heated up to 95°C for 5 minutes and immediately centrifuged at 14,000 rpm (Eppendorf centrifuge 5427R). Isolated DNA in the supernatant was stored at -20°C.

##### 4.1.2 Polymerase chain reaction

*Myh9*<sup>R702C/+</sup> and *Myh9*<sup>D1424N/+</sup> and respective control *Myh9*<sup>+/+</sup> mice were genotyped by polymerase chain reaction (PCR). Genotype specific DNA-fragments were amplified from isolated murine genomic DNA. Genotyping protocols and primer sequences were provided by Mutant Mouse Resource and Research Center at University of North Carolina.

## Methods

### *Myh9*<sup>R702C/+</sup>

Primer sequences 5' to 3'

- Primer 1: CTGTCACATGGCTCATGTTC
- Primer 2: GCCGGACACGCTGAACTTGT
- Primer 3: GCCCTGAGTAGTATCGCTCC

PCR-Mix:

Reagent	Stock concentration	Volume
H <sub>2</sub> O		17.875 µL
DreamTaq buffer	10x	2.5 µL
dNTPs	10 mM	0.5 µL
Primer 1	0.1 µg/µL	1 µL
Primer 2	0.1 µg/µL	1 µL
Primer 3	0.1 µg/µL	1 µL
DreamTaq polymerase	20U	0.125 µL
Template DNA		1 µL
		25 µL

PCR-program:

Cycles	Temperature	Duration
1 cycle	94°C	5 minutes
35 cycles	94°C	30 seconds
	58°C	30 seconds
	72°C	30 seconds
1 cycle	72°C	7 minutes
	4°C	∞

Expected bands: Wildtype allele = 394 bp (Primer 1 + 3)  
 Mutant allele = 200 bp (Primer 1 + 2)

## Methods

### *Myh9*<sup>D1424N/+</sup>

Primer sequences 5' to 3':

- Primer 1: CGCTCTTCTAGAGGACAAGTTCCA
- Primer 2: CAGAGACTCCTCTAGCACTGTA

PCR-Mix:

Reagent	Stock concentration	Volume
H <sub>2</sub> O		18.875 µL
DreamTaq buffer	10x	2.5 µL
dNTPs	10 mM	0.5 µL
Primer 1	0.2 µg/µL	1 µL
Primer 2	0.1 µg/µL	1 µL
DreamTaq polymerase	20U	0.125 µL
Template DNA		1 µL
		25 µL

PCR-program:

Cycles	Temperature	Duration
1 cycle	94°C	5 minutes
35 cycles	94°C	30 seconds
	55°C	30 seconds
	72°C	30 seconds
1 cycle	72°C	7 minutes
	4°C	∞

Expected bands: Wildtype allele = 200 bp  
 Mutant allele = 250 bp

## Methods

### 4.1.3 Agarose gel electrophoresis

DNA ladder (GeneRuler Plus 100bp) and PCR samples were loaded on a 2% agarose gel (agarose solved in 1x TAE-buffer) containing Midori green (1:20,000). Separation of amplified DNA was performed in an electrical field with constant voltage of 120 V for 40 minutes. DNA amplicons were detected with a Herolab using UV light.

### 4.1.4 Real-time PCR

*Myh9<sup>E1841K/+</sup>* and respective control *Myh9<sup>+/+</sup>* mice were genotyped by real-time PCR. Genotype specific DNA-fragments were amplified from isolated murine genomic DNA. Genotyping protocol was performed using iTAQ Universal SYBR Green Supermix from Bio-Rad. Reaction was run on a 7500 Fast Real-Time PCR System from Applied Biosystems. Genotyping protocol and primer sequences were provided by Mutant Mouse Resource and Research Center at University of Missouri.

Primer sequences 5' to 3':

- Primer 1: CCC CTT TCA GTC AGC ATT TC (forward)
- Primer 2: GCA CGT CCT TCA GCT TCT TC (reverse)

PCR-Mix:

Reagent	Stock concentration	Volume
H <sub>2</sub> O		108.7 µL
iTAQ Universal SYBR Green Supermix	2x	143 µL
Primer 1	2 µM	2.9 µL
Primer 2	2 µM	2.9 µL
Template DNA	5 ng/µL	2 µL

## Methods

PCR-program:

Cycles	Temperature	Duration
1 cycle	95°C	2 minutes
40 cycles	95°C	10 seconds
	60°C	30 seconds
	72°C	30 seconds
1 cycle	95°C	30 seconds
1 cycle	60°C	1 minute
1 cycle	65 – 95°C	~10 seconds per 0.2°C

Expected result: Mutant: shifted melt curve due to increased break of hydrogen bonding (nucleotide exchange of guanine to adenine)

### 4.1.5 Blood parameters

*Mouse:* Platelet count and size, as well as all other blood parameters were determined using a hematology analyzer Scil Vet abc Plus +. Blood was taken from mice with heparinized capillaries into ethylenediaminetetraacetic acid (EDTA) tubes. Studies on magnesium supplementation were performed with magnesium-supplemented food (Altromin; 0.75%) for 14 days and platelet count was measured before magnesium supplementation and after 14 days of supplementation.

*Human:* Blood parameters were measured with a Sysmex Hemato Analyzer poCH-100i in Greifswald.

## 4.2 Platelet function analyses

### 4.2.1 Platelet preparation

*Mouse:* Mice were anesthetized with isoflurane and blood was collected in a tube containing heparin (20 U/mL in TBS, pH 7.3). Platelet-rich plasma (PRP) was obtained by two times centrifugation at 800 rpm for 6 minutes (Eppendorf centrifuge 5415C) at RT. To prepare the washed platelets, the PRP supplemented with prostaglandin (PGI<sub>2</sub>; 0.5 µM) and apyrase (0.02 U/mL) was centrifuged at 2800 rpm (~ 736 g; Eppendorf

## Methods

centrifuge 5424) for 5 minutes at RT. The platelet pellet was washed in modified Tyrode's-HEPES buffer in the presence of PGI<sub>2</sub> (0.5 µM) and apyrase (0.02 U/mL). Platelet concentration was determined with a hematology analyzer Sysmex KX 21N. Desired platelet count was obtained after centrifugation at 2800 rpm (~ 736 g; Eppendorf centrifuge 5424) for 5 minutes at RT. Finally, platelets were resuspended in the calculated volume of modified Tyrode's-HEPES buffer with 0.02 U/mL apyrase and incubated at 37°C for 30 minutes before use.

*Human:* Donors had not taken any medication in the ten days prior to blood collection. Whole blood was collected by venipuncture into BD Vacutainer® tubes containing ACD-A and 3.8% buffered trisodium citrate (sodium-citrate). Whole blood was stored at 37°C for at least 30 minutes. Centrifugation was not performed because the large platelets of *MYH9*-RD patients would sediment with the other blood cells due to their size. To maximize the number of platelets available for the experiments (because of their smaller number in the patient sample), the ACD-A whole blood tubes were held at a 45° angle, and the PRP was transferred to a new polypropylene tube. All experimental measurements in Greifswald were performed within 3 hours of blood collection. For spreading experiments PRP was supplemented with PGI<sub>2</sub> (0.5 µM) and apyrase (0.02 U/mL) and 1/10 of the volume ACD. After 10 minutes rest at 37°C, the platelet suspension was centrifuged twice at 500 g for 10 minutes. Supernatant was removed and the pellet was resuspended in Tyrode's-HEPES buffer without Ca<sup>2+</sup> to desired platelet concentrations and set to rest for 30 minutes at 37°C prior to the experiment.

### 4.2.2 Aggregometry

Washed platelets (50 µL with 5 x 10<sup>5</sup> platelets/µL) were analyzed in the presence (HORM collagen [Takeda]) or absence (thrombin) of 70 µg/mL human fibrinogen (Sigma) and were added to 110 µL of Tyrode's-HEPES buffer with calcium. Light transmission was recorded for 10 minutes with an Apact four-channel aggregometer and reported in arbitrary units, where Tyrode's-HEPES buffer supplemented with calcium indicates 100% light transmission.



## Methods

### 4.2.3 Platelet spreading

Coverslips were coated with 100 µg/ml human fibrinogen (Sigma) for 2 hours at 37°C. After blocking with 1% BSA in PBS, the coverslips were washed three times with PBS. Platelets ( $3 \times 10^5$  platelets/µL) were allowed to spread on the coated surface after addition of 0.01 U/mL thrombin (Roche) and in Tyrode's-HEPES buffer with  $\text{Ca}^{2+}$ . After 5, 15, or 30 minutes, platelets were fixed with PHEM fixation buffer, including 4% PFA and permeabilized with IGEPAL CA-630. Images were acquired with a Zeiss incubation microscope (100x objective, Differential interference contrast (DIC) microscopy).

### 4.2.4 Platelet adhesion and thrombus formation under flow conditions

*Mouse:* Heparinized whole blood was diluted 2:1 in Tyrode's-HEPES buffer with  $\text{Ca}^{2+}$ .<sup>96</sup> Whole blood or mixed blood (washed platelets with adjusted platelet count  $5 \times 10^5$  platelets/µL, washed RBCs, 214 µg/mL fibrinogen, 1.7 mM  $\text{CaCl}_2$ ) was incubated with 0.2 µg/mL of an anti-GPIX antibody derivative conjugated to FITC at 37°C for 5 minutes. Coverslips were coated with 200 µg/mL HORM collagen (Takeda) overnight at 37°C and blocked with 1% BSA in PBS for 30 minutes. Whole blood was perfused over the coverslips in a custom made flow chamber (slit depth 50 µm) at a shear stress corresponding to a wall shear rate of  $1000 \text{ s}^{-1}$  (Maastricht chamber<sup>97</sup>). Videos and images were acquired using a Leica DMI6000 B inverted microscope (63x objective, Leica EL 6000 light source, Leica CTR6000 microscope control). Analysis was performed using the software ImageJ.

*Human:* *Ex vivo* thrombus formation assays were performed at a wall shear rate of  $1000 \text{ s}^{-1}$  on collagen-passivated surfaces (200 µg/mL HORM collagen [NYCOMED]) in a microfluidic parallel platelet flow chamber (on ibidi µ-Slide VI 0.1 with physical dimensions: 1 mm width, 100 µm height, and 17 mm length). To visualize thrombus formation, platelets in anticoagulated ACD-A whole blood were stained with a FITC-labeled anti-human CD61 antibody (Clone: RUU-PL7F12, used at a final ratio of 1:100) before perfusion. Fibrin formation was visualized by adding human fibrinogen conjugated with Alexa Fluor 647 (used at a final concentration of 7.5 µg/ml) to whole blood. Whole blood was recalcified immediately before perfusion. Time-lapse confocal imaging (intervals of 10 seconds per image) was performed with a Leica SP5 confocal

## Methods

laser scanning microscope equipped with an HCX PL APO  $\lambda$  blue 40.0x/1.25-oil objective. For image acquisition, FITC and Alexa Fluor 647 fluorophores were excited with argon-krypton (488 nm) and helium-neon (HeNe, 633 nm) laser lines, respectively, selected with an acousto-optic tunable filter (AOTF). Fluorescence emission was detected between 505-515 nm for FITC (detector HyD) and 640-655 nm for Alexa Fluor 647 (detector HyD). To evaluate the effects of TXA in some experiments, whole blood was preincubated with TXA (100  $\mu$ M) for 10 minutes before perfusion over collagen. The effects of recombinant tissue plasminogen activator (rtPA) (137 ng/mL) on fibrin degradation were assessed under a shear flow of 100  $s^{-1}$  added after 10 minutes of thrombus formation. Quantitative assessment of platelet adhesion and thrombus formation was performed to determine the percentage area covered by thrombus over time by computerized image analysis, using the surface generation algorithm in Bitplane Imaris (version 7.65; Oxford Instruments, Abingdon, United Kingdom). Experiments were performed according to the recommendations of the Biorheology Subcommittee of the International Society on Thrombosis and Haemostasis Scientific and Standardization Committee.<sup>98</sup>

### 4.2.5 Bleeding time

Mice were anesthetized with a combination of analgesics and narcotics (0.05 mg/kg fentanyl, 5 mg/kg midazolam, 0.5 mg/kg medetomidine), and a segment of 1-mm length of the tail tip was removed with a scalpel.

*Saline:* Tail tip was dipped into sodium chloride (0.9%) and bleeding was observed until stopped. Observation of rebleeding was performed for one additional minute.

*Filter-paper:* Tail bleeding was monitored by carefully collecting blood drops with a filter paper at 20-second intervals without touching the wound site. When no more blood was seen on the filter paper, bleeding was considered to ceased. Otherwise, the experiments were manually stopped after 20 minutes. Bleeding times longer than 20 minutes were not considered in the statistical analysis. TXA (10  $\mu$ g/g), or sodium chloride, as control, was injected intravenously 5 minutes before tail cutting.

## Methods

### 4.2.6 Clot retraction

PRP from citrated mouse blood was filled up until a volume of 250  $\mu\text{L}$  with Tyrode's-HEPES buffer without  $\text{Ca}^{2+}$  to achieve a platelet concentration of  $3 \times 10^5$  platelets/ $\mu\text{L}$ . To study clot retraction of unadjusted platelet count, 50  $\mu\text{L}$  of PRP was filled up until a volume of 250  $\mu\text{L}$  with Tyrode's-HEPES buffer and 1  $\mu\text{L}$  of erythrocytes. After addition of 0.2 U/ml thrombin and 20 mmol/L  $\text{CaCl}_2$ , clot retraction was monitored over a period of one hour. To study treatment with TXA and rtPA, concentrations of 1  $\mu\text{M}$ , 100  $\mu\text{M}$ , and 10,000  $\mu\text{M}$  TXA and 0.0138 nM rtPA were used and added together with thrombin and  $\text{CaCl}_2$ .

### 4.2.7 Migration

Blood from mice was drawn with non-heparinized capillaries into ACD (1:10). Whole blood was mixed with ACD (1:7) and Miakawa Tyrode's-HEPES buffer (1:2; pH 6.5) and centrifuged at 100 g for 10 minutes with slow deceleration (VWR MEGA STAR 1.6R). The PRP was transferred into a new tube and mixed with the double volume of Miakawa Tyrode's-HEPES buffer (pH 6.5). To pellet the platelets centrifugation was performed at 1,200 g for 5 minutes. Supernatant was discarded and the platelet pellet resuspended in Miakawa Tyrode's-HEPES (pH 6.5) to a platelet concentration of  $2 \times 10^5$  platelets/ $\mu\text{L}$ . Coverslips (ThermoFisher 24x24) were acid washed with 20%  $\text{HNO}_3$  for 1 hour at RT and rinsed with  $\text{H}_2\text{O}$  for 15 minutes under shaking. Cleaned coverslips were dried with a spin-coater (SCI-20) and silanized with hexamethyldisilazane (HMDS) by spin-coating at 80 rps for 30 seconds. To build a custom-made migration chamber, ibidi sticky slides (VI 0.4 part of 80608) were cut into single chambers and immediately after coating glued onto the coverslip. Channels were incubated for 10 minutes with 120  $\mu\text{L}$  Miakawa Tyrode's-HEPES buffer (pH 7.4) supplemented with 0.2% albumin from human serum and 37.5 mg/mL fluorescently labeled fibrinogen (Alexa Fluor 488; Sigma) and washed five times with 150  $\mu\text{L}$  Miakawa Tyrode's-HEPES buffer (pH 7.4). Migration buffer containing Miakawa Tyrode's-HEPES buffer (pH 7.4) was supplemented with anti-adhesive proteins (casein), platelet activators (ADP and U46619), and divalent cations (calcium chloride) at following concentrations: 0.003% casein, 200  $\mu\text{M}$  calcium chloride, 4  $\mu\text{M}$  ADP, and 2  $\mu\text{M}$  U46619. Washed platelets (10  $\mu\text{L}$  of  $2 \times 10^5$  platelets/ $\mu\text{L}$ ) were added to the migration buffer to reach a final concentration of  $8 \times 10^3$  platelets/ $\mu\text{L}$ . 150  $\mu\text{L}$  of the

## Methods

migration buffer, including platelets, was added to the migration chamber and visualized with a Leica Thunder Imaging System.

### 4.2.8 Thromboelastometry

Rotational thromboelastometry (ROTEM) was used together with a modified version of the commercial extrinsic tissue factor-activated thromboelastometry assay (EXTEM) to detect changes in fibrinolytic activity.<sup>99</sup> Specifically, we induced lysis *ex vivo* by adding rtPA at a final concentration of 137 ng/mL, as reported.<sup>99</sup> In parallel, we attempted to abrogate lysis by the simultaneous addition of TXA at a final concentration of 100  $\mu$ M, which was reported to inhibit fibrinolysis.<sup>100</sup> The maximum run time was set to 150 minutes. The following standard parameters were analyzed: Lysis Onset Time (LOT), Lysis Time (LT), Clotting Time (CT), and Clot Formation Time (CFT).

## 4.3 Flow cytometric analysis of platelet function

### 4.3.1 Glycoprotein expression

Whole blood was collected from anesthetized mice in heparin and diluted in Tyrode's-HEPES buffer. To determine GP expression, blood was incubated for 15 minutes with the indicated fluorophore-conjugated antibodies (FITC-labeling of antibodies: D1424N, E1841K; APC-labeling of antibodies: R702C). Measurements were performed using a FACSCelesta.

### 4.3.2 Activation

Whole blood was collected from anesthetized mice in heparin and diluted in Tyrode's-HEPES buffer. For activation studies, blood samples were washed twice with Tyrode's-HEPES buffer. Washed blood was resuspended in calcified Tyrode's-HEPES buffer (2 mM  $\text{Ca}^{2+}$ ). Platelets were incubated with agonists and stained with fluorophore-conjugated antibodies against active  $\alpha$ IIb $\beta$ 3 (PE) and P-selectin (FITC) for 7 minutes at 37°C and 7 minutes at RT. Measurements were performed using a FACSCelesta.

## Methods

### 4.3.3 F-actin content and assembly

Whole blood was collected from anesthetized mice in heparin and diluted in Tyrode's-HEPES buffer. For analysis of F-actin content, washed platelets were incubated with an anti-GPIX antibody derivative labeled with APC (20 µg/mL, homemade clone 56F8) and either left unstimulated (resting) or were treated with indicated agonists for 3 minutes at 37°C. Cells were fixed in 10% PFA, centrifuged, and resuspended in Tyrode's-HEPES buffer in the presence of Ca<sup>2+</sup> and 0.1% Triton X-100. The permeabilized cells were stained with 10 µM phalloidin-FITC for 30 minutes. Measurements were performed using a FACSCalibur (mouse line D1424N) or FACSCelesta (mouse line E1841K).

## 4.4 Biochemical analyses

### 4.4.1 Immunoblotting with SDS-PAGE

Washed platelets were lysed with 2x protein lysis buffer at a platelet concentration of 5 x 10<sup>5</sup> platelets/µL. Samples were boiled for 5 minutes at 95°C and separated by sodium dodecyl sulfate-polyacrylamide gel electrophoresis (SDS-PAGE). Gels were poured one day in advance with 5% stacking gel and a 10% or 7.5% separating gel. Protein samples and a molecular-weight size marker (Page Ruler PLUS Prestained) were loaded onto the gel in the electrophoresis chamber filled with SDS running buffer.<sup>101</sup> Electrophoresis occurred at constant 25 mA per gel until loading dye nearly traversed the gel. Gels were blotted onto polyvinylidene difluoride (PVDF) membranes in 1x Tankblot buffer. Membranes were blocked with 1x Blue Block and incubated with the appropriate antibodies against Glyceraldehyd-3-phosphat-dehydrogenase (GAPDH) (1:1000), myosin IIA (1:200), ROCK1 (1:500), RhoA (1:500), and β-actin (1:1000) diluted in 1x Blue Block. After washing thrice with TBS-T, membranes were incubated with horseradish peroxidase-conjugated secondary antibodies and enhanced chemiluminescent solution was used for visualization on an Amersham Imager 680. If necessary, membranes were incubated with stripping buffer for 30 minutes at RT to provide clean and efficient removal of primary and secondary antibodies, to visualize other proteins at similar molecular weight.

## Methods

### 4.4.2 Immunoblotting with ProteinSimple Jess

Protein levels of MLC2, myosin IIA, myosin phosphatase 1 (MYPT1), and phosphorylation levels of MLC2 were analyzed using an automated capillary-based immunoassay platform; Jess (ProteinSimple).<sup>102</sup>  $5 \times 10^5$  platelets/ $\mu$ L were lysed by adding the same volume of ice-cold 2x lysis buffer. Lysates were diluted to the required concentration with 0.1x sample buffer 2 (diluted from 10x sample buffer 2). Lysates were prepared by adding 5x master mix containing 200 mM dithiothreitol, 5x sample buffer, and fluorescent standards (Standard Pack 1) and boiled at 95°C for 5 minutes according to the manufacturers' instructions from Protein Simple. The optimized antibody dilutions and respective lysate concentrations for each antibody (all from CST) are listed below: anti-MLC2 antibody 1:10, 0.1 mg/mL; anti-myosin IIA antibody 1:10, 0.025 mg/mL; anti-MLC2-p-S19 antibody 1:10, 0.4 mg/mL; anti-MLC2-p-T18/S19 1:10, 0.4 mg/mL; anti-MYPT1 antibody 1:10, 0.1 mg/mL. For most antibodies, either a secondary anti-rabbit horseradish peroxidase (HRP) conjugated antibody (DM-001) or a secondary anti-mouse HRP conjugated antibody was used, and the chemiluminescence signal was recorded using the high dynamic range (HDR) profile. For detection of myosin IIA and MYPT1 signals in the R702C and E1841K knock-in samples, a secondary anti-rabbit NIR antibody was used with the corresponding fluorescence profile. The NIR signal is shown in gray scale. All antibodies were diluted in antibody diluent 2. Samples, antibody diluent 2, primary and secondary antibodies, luminol S and peroxide mixture, and wash buffer were placed in prefilled 12-230 kDa microplates (prefilled with Separation Matrix 2, Stacking Matrix 2, Split Running Buffer 2, and Matrix Removal Buffer). The microplate was centrifuged at 2500 rpm for 5 minutes at RT. To start the assays, the capillary cartridge was placed in the cartridge holder and the microplate was placed on the plate holder. Compass Software for Simple Western was used to operate Jess and analyze the results (version 4.1.0, ProteinSimple). The loading time for the separation matrix was set to 200 seconds, the loading time for the stacking matrix was set to 15 seconds, the sample loading time was set to 9 seconds, the separation time was set to 30 minutes, the separation voltage was set to 375 volts, the antibody dilution time was set to 5 minutes, the incubation time for the primary antibody was set to 90 minutes, and the incubation time for the secondary antibody was set to 30 minutes. All of the reagents used for this method are available in the Kit for Jess experiments from Protein Simple (12- 230 kDa Jess

## Methods

Separation Module (#SM-W004) and Anti-Rabbit Detection Module for Jess (#DM-001)).

### 4.4.3 Actin sedimentation

190  $\mu\text{L}$  of washed platelets in Tyrode's-HEPES buffer ( $3 \times 10^5$  platelets/ $\mu\text{L}$ ) were lysed with 20  $\mu\text{L}$  lysis solution containing 10x PHEM buffer, 1% Triton X-100, 60  $\mu\text{M}$  taxol, 20  $\mu\text{M}$  phalloidin, and protease inhibitor cocktail for 5 minutes at RT. One set of 105  $\mu\text{L}$  served as total protein cell lysate (sample: total protein), whereby the other set of 105  $\mu\text{L}$  was separated into polymerized and soluble fraction by centrifugation. Ultracentrifugation (Optima™ L-80 XP Ultracentrifuge) was performed at 42,000 rpm for 30 minutes at 37°C in a 42.2 Ti rotor (Beckman coulter). Supernatant was transferred to a new tube (sample: supernatant) and the pellet was resuspended in 200  $\mu\text{L}$  10x PHEM buffer. Centrifugation was performed to wash the pellet at 42,000 rpm for 30 minutes at 37°C. The supernatant was transferred to a new tube (sample: wash) and the pellet (sample: pellet) was resuspended in 105  $\mu\text{L}$  1x SDS sample buffer. Total protein, supernatant, and supernatant of washing step were supplemented with 1x SDS sample buffer. Immunoblotting was performed as described in section 4.4 *Biochemical analyses*.

## 4.5 Imaging

### 4.5.1 Immunostaining of platelets

Washed platelets were added onto 0.01% PLL-coated coverslips for 20 minutes, fixed with 4% PFA in PHEM and permeabilized with IGEPAL CA-630. Fixed and permeabilized spread platelets (30 minutes; described in section 4.2.4 *platelet spreading*) were stained for myosin IIA with anti-myosin IIA (1:200 in PBS) antibody from rabbit and secondary donkey anti-rabbit IgG-Cy3 (1:350 in PBS) for wildtype platelets of mouse line R702C, and wildtype and heterozygous platelets of mouse lines D1424N and E1841K. F-actin was stained with phalloidin-Atto647N (1:500 in PBS) and  $\alpha$ -tubulin either with Alexa Fluor 488-conjugated anti- $\alpha$ -tubulin antibody (1:500 in PBS) or Alexa Fluor 546-conjugated anti- $\alpha$ -tubulin antibody (1:500 in PBS; heterozygous platelets of mouse line R702C). Visualization was performed with a Leica TCS SP8 confocal microscope (100x oil objective; NA 1.4). Confocal microscopy was performed

## Methods

with HC PL APO CS2 objectives. Depending on the staining, a series of monochromatic lasers (488 nm; 561 nm; HeNe 633 nm) tuned to specific wavelengths were used. The detection filters (PMT trans or ultrasensitive hybrid detectors) were adjusted to match the spectral characteristics of the fluorochromes.

### 4.5.2 Transmission electron microscopy of platelet ultrastructure

Washed platelets at a concentration of  $3 \times 10^5$  platelets/ $\mu\text{L}$  were fixed with 2.5% glutaraldehyde in cacodylate buffer (pH 7.2). Epon 812 was used to embed the platelets. Ultra-thin sections of platelets were stained with 2% uranyl acetate and lead citrate. The sections were analyzed using a Zeiss EM900 electron microscope.

### 4.5.3 Platinum replica electron microscopy of platelet cytoskeleton

The cytoskeleton of resting platelets and spread platelets after 15 minutes on fibrinogen were visualized by platinum replica electron microscopy (PREM). Washed platelets (5  $\mu\text{L}$  of  $2 \times 10^5$  platelets/ $\mu\text{L}$ ) for resting conditions were spun (5 minutes at 280 g) onto PLL-coated coverslips in 1x PHEM buffer containing 0.75% Triton X-100, 1  $\mu\text{M}$  phalloidin, 1  $\mu\text{M}$  taxol, and 0.1% glutaraldehyde. To prepare spread platelets, washed platelets (2.5  $\mu\text{L}$  of  $2 \times 10^5$  platelets/ $\mu\text{L}$ ) were spun for 5 minutes at 280 g onto fibrinogen-coated slides (100  $\mu\text{g}/\text{mL}$ ) in Tyrode's-HEPES buffer with calcium. Platelets were stimulated with 0.01 U/mL thrombin for 15 minutes. Resting and spread platelets on coverslips were washed with 1x PHEM buffer supplemented with 0.1  $\mu\text{M}$  phalloidin and taxol and fixed for 10 minutes in 1x PHEM buffer with 1% glutaraldehyde. Samples were sequentially incubated with 0.1% tannic acid and 0.2% uranyl acetate and dehydrated by transferring samples through acetone. Using a Leica EM CPD300 critical point drying was performed. Samples were coated with 1.2 nm of platinum under rotation at 45°C and 3 nm carbon at 90°C without rotation under high vacuum (Leica EM ACE600). Replicas were floated and picked up on formvar-carbon-coated grids. Samples were examined on a JEOL JEM-2100.



## Methods

### 4.5.4 Cryo sectioning and staining

Isolated femora were fixed for at least 30 minutes at RT with PBS fixation buffer (4% PFA in PBS). Dehydration was performed with a graded sucrose series of 10%, 20%, and 30% sucrose in PBS for 24 hours each. The samples were subsequently embedded in super cryo embedding medium and frozen at -20°C. Cryosections (7 µm) were generated using the Kawamoto method<sup>103</sup> and probed with FITC-conjugated anti-GPIX antibody (homemade, clone 56F8; 1:500) to label platelets and MKs, and Alexa Fluor 647-conjugated anti-CD105 antibody (MJ7/18; 1:400) to stain the endothelium. Nuclei were stained using Fluoroshield with 4',6-Diamidino-2-phenylindol (DAPI). Samples were visualized with a Leica TCS SP8 confocal microscope.

### 4.5.5 Image processing and analysis

Adjustment of brightness and contrast of images taken with confocal microscopes was performed with ImageJ. Adjustments were made linearly to the whole image.

## 4.6 Biophysical analyses

All biophysical analyses were performed together with collaboration partners. Bleeding of mice, platelet preparation, and measurement assistance was performed by Juliane Baumann. The measurements and analysis were performed by the following collaboration partners: Laura Sachs and Prof. Dr. Oliver Otto (4.6.1), Laura Sachs (4.6.3), Dr. Raghavendra Palankar (4.6.2), Dr. Ingmar Schön and Martin Kenny (4.6.4), and Prof. Dr. Tilman E. Schäffer, Hendrik von Eysmond, and Johanna Rodriguez (4.6.5). Further information about the methods performed in Greifswald (4.6.1, 4.6.2, and 4.6.3) is provided in the doctoral thesis "*Application of biophysical methods to assess the role of platelet cytoskeletal proteins in platelet biomechanics*" of Laura Sachs (submission 2022/03/25).

### 4.6.1 Real-time fluorescence deformability cytometry

*Mouse:* 25 µL whole blood in citrate was resuspended in 425 µL CellCarrier B. The measurement was stopped after 10,000 individual platelets had been counted (hard

## Methods

gate area 0 - 40  $\mu\text{m}^2$ ). Kernel density estimate (KDE) plots of event density were generated using shape-out analysis software (<https://github.com/ZELLMECHANIK-DRESDEN/ShapeOut2/releases/tag/2.3.0> version 2.3, Zellmechanik Dresden, Germany), and statistical analysis was performed using the Holm-Sidak method, to determine median values for deformation and size of platelets and RBCs. For the analysis of platelets, the area-area ratio was limited from 0 to 1.1 and the cell size was limited from 0 to 10  $\mu\text{m}^2$ , respectively, for RBCs the area-area ratio was limited from 0 to 1.1 and cell size from 15 to 40  $\mu\text{m}^2$ , respectively.

*Human:* Platelets in PRP were labeled with a monoclonal mouse anti-human antibody CD61-PE. Samples were incubated at RT for 10 minutes in the dark. Deformation measurements were performed in a microfluidic chip FLic15 with a constriction of 15  $\mu\text{m}$  x 15  $\mu\text{m}$  cross-section and a length of 300  $\mu\text{m}$ . Real-time fluorescence deformability cytometry (RT-FDC) measurements were performed in CellCarrier B buffer, consisting of 0.6% (w/v) methylcellulose in PBS (without  $\text{Ca}^{2+}$ ,  $\text{Mg}^{2+}$ ). Here, 50  $\mu\text{L}$  of immunofluorescently labeled human PRP was added to 450  $\mu\text{L}$  of CellCarrier B. The human PRP suspension was then infused into the microfluidic chip at a flow rate of 0.006  $\mu\text{L/s}$ , and measurement was stopped after reaching 5,000 individual platelets (hard-gate 150-33000 arbitrary units, A.U. for CD61-PE of fluorescence intensity), or after 10 minutes. RT-FDC data was acquired using ShapeIn software (version 2.0, Zellmechanik Dresden, Germany). KDE plots of event density were generated with the Shape-Out analysis software, and statistical analysis was performed to determine the median values for platelet deformation and its size. For the analysis, the area-area ratio was limited to 0 - 1.1 and the cell size to 0 - 25  $\mu\text{m}^2$ . The RT-FDC setup (AcCellerator) is built around an inverted microscope (Axio Observer A1) with a Zeiss A-Plan 100x NA 0.8 objective.<sup>104-106</sup>

### 4.6.2 Single platelet force spectroscopy

Silicon CSC12, 0.6 N/m tipless cantilevers and 35-mm glass bottom trays were exposed to a UV cleaner for 30 minutes. Prior to coating, the spring constants of the cantilevers were independently measured using a thermal tuning technique (JPK). The cantilevers were incubated with 50  $\mu\text{g/mL}$  collagen G for 3 hours at 37°C and rinsed three times with Tyrode's-HEPES buffer. An aliquot of 15 x 10<sup>3</sup> platelets/ $\mu\text{L}$  in Tyrode's-

## Methods

HEPES buffer containing 1 mM CaCl<sub>2</sub> and 0.5 mM MgCl<sub>2</sub> was dropped onto the passaged glass immediately before each measurement (10 minutes, RT). Unbound platelets were removed with Tyrode's-HEPES buffer. To immobilize a single platelet on the cantilever, the collagen-passivated cantilever was brought into contact with a non-activated platelet on a BSA-passivated glass slide (set point 200 pN) until a single platelet adhered firmly to the ventral surface at the tip of the cantilever. The cantilever with the attached platelet was then moved to a surface passivated with HORM collagen (NYCOMED) or to firmly attached platelets on HORM collagen (NYCOMED) to perform measurements of platelet-substrate or platelet-platelet interaction with single platelet force spectroscopy (SPFS), respectively. All measurements were performed in Tyrode's-HEPES with Ca<sup>2+</sup>, glucose, and BSA. Using a JPK NanoWizard 3, force-distance (F-D) curves were recorded with a Z length of 7 μm and a set point of 200 pN to control the maximum force of the cantilever against the surface. A velocity of 15 μm/s was used for all measurements to avoid fusion of two platelets during contact and to completely tear two platelets away from each other. For each passivated substrate, the last 500 force-displacement curves of 7 to 10 individual platelets were recorded.

### 4.6.3 Colloidal probe spectroscopy

To determine the elastic modulus of platelet aggregates, penetration experiments were performed by colloidal force spectroscopy using an atomic force microscope. The atomic force microscope is combined with an optical system consisting of an inverted optical microscope (IX8, 20x objective). Gold-coated cantilevers (tip: spherical 1.5 - 3 μm) coated with 8.45 mM poly(ethylene glycol)methyl ether thiol solution for 2 h at RT were used. Measurements were performed in suspension buffer. Prior to each experiment, the sensitivity and spring constant of each cantilever were determined individually in suspension buffer. To calibrate the sensitivity, the deflection of the cantilever upon contact with a freshly cleaved mica surface was analyzed (ensemble average 23.3 ± 3.1 nm/V), and the spring constant was measured using the thermal noise technique (ensemble average 98 ± 30 mN/m). One mL of ACD-A human whole blood was treated with 7.5 μL of 1 M CaCl<sub>2</sub> × 2H<sub>2</sub>O and 1.88 μL of 2 M MgCl<sub>2</sub> × 6H<sub>2</sub>O solution. Heparinized whole blood was used for mouse experiments. Cover slips were coated with 80 μg/mL HORM collagen (NYCOMED) overnight at 37°C and blocked

## Methods

with 1% BSA in PBS for 10 minutes and then placed in a flow chamber with a slit depth of 55  $\mu\text{m}$  (Straight Channel Chip). Recalcified whole blood was perfused for 5 minutes at a shear rate of 1000  $\text{s}^{-1}$ . The coverslips were washed three times with suspension solution. The cantilever was brought into contact with platelet aggregates at a rate of 2.7  $\mu\text{m}/\text{s}^{-1}$ , with a force set point of 2 nN. Measurements were performed at RT in suspension buffer. The elastic modulus  $E$  of platelets was calculated from the atomic force microscopy (AFM) penetration force curves by applying the Hertz model, which describes how the force increases as the AFM probe penetrates the cell. Briefly, the cantilever deflection force  $F$  was fitted to the equation:

$$F(z) = \frac{4}{3} E \cdot R_{\text{sphere}}^{\frac{1}{2}} \cdot z^{\frac{3}{2}} / (1 - \nu^2)$$

Here  $R_{\text{sphere}}$  is the radius of the AFM sphere probing the cells,  $z$  is the cell indentation, and Poisson's ratio  $\nu$  was set to 0.5, assuming conservation of cell volume. Details can be found elsewhere.<sup>107,108</sup> Five platelet aggregates were recorded per coverslip with at least 25 force curves per aggregate, and each force curve was evaluated individually. Therefore, for each experimental condition, the platelet elastic modulus is reported as the mean of more than 100 individual force curves.

For TXA measurements, 1 mL of whole blood was incubated with 100  $\mu\text{M}$  TXA for 10 minutes. For rtPA measurements, 500  $\mu\text{l}$  of 137 ng/ml rtPA was added to the coverslip immediately after measurement of the untreated or TXA sample and incubated for 5 minutes.

### 4.6.4 Micropost assay

Micropost arrays were fabricated from hPDMS by replica molding from negative molds, containing cylindrical posts with 1.05  $\mu\text{m}$  diameter and 2.6  $\mu\text{m}$  height arranged on a hexagonal grid (2.0  $\mu\text{m}$  center-to-center spacing). The Young's modulus of hPDMS was 4.7 MPa. Flat stamps for microcontact printing were made from Sylgard 184 (Dow Corning Inc). Fluorescently labeled (Alexa Fluor 488 NHS ester) fibrinogen (0.1 mg/mL in PBS) was physisorbed from solution onto stamps for one hour, immediately washed with distilled water and blown dry under nitrogen. After pre-activation by UV/ozone treatment for 7 minutes, coated stamps were brought into conformal contact with

## Methods

micropost arrays, pressed down using a forceps, and removed. The transfer efficiency of fibrinogen was confirmed by fluorescence microscopy of stamps and microposts (typically >90%). Micropost arrays were passivated using a 1:2 mix (0.5 mg/mL in PBS) of fluorescently labeled (DyLight 405 NHS ester) endotoxin-free BSA to non-labeled BSA for 30 minutes. This was followed by passivation with Pluronic F127 (0.5% w/v in PBS) for 30 minutes and washing three times with PBS. Washed platelets were resuspended in Tyrode's-HEPES buffer and seeded in the presence of 0.01 U/mL thrombin onto the coverslips at a density of  $\sim 2$  million  $\text{cm}^{-2}$  for 60 minutes at 37°C. Platelets were fixed in 3% PFA in PBS for 15 minutes and washed three times in PBS. Samples were permeabilized with IGEPAL CA-630, blocked with BSA and stained for F-actin (phalloidin-Alexa Fluor 647; 1:100 in 3% BSA in PBS) for 30 minutes. Slides were washed with PBS and mounted in a chamber (Chamlide) containing PBS. Confocal images were obtained on a confocal microscope Leica TCS SP8 from top and bottom slices of the microposts. Image analysis of traction forces was performed by custom MATLAB code. Posts were detected by template matching and their positions were refined by radial symmetry matching. Post deflections were derived from the positions of the same post in the upper and lower layers after systematic displacements between layers were removed. Traction forces were calculated from the post deflections using Hooke's law and a spring constant of 34.51 nN/ $\mu\text{m}$ .<sup>109</sup> Spreading area and actin fiber alignment was analyzed with spread platelets on fibrinogen (30 minutes; described in section 4.2.4 *platelet spreading*) stained for F-actin (Phalloidin-Alexa Fluor 647, 1:100 in 3% BSA in PBS) and vinculin (mouse-anti-vinculin, 1:100 in 3% BSA in PBS; secondary antibody donkey anti-mouse IgG Alexa Fluor 546, 1:100 in 3% BSA in PBS).

### 4.6.5 Scanning ion conductance microscopy

For scanning ion conductance microscopy (SICM) 35 mm round polystyrene cell culture dishes were coated with fibrinogen (0.1 mg/mL) and incubated at 37°C for 1 hour. Washed mouse platelets were resuspended in Tyrode's-HEPES buffer supplemented with 1 mM  $\text{Ca}^{2+}$  and spread in the presence of thrombin (0.01 U/mL) for 15 minutes at RT. Culture dishes were then washed three times with Tyrode's-HEPES buffer to remove non-adherent platelets. The dishes were then placed in custom-made SICM arrays<sup>110</sup> and imaged within an hour. Platelet morphology and elastic modulus

## Methods

were visualized using borosilicate pipettes with an inner radius of ~90 nm and a pressure of 10 kPa. Imaging was performed at a pixel rate of 20 Hz, with 32 x 32 or 64 x 64 pixels at scan sizes between 6 x 6 and 12 x 12  $\mu\text{m}^2$ . Data from two mice were pooled. Elastic modulus E analysis was calculated as previously described.<sup>111</sup>

### 4.7 Data analysis

Results are from at least two independent experiments per group unless otherwise stated. Correction for multiple comparisons was analyzed by the Holm-Sidak method, and differences between the control and mutant samples were statistically analyzed by the Mann-Whitney U test. P values <0.05 were considered statistically significant: \*0.05 > p  $\geq$  0.01; \*\*0.01 > p  $\geq$  0.001; \*\*\*p < 0.001. Results with a P value  $\geq$  0.05 were considered not significant.

## Results

### 5 Results

#### 5.1 Characterization of *Myh9* mutant mice

##### 5.1.1 Unaltered protein expression of the RhoA-ROCK-myosin IIA pathway

In 2012, three mouse lines were generated each with a mutation in the *Myh9* gene, leading to amino acid exchanges at different positions representing the most common mutations found in *MYH9*-RD patients.<sup>16</sup> Via homologous recombination the amino acid arginine at position 702 was exchanged to cysteine (R702C, further referred to as *Myh9<sup>R702C/+</sup>*), aspartic acid at position 1424 was exchanged to asparagine (D1424N, referred to as *Myh9<sup>D1424N/+</sup>*) and at amino acid position 1841 glutamic acid was replaced by lysine (E1841K, further referred to as *Myh9<sup>E1841K/+</sup>*). Littermates of each mouse line were used as controls and are further referred to as *Myh9<sup>+/+</sup>* (+ indicates the wildtype allele). To investigate the expression of the myosin IIA protein in the knock-in mutant mouse lines compared to their corresponding littermate controls, myosin IIA HC immunoblot analysis was performed. Platelet lysates of *Myh9<sup>+/+</sup>* as well as *Myh9<sup>R702C/+</sup>*, *Myh9<sup>D1424N/+</sup>*, and *Myh9<sup>E1841K/+</sup>* mice showed normal myosin IIA expression as reflected by a protein band at 200 kDa (Figure 17A – C; and reference<sup>16</sup>). Especially for *Myh9<sup>R702C/+</sup>*, human cDNA, fused to GFP, encoding for the exchange of the amino acid at position 702 was inserted into the mouse *Myh9* gene. For this reason, immunoblot of platelet lysates from *Myh9<sup>R702C/+</sup>* mice performed with a low percentage gel revealed two bands, the GFP-tagged mutant human myosin IIA protein (Figure 17A; \*) and the endogenous mouse myosin IIA protein (Figure 17A; #). The expression of upstream proteins of the RhoA-ROCK-myosin IIA pathway (RhoA, ROCK1; Figure 17A), as well as of MYPT1, required for dephosphorylation of myosin light chain (Figure 17B), was unaltered. These results show that point mutations at three different positions in the *Myh9* gene do not interfere with the expression of myosin IIA and upstream proteins in platelets.

## Results

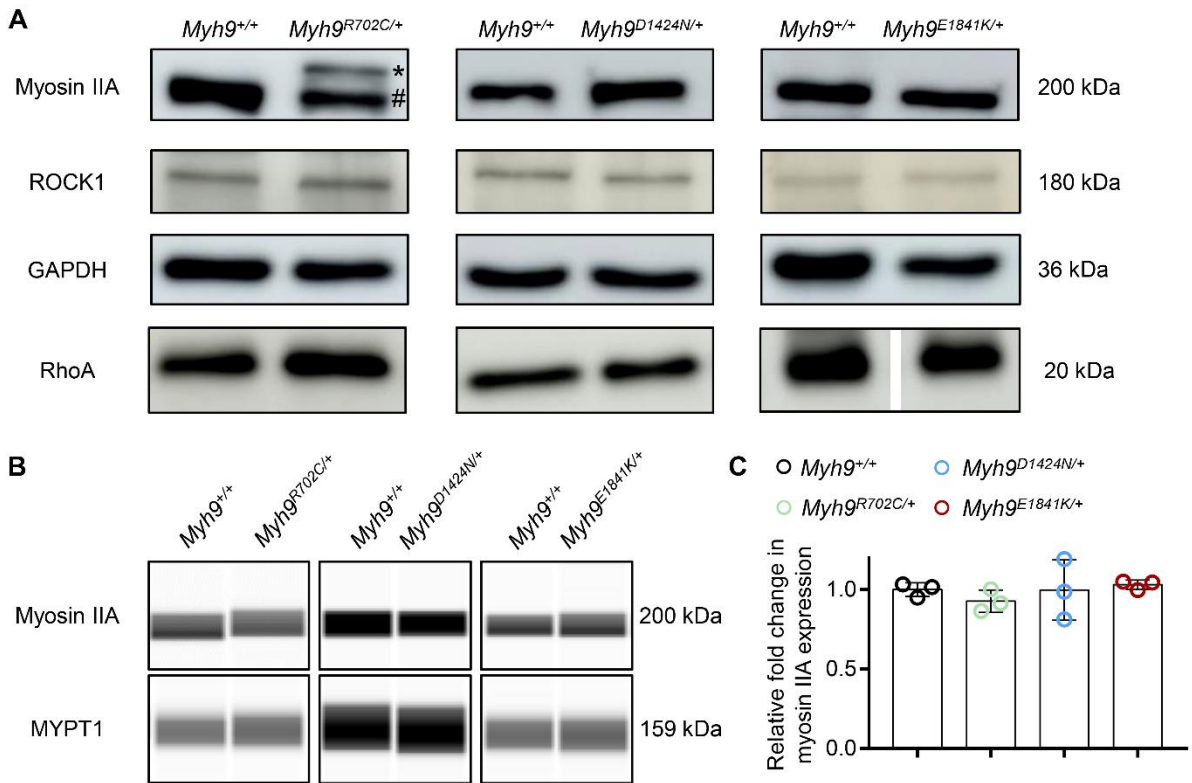


**Figure 17. RhoA-ROCK-myosin IIA pathway proteins are normally expressed in platelets of *Myh9* mutant mice.** (A) The expression of RhoA, ROCK, and myosin IIA in *Myh9* mutant and control platelet lysates was assessed by immunoblot analysis. Myosin IIA immunoblotting of *Myh9*<sup>R702C/+</sup> and control lysates was performed on a 7.5% SDS-PAGE, all other immunoblots with a 10% SDS-PAGE. GFP-tagged mutant human myosin IIA (\*) and endogenous mouse myosin IIA (#) in platelet lysates of *Myh9*<sup>R702C/+</sup> were detected. Loading control is the housekeeping protein GAPDH (n=3). (B) A capillary-based immunoassay approach was used to confirm the expression of myosin IIA and MYPT1. Fold change of myosin IIA expression of *Myh9* mutant platelets relative to corresponding wildtype myosin IIA expression are quantified in (C). Control shown corresponds to *Myh9*<sup>+/+</sup> of mouse line D1424N (n=3).

### 5.1.2 *Myh9* mutant mice display macrothrombocytopenia

*Myh9* mutant mice exhibited a significantly reduced platelet count (Figure 18A) and a significantly increased platelet size (Figure 18B) in the peripheral blood compared to control mice, as confirmed by a hematology analyzer. Transmission electron micrographs (TEM) of platelet thin sections confirmed the increased size of *Myh9* mutant platelets and a heterogeneous population of platelet size in *Myh9* mutant samples. TEM analysis of *Myh9* mutant platelets revealed an overall normal ultrastructure comparable to controls (Figure 18C).



## Results

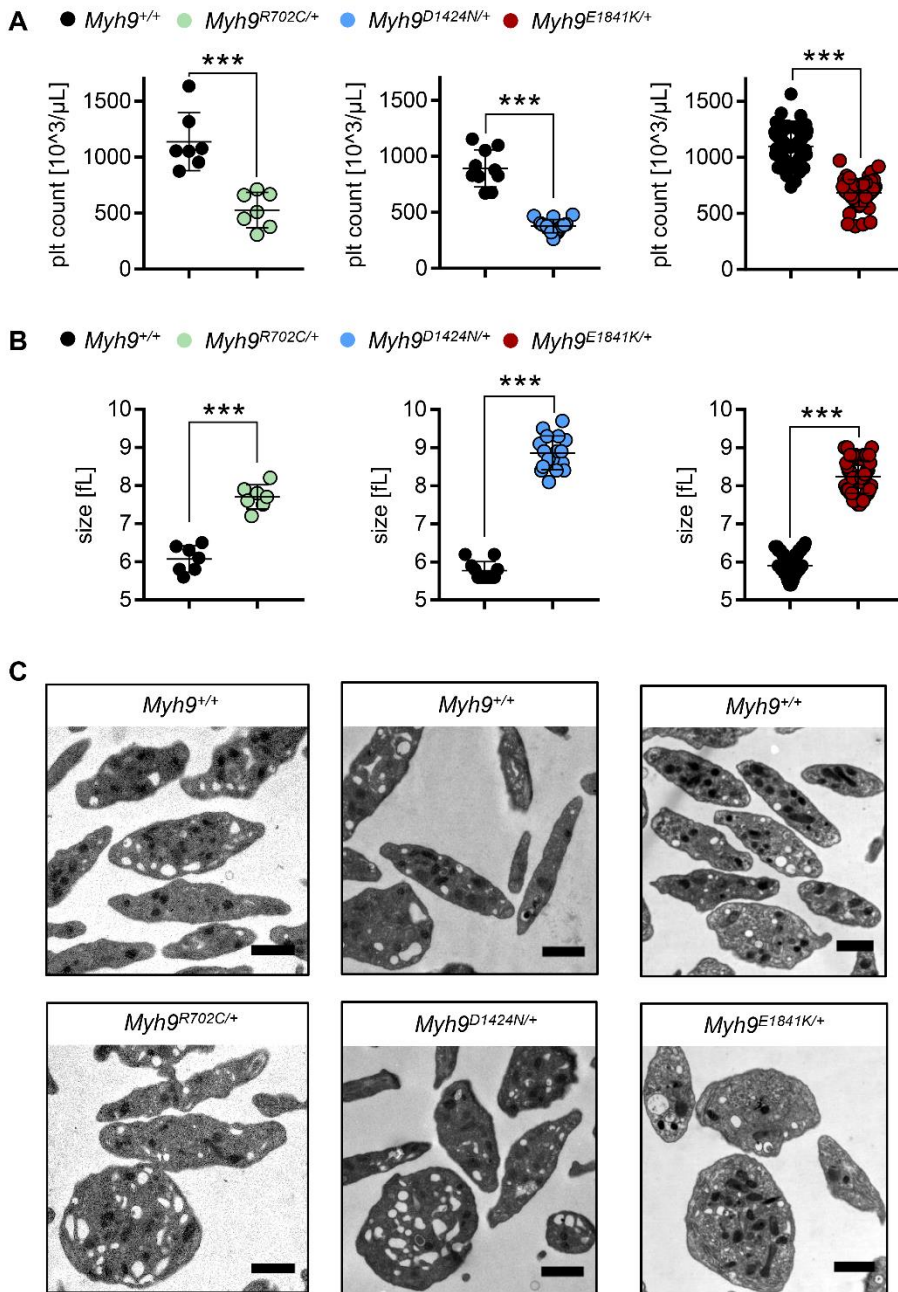


**Figure 18. *Myh9* mutant mice display macrothrombocytopenia.** (A) Platelet count and (B) size were determined using a hematology analyzer Scil Vet abc Plus +. Each symbol represents one individual mouse (values are mean  $\pm$  S.D.; statistics: Mann-Whitney U-test \*\*\* $p < 0.001$ ). (C) Representative transmission electron micrographs of *Myh9*<sup>+/+</sup> and corresponding *Myh9* mutant platelets (scale bars 1  $\mu$ m;  $n=3$ ).

These data show that the macrothrombocytopenia of *MYH9*-RD patients is recapitulated in *Myh9* mutant mice.<sup>68</sup> Other blood cell parameters were not affected by the heterozygous point mutations in the *Myh9* gene. Although myosin IIA is expressed in red blood cells,<sup>112</sup> RBC count, hemoglobin level and hematocrit of mutant mice were comparable to control mice (Table 1).

## Results

**Table 1. Blood cell parameters of *Myh9* mutant mice are comparable to controls.** Blood cell parameters of *Myh9* mutant and control blood were measured with a hematology analyzer Scil Vet abc Plus + (mean  $\pm$  S.D.; n=7). Abbreviations: WBC white blood cell; LYM lymphocyte; MON monocyte; GRA granulocyte; EOS eosinophils RBC red blood cell; HGB hemoglobin; HCT hematocrit. Statistics: Mann-Whitney U-test, all values are statistically not significant ( $p \geq 0.05$ ).

	<i>Myh9</i> <sup>+/+</sup>	<i>Myh9</i> <sup>R702C/+</sup>	<i>Myh9</i> <sup>+/+</sup>	<i>Myh9</i> <sup>D1424N/+</sup>	<i>Myh9</i> <sup>+/+</sup>	<i>Myh9</i> <sup>E1841K/+</sup>
WBC [10 <sup>3</sup> / $\mu$ L]	5.4 $\pm$ 1.6	6.3 $\pm$ 1.2	7.2 $\pm$ 1.2	6.6 $\pm$ 0.7	9.2 $\pm$ 2.1	10.5 $\pm$ 1.3
LYM [10 <sup>3</sup> / $\mu$ L]	3.5 $\pm$ 1.2	4.5 $\pm$ 0.9	5.9 $\pm$ 1.1	5.3 $\pm$ 0.5	7.4 $\pm$ 1.7	8.5 $\pm$ 1.0
MON [10 <sup>3</sup> / $\mu$ L]	0.2 $\pm$ 0.1	0.2 $\pm$ 0.1	0.2 $\pm$ 0.1	0.2 $\pm$ 0.1	0.3 $\pm$ 0.1	0.3 $\pm$ 0.1
GRA [10 <sup>3</sup> / $\mu$ L]	1.7 $\pm$ 0.9	1.6 $\pm$ 0.3	1.1 $\pm$ 0.3	1.1 $\pm$ 0.3	1.5 $\pm$ 0.4	1.7 $\pm$ 0.3
EOS [10 <sup>3</sup> / $\mu$ L]	0.04 $\pm$ 0.01	0.05 $\pm$ 0.01	0.04 $\pm$ 0.01	0.04 $\pm$ 0.01	0.06 $\pm$ 0.01	0.06 $\pm$ 0.01
RBC [10 <sup>6</sup> / $\mu$ L]	8.7 $\pm$ 0.6	9.2 $\pm$ 0.6	8.2 $\pm$ 0.3	8.0 $\pm$ 0.3	8.6 $\pm$ 0.3	8.9 $\pm$ 0.3
HGB [g/dL]	16.1 $\pm$ 1.0	16.7 $\pm$ 0.6	15.4 $\pm$ 0.6	15.1 $\pm$ 0.3	14.2 $\pm$ 0.3	14.4 $\pm$ 0.4
HCT [%]	47.7 $\pm$ 1.9	50.0 $\pm$ 2.2	46.7 $\pm$ 1.3	45.8 $\pm$ 2.6	42.4 $\pm$ 1.1	43.6 $\pm$ 1.6

## Results

To understand the decreased platelet count in the circulation of mutant mice and patients, we investigated the MKs in the BM, which are responsible for platelet production. The count of MKs in the BM of *Myh9*<sup>D1424N/+</sup> mice was increased, suggesting an attempt to compensate for the low platelet count in blood circulation (reference <sup>16</sup> and Figure 19A). Morphology and distance to vessels of mutant BM MKs were overall comparable to control MKs (Figure 19B).

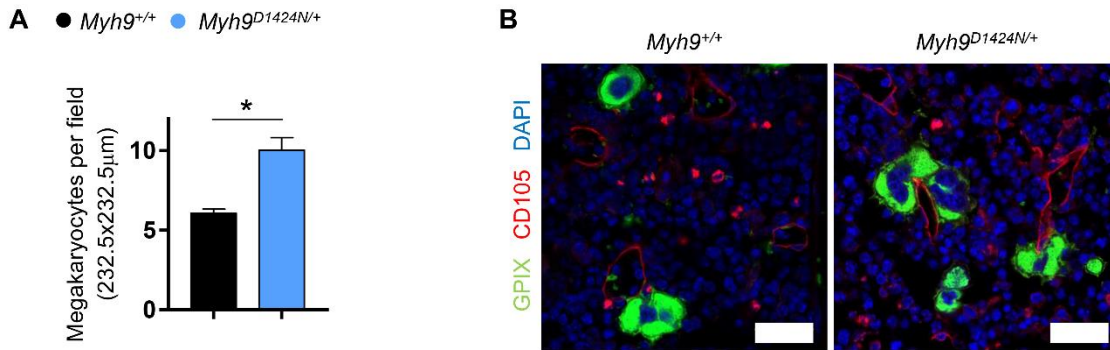


**Figure 19. MK count is increased in BM of *Myh9* mutant mice.** (A) Quantification of MK number in BM of *Myh9*<sup>D1424N/+</sup> mice and corresponding controls. Statistics: unpaired t-test (\*0.05 > p ≥ 0.01). (B) Representative images obtained by confocal microscopy from femoral BM cryosections of *Myh9*<sup>D1424N/+</sup> mice and corresponding controls. Sections were stained for MKs (GPIX, green), vessels (CD105, red) and nuclei (DAPI, blue). Scale bars represent 30 µm (n=3).

Due to the heterogeneous platelet size and the increased platelet volume in the mutant mice, gating strategies had to be optimized in flow cytometry. To compare platelet populations with similar size, a small gate was set to a size (forward scatter, FSC) where the sizes of control and mutant platelets overlapped (Figure 20).

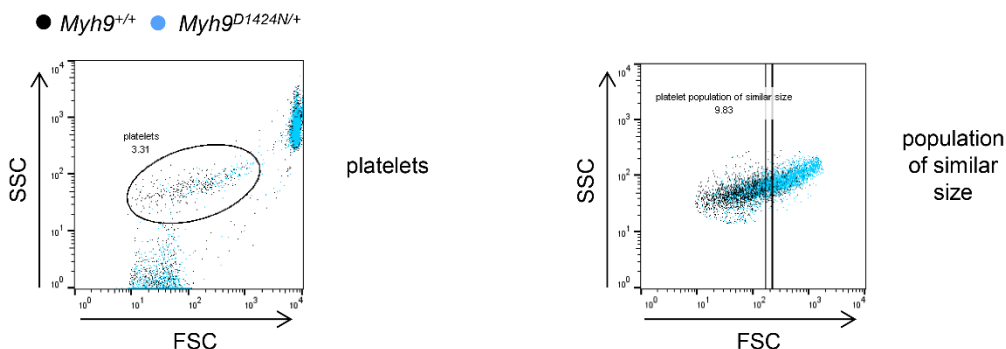


**Figure 20. Gating strategy to compare platelet populations with similar size.** Left: gating strategy to compare the whole population of platelets determined by the individual size (FSC) and granularity (sideward scatter (SSC)). Right: whole platelet population was gated to obtain a small area of similar sized platelet (FSC). Representative gating strategy for GP expression of CD9.

## Results

Flow cytometric analysis of the expression of prominent platelet surface proteins revealed moderate differences between *Myh9* mutant platelets and corresponding controls. Some receptors, most notably the GPIb-V-IX complex, were increased on mutant platelets even when comparing platelet populations of similar sized platelets (Table 2).

**Table 2. Surface proteins on *Myh9* mutant platelets show only moderate differences to surface proteins on control platelets.** GP expression on the platelet surface of *Myh9* mutant and control samples was analyzed with flow cytometry (n=4-7) by comparing platelet populations of similar size. Data are expressed as mean fluorescence intensity (MFI) of FITC-labeled antibodies against platelet surface proteins. Statistics: Multiple comparison using Holm-Sidak (ns  $p \geq 0.05$ ; \* $0.05 > p \geq 0.01$ ; \*\* $0.01 > p \geq 0.001$ ; \*\*\* $p < 0.001$ ).

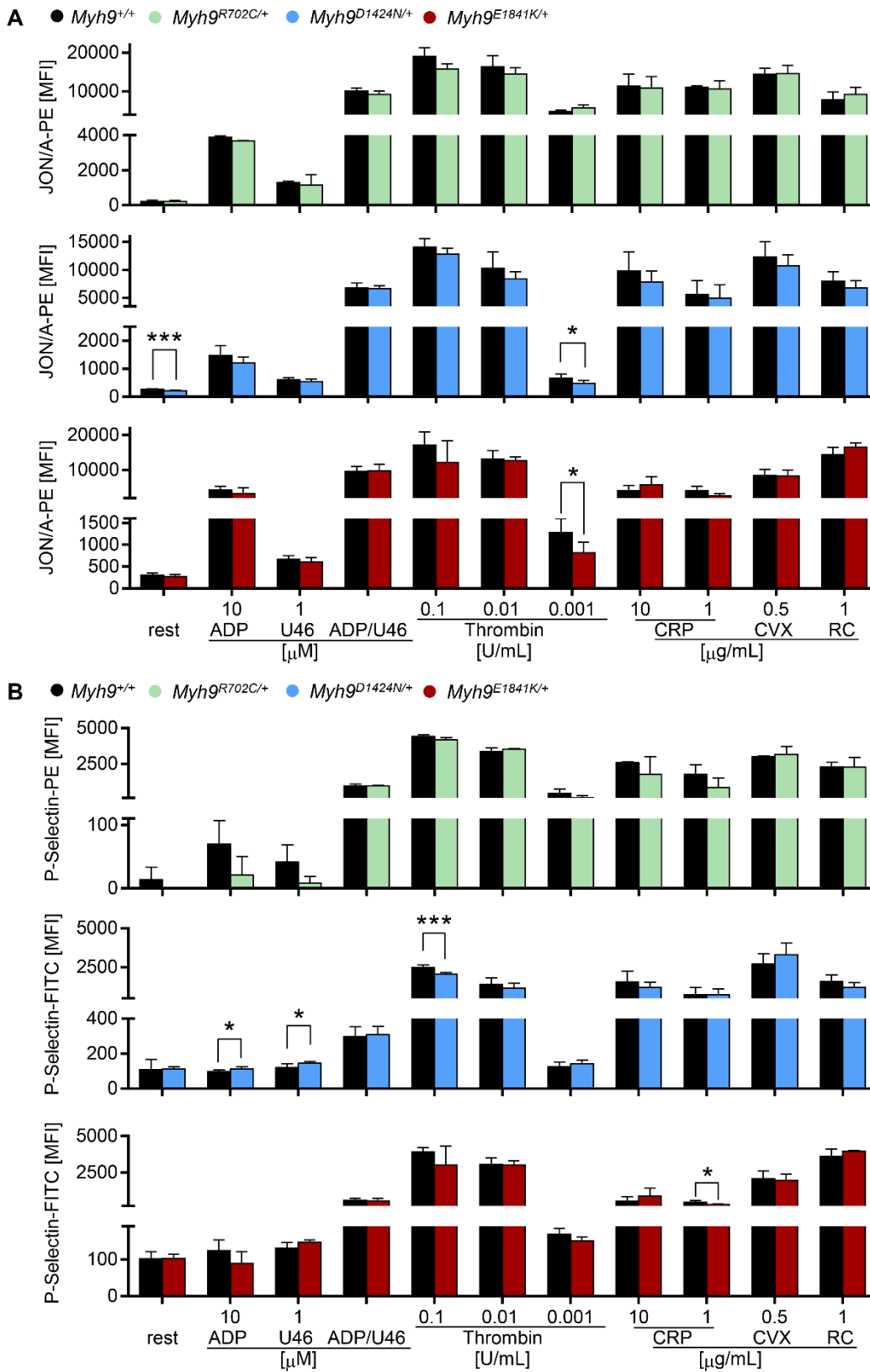
	<i>Myh9</i> <sup>+/+</sup>	<i>Myh9</i> <sup>R702C/+</sup>		<i>Myh9</i> <sup>+/+</sup>	<i>Myh9</i> <sup>D1424N/+</sup>		<i>Myh9</i> <sup>+/+</sup>	<i>Myh9</i> <sup>E1841K/+</sup>	
GPIb	10930 ± 461	12225 ± 737	*	7669 ± 146	10098 ± 1302	***	8370 ± 296	9694 ± 746	**
GPV	9337 ± 414	10129 ± 922	ns	5660 ± 468	6910 ± 739	**	5244 ± 1520	7442 ± 178	**
GPIX	15084 ± 1491	15826 ± 1028	ns	9317 ± 1184	12735 ± 605	***	7640 ± 4253	12564 ± 270	*
αIIbβ3	10573 ± 500	10669 ± 320	ns	13785 ± 461	13055 ± 1378	ns	9882 ± 5074	13384 ± 759	ns
α2	463 ± 24	483 ± 12	ns	1042 ± 126	1026 ± 154	ns	1437 ± 93	1551 ± 76	ns
CD9	27814 ± 775	29337 ± 1791	ns	28482 ± 1130	26244 ± 1159	**	32612 ± 2048	34219 ± 2280	ns
GPVI	1591 ± 213	1795 ± 174	ns	990 ± 49	904 ± 63	*	843 ± 479	1202 ± 74	ns
CLEC-2	3158 ± 80	3498 ± 115	***	3213 ± 301	3267 ± 139	ns	1694 ± 1414	3583 ± 230	*

### 5.1.3 Comparable activation and aggregation of *Myh9* mutant platelets

Next, we performed flow cytometric studies to investigate platelet signaling in *Myh9* mutant platelets. αIIbβ3 activation and P-selectin exposure of *Myh9* mutant platelets were measured in response to classical agonists, when comparing populations of similar sized platelets (Figure 20). Overall comparable results were obtained for mutant platelets in comparison to control platelets after stimulation of several platelet receptors (Figure 21A, B). Stimulation of G-protein coupled receptors with either ADP, the thromboxane A2 analog U46619 (U46), a combination of ADP and U46619, or thrombin revealed comparable platelet activation. Similar αIIbβ3 activation and P-selectin exposure of *Myh9* mutant platelets was achieved via stimulation of the GPVI-immunoreceptor tyrosine-based activation motif (GPVI-ITAM) pathway with collagen-related peptide (CRP) or convulxin (CVX). An unaltered degree of activation of *Myh9*

## Results

mutant platelets was also observed after stimulation of the hemITAM receptor CLEC2 (C-type lectin-like receptor 2) with rhodocytin (RC).



## Results

**Figure 21. Unaltered inside-out activation of *Myh9* mutant platelets.** (A) Activation of platelet  $\alpha\text{IIb}\beta\text{3}$ -integrin (JON/A-phycoerythrin [PE]) and (B) P-selectin exposure (anti-P-Selectin-fluorescein isothiocyanate [FITC]). Flow cytometry was performed under resting (rest) conditions and upon stimulation with different agonists ( $n=5-6$ , MFI). Statistics: Multiple comparison using Holm-Sidak ( $ns \geq 0.05$ ;  $*0.05 > p \geq 0.01$ ;  $**0.01 > p \geq 0.001$ ;  $***p < 0.001$ ).

Platelets from *MYH9*-RD patients display a lack of shape change upon activation, but a normal platelet aggregation.<sup>23,68,79</sup> In contrast, we could not detect impaired shape change of *Myh9* mutant platelets upon activation with thrombin (Figure 22A) or collagen (Figure 22B).

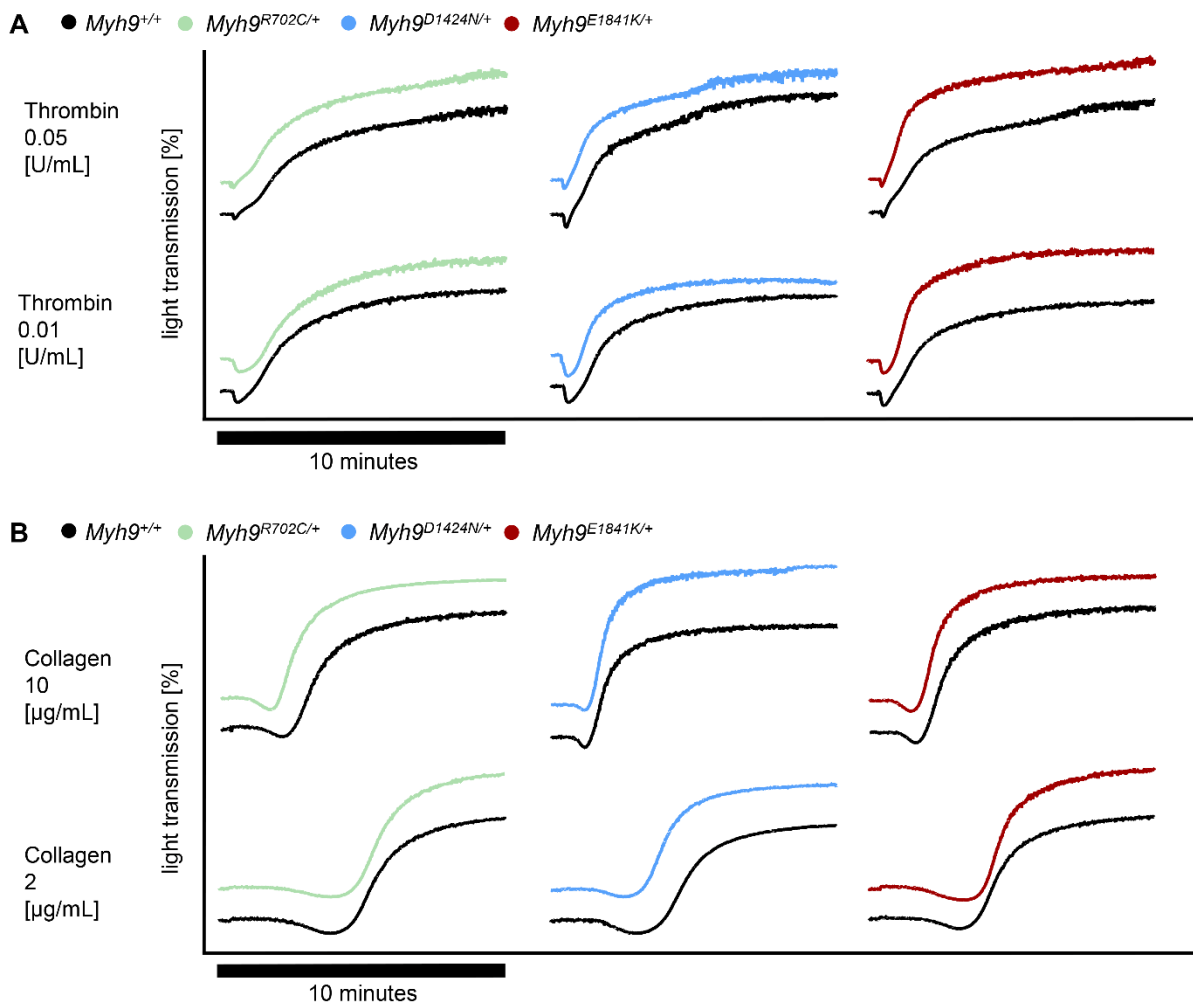


**Figure 22. *Myh9* mutant platelets change their shape and aggregate.** Washed platelets of all three mouse lines were stimulated with (A) thrombin or (B) collagen. Light transmission was recorded using a 4-channel aggregometer. Representative curves of two individual experiments are shown ( $n=2$ ).

Further, data on the onset and degree of aggregation was collected from aggregometry curves. The parameters maximum aggregation, maximum gradient and time until shape change was determined by analyzing the aggregometry curves. The maximum

## Results

aggregation of *Myh9* mutant platelets was not impaired for all three mouse lines and different agonists and concentrations (Table 3). Maximum gradient of *Myh9*<sup>E1841K/+</sup> platelets was increased in response to G-protein-coupled receptor agonist thrombin at a low concentration (Table 3). *Myh9*<sup>R702C/+</sup> platelets showed enhanced ability to change their shape in response to high doses of the GPVI agonist collagen (Table 3). Overall, the onset and degree of aggregation of *Myh9* mutant platelets were not impaired (Table 3). Taken together, murine *Myh9* mutant platelets could be activated, underwent shape change and formed aggregates in response to classical platelet agonists.

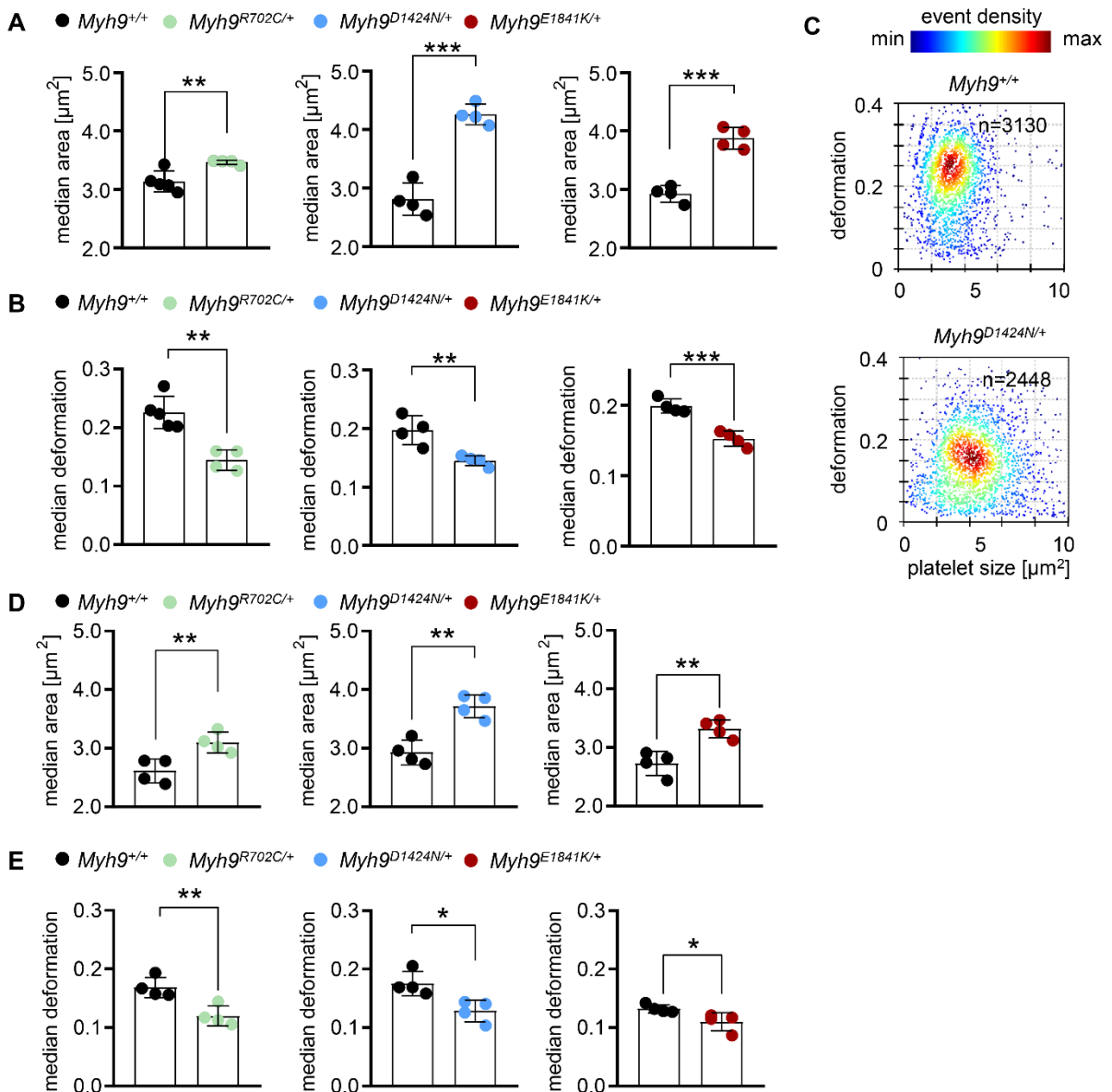
**Table 3. Degree and slope of *Myh9* mutant platelet aggregation is unaltered.** Washed platelets were activated with either thrombin (upper two) or collagen (lower two) and light transmission was recorded. Maximum aggregation (Max. Agg.), maximum gradient (Max. Grad.), and time until shape change occurred (lag time) were determined (mean ± S.D.; Mann-Whitney U-test: ns p ≥ 0.05; \*0.05 > p ≥ 0.01; \*\*0.01 > p ≥ 0.001).

Thrombin 0.05 U/ml	<i>Myh9</i> <sup>+/+</sup>	<i>Myh9</i> <sup>R702C/+</sup>	sig.	<i>Myh9</i> <sup>+/+</sup>	<i>Myh9</i> <sup>D1424N/+</sup>	sig.	<i>Myh9</i> <sup>+/+</sup>	<i>Myh9</i> <sup>E1841K/+</sup>	sig.
Max. Agg. [%]	70.5 ± 4.8	71.2 ± 2.0	ns	81.7 ± 10.1	74.2 ± 14.4	ns	77.1 ± 8.5	69.7 ± 5.1	ns
Max. Grad. [%/min]	40.4 ± 18.3	33.0 ± 1.9	ns	44.9 ± 6.6	48.5 ± 4.6	ns	50.8 ± 8.5	64.6 ± 19.8	ns
lag time [sec]	25.2 ± 2.0	25.3 ± 1.7	ns	32.0 ± 6.7	32.7 ± 5.9	ns	25.2 ± 2.3	25.0 ± 1.4	ns
Thrombin 0.01 U/ml	<i>Myh9</i> <sup>+/+</sup>	<i>Myh9</i> <sup>R702C/+</sup>	sig.	<i>Myh9</i> <sup>+/+</sup>	<i>Myh9</i> <sup>D1424N/+</sup>	sig.	<i>Myh9</i> <sup>+/+</sup>	<i>Myh9</i> <sup>E1841K/+</sup>	sig.
Max. Agg. [%]	71.7 ± 3.5	68.8 ± 4.3	ns	64.2 ± 16.5	56.2 ± 3.0	ns	65.2 ± 21.5	70.5 ± 6.2	ns
Max. Grad. [%/min]	34.2 ± 3.1	41.3 ± 8.7	ns	49.6 ± 10.7	59.9 ± 14.2	ns	52.6 ± 8.1	77.2 ± 7.3	**
lag time [sec]	26.0 ± 0.8	26.7 ± 0.6	ns	26.3 ± 1.0	23.8 ± 3.2	ns	28.0 ± 1.4	27.0 ± 2.9	ns
Collagen 10 µg/ml	<i>Myh9</i> <sup>+/+</sup>	<i>Myh9</i> <sup>R702C/+</sup>	sig.	<i>Myh9</i> <sup>+/+</sup>	<i>Myh9</i> <sup>D1424N/+</sup>	sig.	<i>Myh9</i> <sup>+/+</sup>	<i>Myh9</i> <sup>E1841K/+</sup>	sig.
Max. Agg. [%]	82.9 ± 8.3	80.5 ± 17.8	ns	88.0 ± 10.2	85.0 ± 8.4	ns	83.8 ± 15.8	79.4 ± 9.9	ns
Max. Grad. [%/min]	49.5 ± 15.4	69.1 ± 27.5	ns	84.0 ± 12.0	92.2 ± 19.1	ns	58.0 ± 18.7	69.0 ± 17.2	ns
lag time [sec]	81.7 ± 21.2	61.5 ± 6.9	*	55.8 ± 15.5	63.0 ± 8.7	ns	64.5 ± 4.2	62.5 ± 21.4	ns
Collagen 2 µg/ml	<i>Myh9</i> <sup>+/+</sup>	<i>Myh9</i> <sup>R702C/+</sup>	sig.	<i>Myh9</i> <sup>+/+</sup>	<i>Myh9</i> <sup>D1424N/+</sup>	sig.	<i>Myh9</i> <sup>+/+</sup>	<i>Myh9</i> <sup>E1841K/+</sup>	sig.
Max. Agg. [%]	70.0 ± 15.1	85.4 ± 8.5	ns	80.4 ± 4.2	82.1 ± 8.3	ns	83.8 ± 3.7	73.7 ± 6.5	ns
Max. Grad. [%/min]	41.8 ± 14.7	48.6 ± 12.4	ns	57.0 ± 10.1	66.0 ± 25.6	ns	54.4 ± 3.3	55.6 ± 10.1	ns
lag time [sec]	155.0 ± 32.6	129.6 ± 33.5	ns	101.7 ± 17.0	102.3 ± 19.0	ns	126.5 ± 8.3	109.2 ± 25.3	ns

## Results

### 5.1.4 Increased stiffness and F-actin content in *Myh9* mutant platelets

RT-FDC is a high-throughput method for continuous mechanical characterization of cells, by which a large cell population can be measured and individual cell populations in whole blood identified. Besides that, this method is sensitive to cytoskeletal alterations,<sup>104</sup> making RT-FDC a promising tool to measure *Myh9* mutant platelets. Resting *Myh9* mutant and control platelets were deformed inside the channel by hydrodynamic forces and RT-FDC revealed mutant platelets to be larger (Figure 23A, D) and stiffer, as indicated by a lower deformability (Figure 23B, E). Representative scatter plots show deformation in relation to platelet size, in which a right shift towards increased platelet size and a shift downwards towards decreased deformability for *Myh9* mutant platelets can be observed (Figure 23C).





## Results

**Figure 23. *Myh9* mutant platelets are stiffer.** RT-FDC measurements show (A) area and (B) deformation of *Myh9* mutant and control platelets in sodium-citrate. (C) Representative KDE scatter plots showing the distribution of single platelet deformability in relation to size of *Myh9*<sup>D1424N/+</sup> mutant and control platelets (n= number of single platelets). (D) Platelet size and (E) deformation measured in whole blood drawn in EDTA with RT-FDC. (A, B, D, E) Bar plots show mean ± S.D. from individual mice (n=4-5) of the median of about 2000 platelets of one mouse. Statistics: Multiple comparison using Holm-Sidak (\*0.05 > p ≥ 0.01; \*\*0.01 > p ≥ 0.001; \*\*\*p < 0.001).

Anticoagulants affect human platelet biomechanics in RT-FDC. Therefore, it is recommended to collect blood in sodium-citrate, while EDTA is supposed to alter the biomechanical properties of platelets.<sup>113</sup> Independent of the anticoagulant used for bleeding mice, platelets of *Myh9* mutant mice appeared to be bigger in size and stiffer when bled in sodium-citrate (Figure 23A – C) or in EDTA (Figure 23D, E). Since red blood cells play a role in thrombus formation and clot retraction<sup>114</sup>, we analyzed RBCs from mice bled in EDTA using RT-FDC. RBC count, hematocrit and hemoglobin was unaltered in *Myh9* mutant mice (Table 1), as well as the size and deformation of RBCs (Figure 24). Similarly, Smith *et al.* showed normal RBC deformability from blood of *MYH9*-RD patients using ektacytometry.<sup>112</sup> In conclusion, RBCs of *Myh9* mutant mice and *MYH9*-RD patients have no or maybe a minor effect on thrombus formation and clot retraction, but the enhanced stiffness of resting platelets rather points to altered platelet mechanical properties, which have to be further investigated.

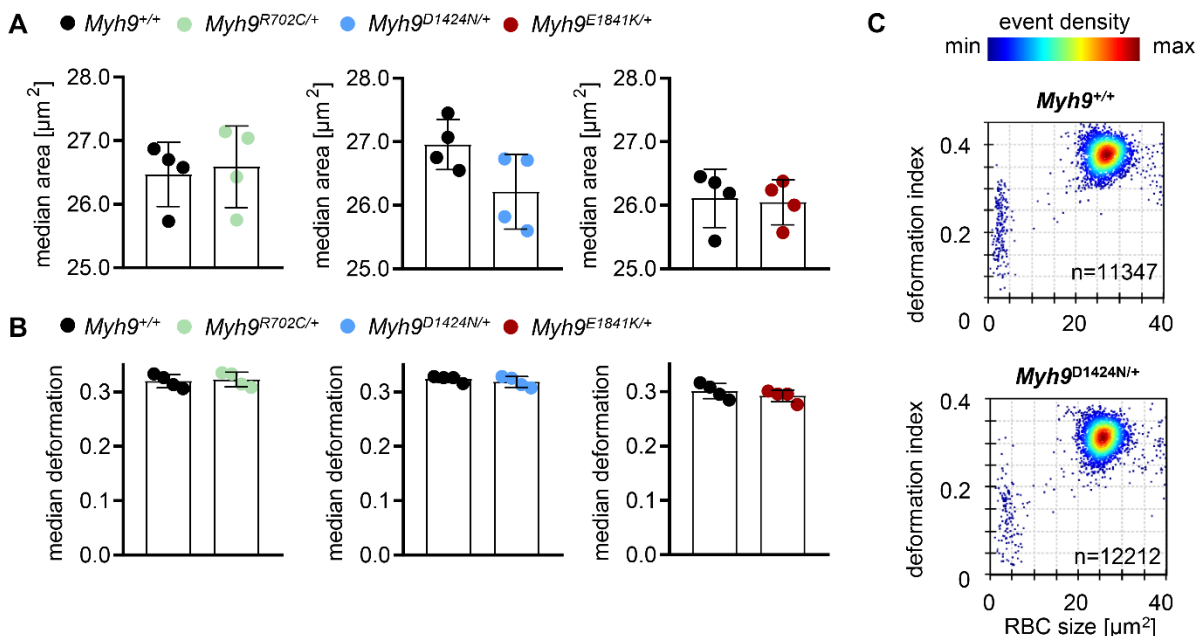


**Figure 24. RBCs of *Myh9* mutant mice are normal in deformation and size.** Red blood cells were measured with RT-FDC for (A) RBC area and (B) deformation. (A, B) Bar plots show mean ± S.D. from individual mice (n=4-5) of the median of about 1000 cells per mouse. Statistics: Multiple comparison

## Results

using Holm-Sidak (ns  $p \geq 0.05$ ). (C) Representative scatter plots of RBCs from *Myh9<sup>D1424N/+</sup>* mutant and control mice for deformation versus size (n= number of RBCs).

To assess the influence of cytoskeletal components on the deformation of resting platelets, PREM and confocal microscopy were performed. The cytoskeletal structure of resting platelets of *Myh9* mutant mice appeared comparable to that of *Myh9<sup>+/+</sup>* platelets. Tubulin was organized in a ring-like structure (Figure 25, arrowhead; Figure 26) and F-actin was homogenously distributed over the whole cell (Figure 25, asterisk; Figure 26).

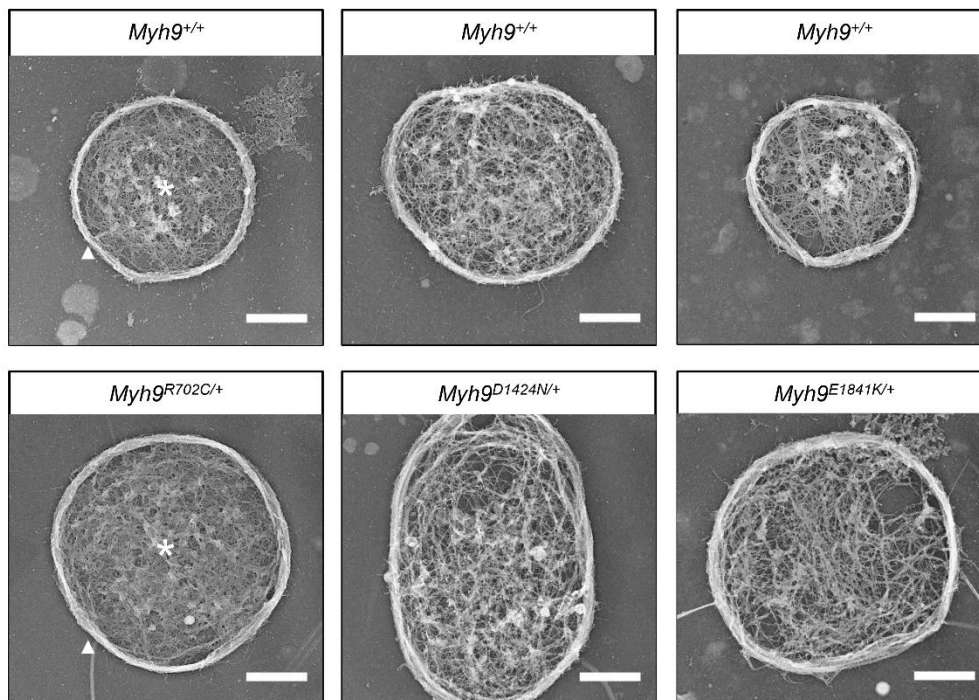
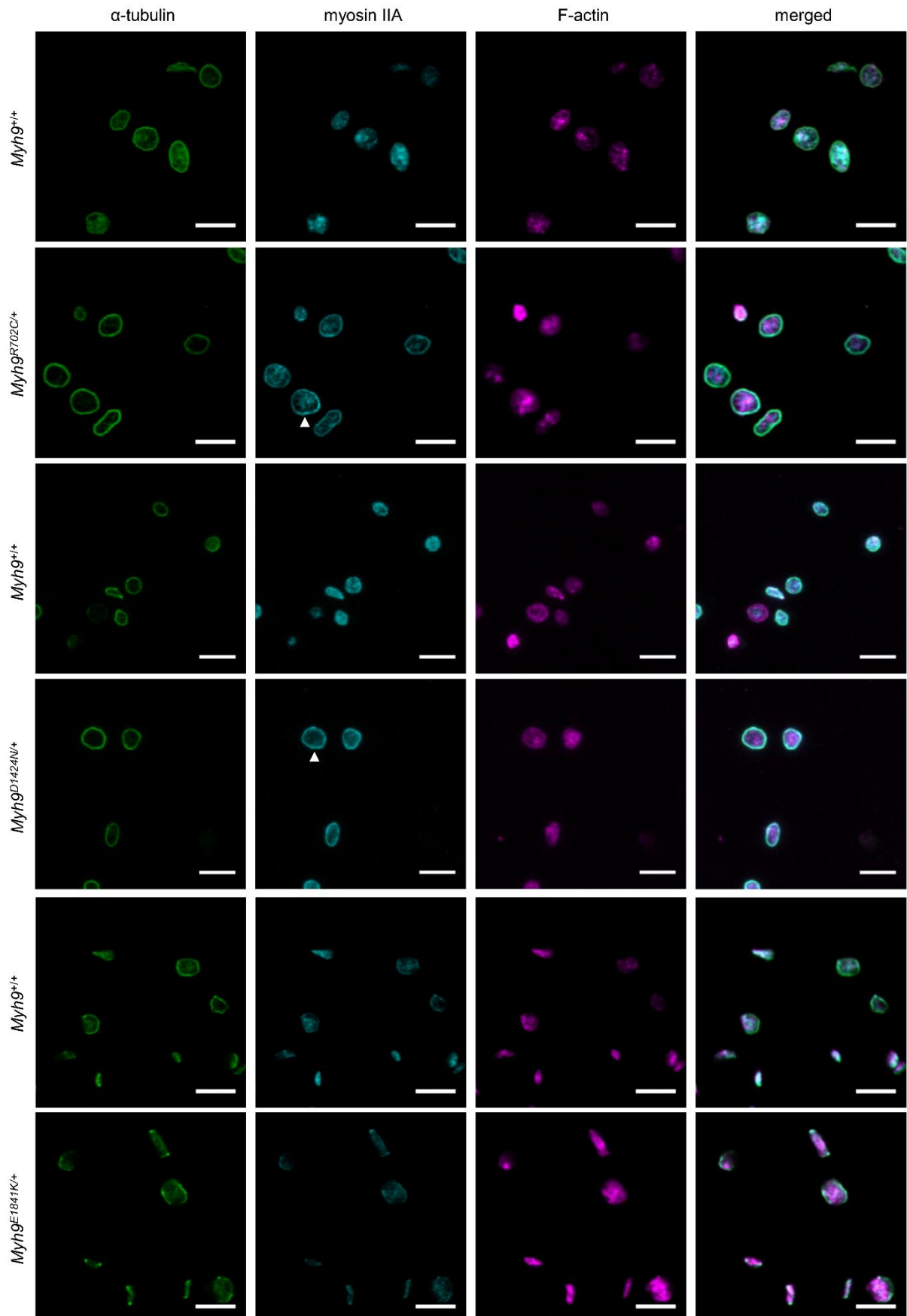


**Figure 25. Unaltered ultrastructure of resting platelets from *Myh9* mutant mice.** Ultrastructure of resting *Myh9* mutant and control platelets was assessed with PREM (scale bars 1  $\mu\text{m}$ ; microtubule ring: arrowhead; F-actin: asterisk).

Previous publications showed colocalization of F-actin and myosin in resting platelets. In human platelets of healthy individuals<sup>115,116</sup> and control platelets of mice (Figure 26; *Myh9<sup>+/+</sup>*) a homogenous pattern of F-actin and myosin distribution was observed with a slight accumulation at the cell periphery. The distribution of myosin IIA in *Myh9* mutant platelets appeared to be localized, like  $\alpha$ -tubulin, in a ring-like structure at the cell periphery (Figure 26, arrowhead).

## Results



## Results

**Figure 26. Distribution of cytoskeletal components in resting *Myh9* mutant platelets.** Representative confocal microscopy images of resting platelets on PLL (scale bars 5  $\mu\text{m}$ ). Platelets were stained for  $\alpha$ -tubulin (green) and F-actin (phalloidin, magenta). Except for *Myh9<sup>R702C/+</sup>* mutant platelets (GFP-labeled myosin IIA), myosin IIA was stained with a fluorophore-coupled antibody (cyan). Arrowheads indicate myosin IIA accumulation at the cell periphery.

Because F-actin was normally distributed in mutant platelets as confirmed by immunostainings and PREM, we wondered whether the ratio of polymerized and monomeric actin is altered in myosin IIA mutant platelets. Typically, G- and F-actin are present in resting platelets at a ratio of about 1:1.<sup>48</sup> Ultracentrifugation of phalloidin-stabilized resting platelet samples revealed a normal ratio of soluble G-actin and insoluble F-actin abundance in mutant platelets of all three mouse lines (Figure 27). In conclusion the mutations in the *Myh9* gene seem to have no effect on G-/F-actin ratio in platelets.

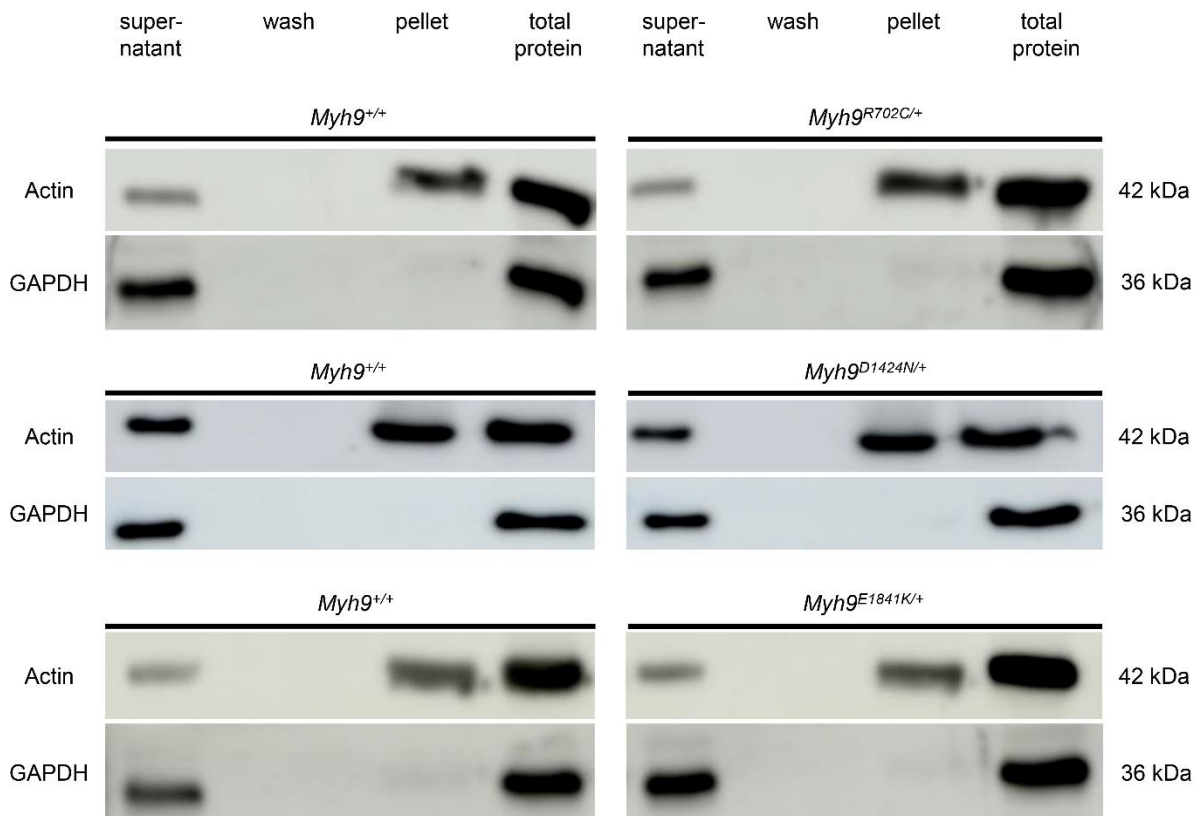


**Figure 27. G- and F-actin ratio is normal in mutant resting platelets.** Ultracentrifugation of platelet samples with phalloidin-stabilized cytoskeleton was performed to pelletize F-actin and detect soluble proteins, like G-actin and GAPDH in the supernatant. GAPDH served as control for successful separation of soluble and solid parts. Representative immunoblots of three independent experiments are shown (n=3).

## Results

Since *Myh9* mutant platelets are enlarged (Figure 18B, C, 23A, D) and myosin IIA interacts directly with actin,<sup>45</sup> we performed flow cytometry to determine F-actin content and ability of platelets to assemble actin after activation. The mouse line *Myh9*<sup>R702C/+</sup> was not analyzed in this assay because of the fluorophore emission overlap from GFP and the FITC-labeled phalloidin used in this experiment. The comparison of whole platelet populations, regardless of the increased mutant platelet size, revealed that the F-actin content in resting *Myh9*<sup>D1424N/+</sup> and *Myh9*<sup>E1841K/+</sup> platelets was increased as compared to controls (Figure 28A). Statistically significant, but only moderate differences in the capability of F-actin assembly in *Myh9*<sup>D1424N/+</sup> mutant platelets was measured after agonist-induced activation. After stimulation of G-protein coupled receptors with ADP/U46619 and thrombin, *Myh9*<sup>E1841K/+</sup> mutant platelets were able to polymerize F-actin to the same extent as *Myh9*<sup>+/+</sup> platelets (Figure 28B). With a different gating strategy, we compared platelet populations of similar platelet size (Figure 20; left) and found that the F-actin content of *Myh9*<sup>D1424N/+</sup> and *Myh9*<sup>E1841K/+</sup> platelets was comparable to levels in *Myh9*<sup>+/+</sup> platelets (Figure 28C), and polymerization of F-actin after activation of *Myh9*<sup>D1424N/+</sup> platelets was reduced (Figure 28D). These results suggest a size-dependent F-actin content in *Myh9* mutant platelets and a slight defect in F-actin polymerization especially in the mutant *Myh9*<sup>D1424N/+</sup> mice.

## Results

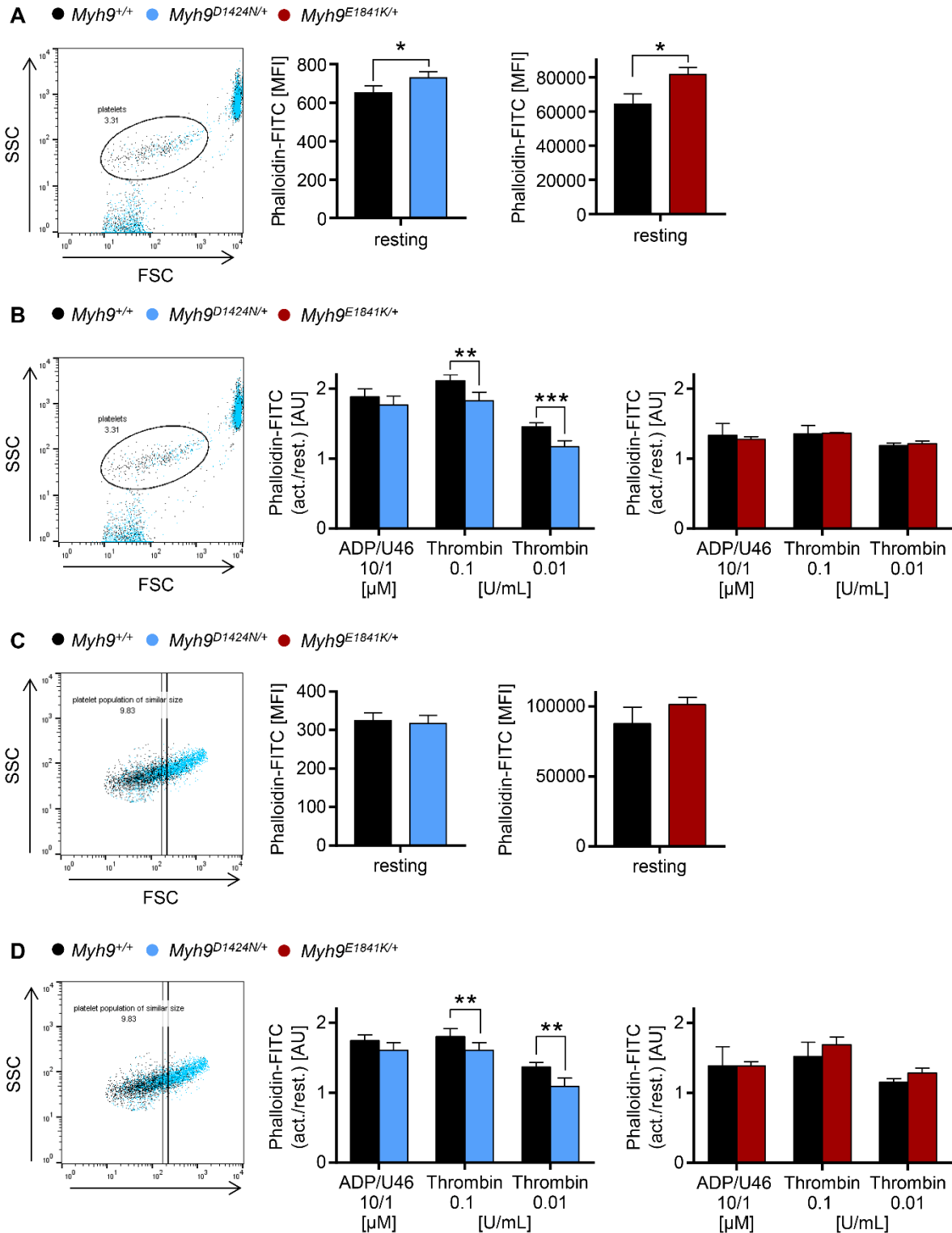


**Figure 28. Higher F-actin content in *Myh9* mutant platelets due to increased size.** (A-B) Whole platelet populations of mouse lines D1424N and E1841K were analyzed for (A) F-actin content in resting platelets and (B) actin filament assembly after activation with indicated agonists. Platelet populations of similar size of *Myh9*<sup>D1424N/+</sup> and *Myh9*<sup>E1841K/+</sup> mutant samples were compared to *Myh9*<sup>+/+</sup> sample regarding (C) F-actin content (resting) and (D) assembly after activation. (A – D) The mean fluorescence intensity is shown (n=3-7). Statistics: Multiple comparison using Holm-Sidak (ns  $p \geq 0.05$ ;  $0.05 > p \geq 0.01$ ;  $0.01 > p \geq 0.001$ ;  $p < 0.001$ ).

## Results

### 5.1.5 Myh9 mutant platelets adhere and fully spread on fibrinogen

Cytoskeletal rearrangement is critical for platelets to undergo shape change after activation. Actin, the most abundant protein in cells, assembles into filaments for filopodia and branched filaments for lamellipodia formation.<sup>23</sup> Flow cytometry data indicated impaired polymerization of F-actin of *Myh9*<sup>D1424N/+</sup> platelets after activation with thrombin (Figure 28B, D). Therefore, a static platelet spreading assay was performed to investigate organization and rearrangement of the cytoskeleton in *Myh9* mutant platelets. Spread platelets can be categorized into four phases: (I) resting platelet adhesion, (II) formation of filopodia, (III) filopodia and the formation of lamellipodia, and (IV) only lamellipodia / “fried-egg like” shape<sup>49</sup> (Figure 29A, lower right). DIC imaging revealed that thrombin-activated *Myh9* mutant platelets adhered normally to fibrinogen under static conditions. Subsequently, *Myh9* mutant platelets formed filopodia and lamellipodia over a time period of 30 minutes. The spreading kinetics were overall comparable to the corresponding control, with a slightly faster spreading of *Myh9*<sup>D1424N/+</sup> platelets and *Myh9*<sup>E1841K/+</sup> platelets after 5 minutes, which might be explained by their increased size and therefore faster sedimentation and adhesion to fibrinogen (Figure 29A). In agreement, the formation of lamellipodia on fibrinogen was unaltered in *Myh9* mutant platelets, as also revealed by PREM. However, microtubules in some spread mutant platelets seemed to be rather organized in a parallel manner as compared to control platelets (Figure 29B, arrowhead).

## Results

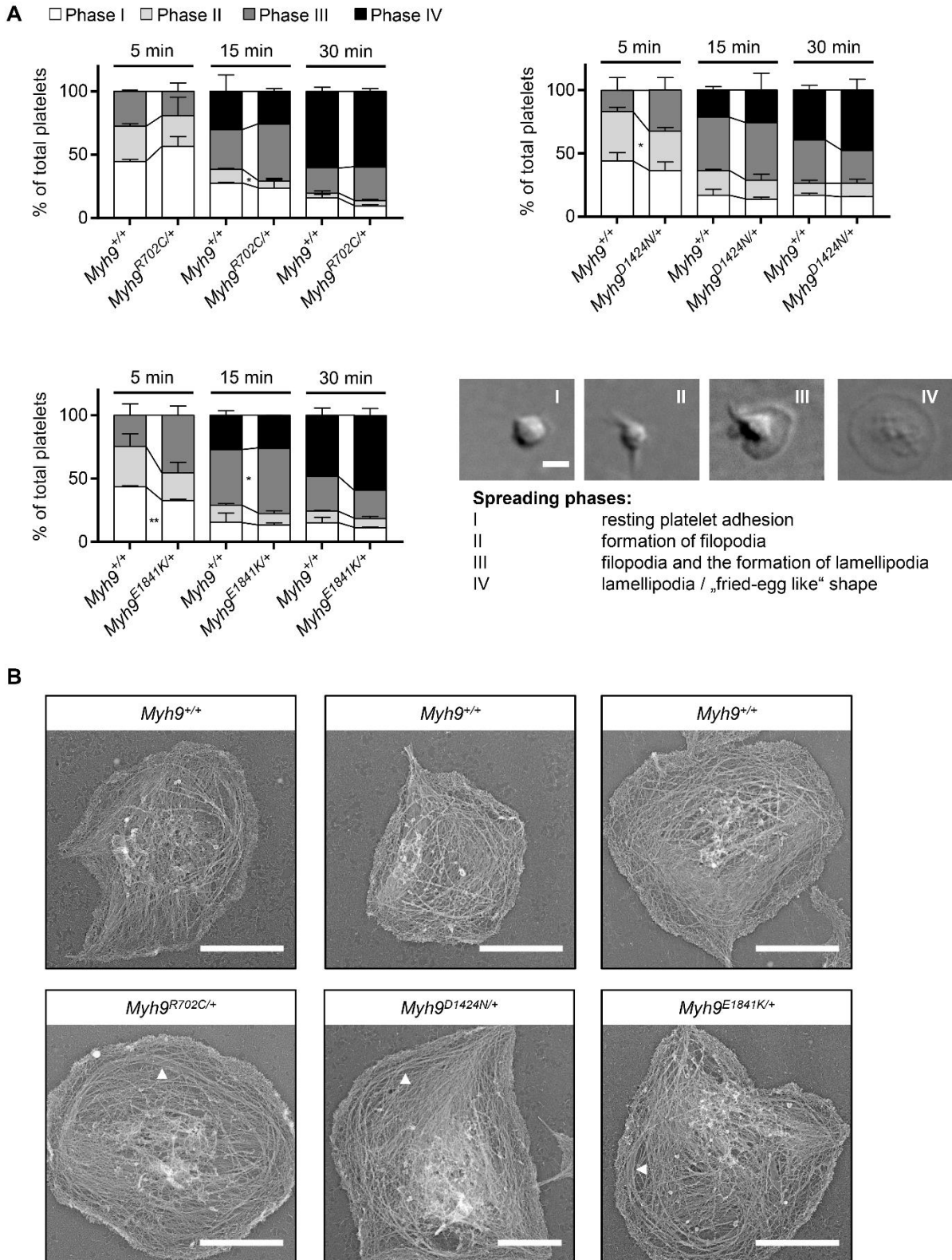


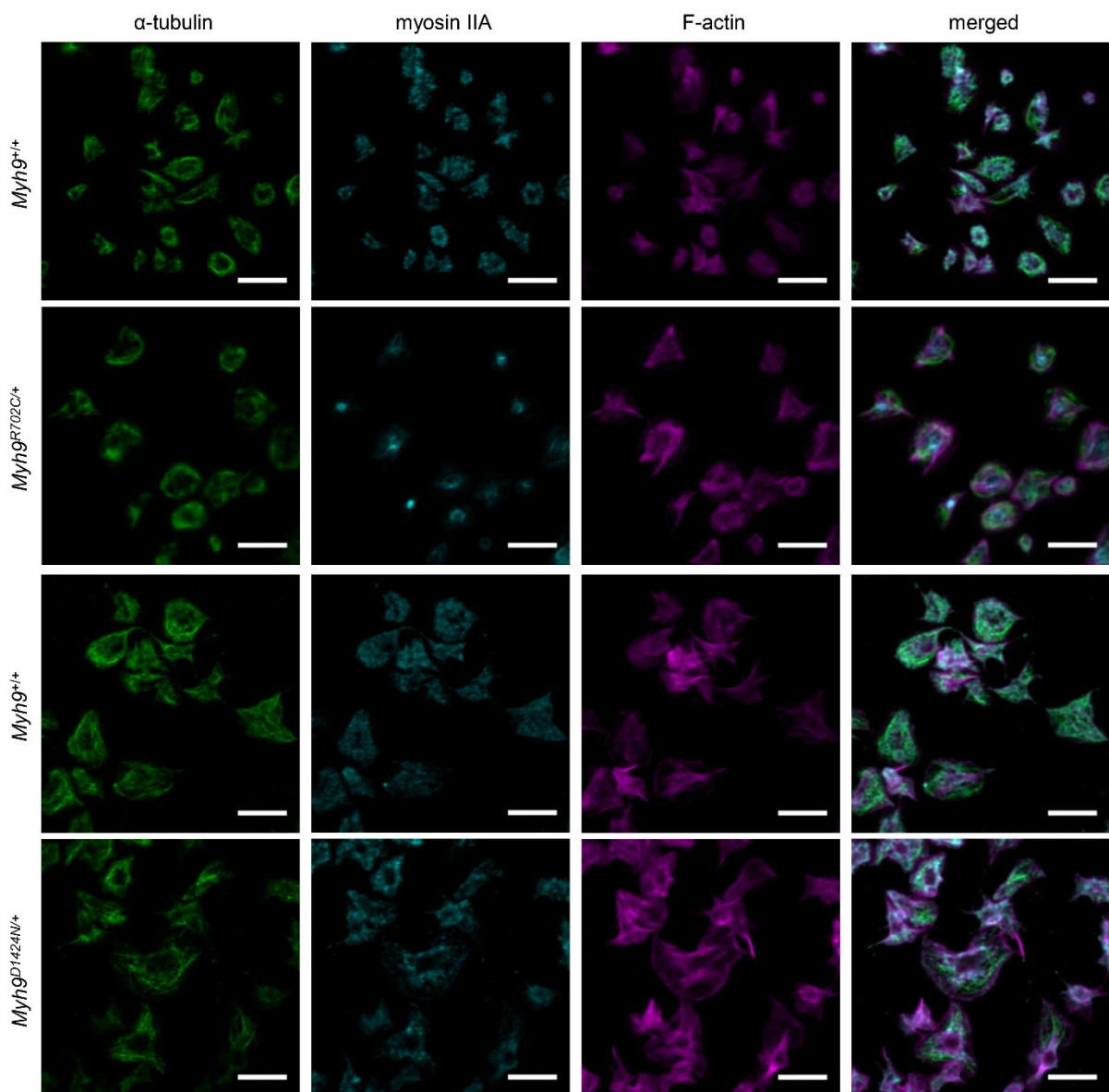
**Figure 29. *Myh9* mutant platelets spread and form lamellipodia on fibrinogen.** (A) Washed platelets were allowed to spread on fibrinogen in the presence of thrombin and were fixed at indicated time points (mean  $\pm$  S.D.;  $n=2$ ). Platelets were categorized into four different spreading phases. Phase I: resting platelets; Phase II: platelets with filopodia; Phase III: platelet with filopodia and lamellipodia; Phase IV: fully spread platelets with only lamellipodia (“fried-egg-like” shape) (scale bar 2  $\mu$ m). Statistics: Multiple



## Results

comparison using Holm-Sidak (ns  $p \geq 0.05$ ;  $*0.05 > p \geq 0.01$ ;  $**0.01 > p \geq 0.001$ ). (B) Representative PREM images of the cytoskeleton ultrastructure of *Myh9* mutant platelets spread on fibrinogen for 15 minutes in the presence of thrombin (scale bars 2  $\mu\text{m}$ ). Arrowheads indicate microtubules arranged in a parallel manner.

Immunostainings for myosin IIA and F-actin revealed overall comparable distribution of cytoskeletal components in spread mutant platelets on fibrinogen. The  $\alpha$ -tubulin was distributed over the whole cell in wildtype and mutant platelets (Figure 30). In agreement with PREM data,  $\alpha$ -tubulin was located in the periphery, predominantly in larger platelets (Figure 30, arrowhead). However, this preliminary observation has to be further analyzed in more detail in future studies.



## Results

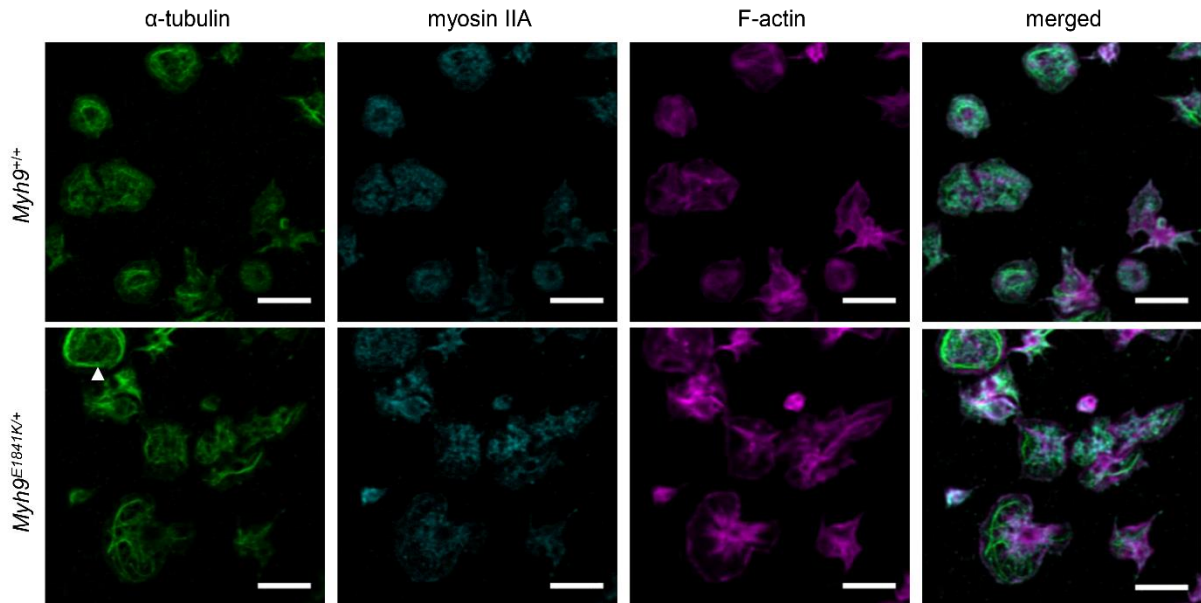


**Figure 30. Immunostaining of *Myh9* mutant platelets spread on fibrinogen.** Cytoskeletal components of mouse lines D1424N and E1841K were stained for  $\alpha$ -tubulin (Alexa Fluor 488; green; arrowhead: parallel organized microtubules), myosin IIA (secondary antibody labeled Cy3; cyan) and F-actin (phalloidin-Atto647N, magenta) after spreading for 30 minutes on fibrinogen in the presence of thrombin and imaged with confocal microscopy. Wildtype platelets of mouse line R702C were stained as described before. Mutant platelets were stained for  $\alpha$ -tubulin (Alexa Fluor 546; green) and F-actin (phalloidin-Atto647N, magenta). Myosin IIA of *Myh9*<sup>R702C/+</sup> mutant platelets was detected via GFP label. Representative images of all three *Myh9* mutant mouse lines are shown (n=3; scale bars 5  $\mu$ m).

The actomyosin complex is not only required for shape change upon activation, but also platelet migration is a highly actomyosin-dependent mechanism. Actin polymerization and myosin IIA-mediated contraction is important for platelets to migrate and pile up adhesive substrate together with collecting deposited bacteria.<sup>27</sup> Once platelets are spread and pro-adhesive fibrinogen and anti-adhesive albumin are balanced, polarization is initiated.<sup>117</sup> Actin polymerization shapes the leading edge morphology and myosin IIA the trailing edge. In the study of Gaertner *et al.*, dose-dependent inhibition of myosin IIA with blebbistatin resulted in a lower platelet migrating capability.<sup>27</sup> We wondered whether heterozygous point mutations in the *Myh9* gene also impair migration, therefore a platelet migration assay was established. *Myh9*<sup>+/+</sup> platelets were able to spread on homogeneously coated fibrinogen, changed their shape and migrated randomly (Figure 31A). The morphology of migrating mutant platelets was comparable to controls, with a fully spread “fried egg”-like shape or large filopodia emanating from platelets (Figure 31A). Quantification of migrating platelets showed that the number of migrating *Myh9*<sup>R702C/+</sup> and *Myh9*<sup>D1424N/+</sup> platelets on fibrinogen was comparable to corresponding controls, but more *Myh9*<sup>E1841K/+</sup> platelets

## Results

were able to migrate in comparison to control platelets (Figure 31B). Interestingly, the distance of platelet migration was increased for all mutant lines as compared to the corresponding control (Figure 31C).

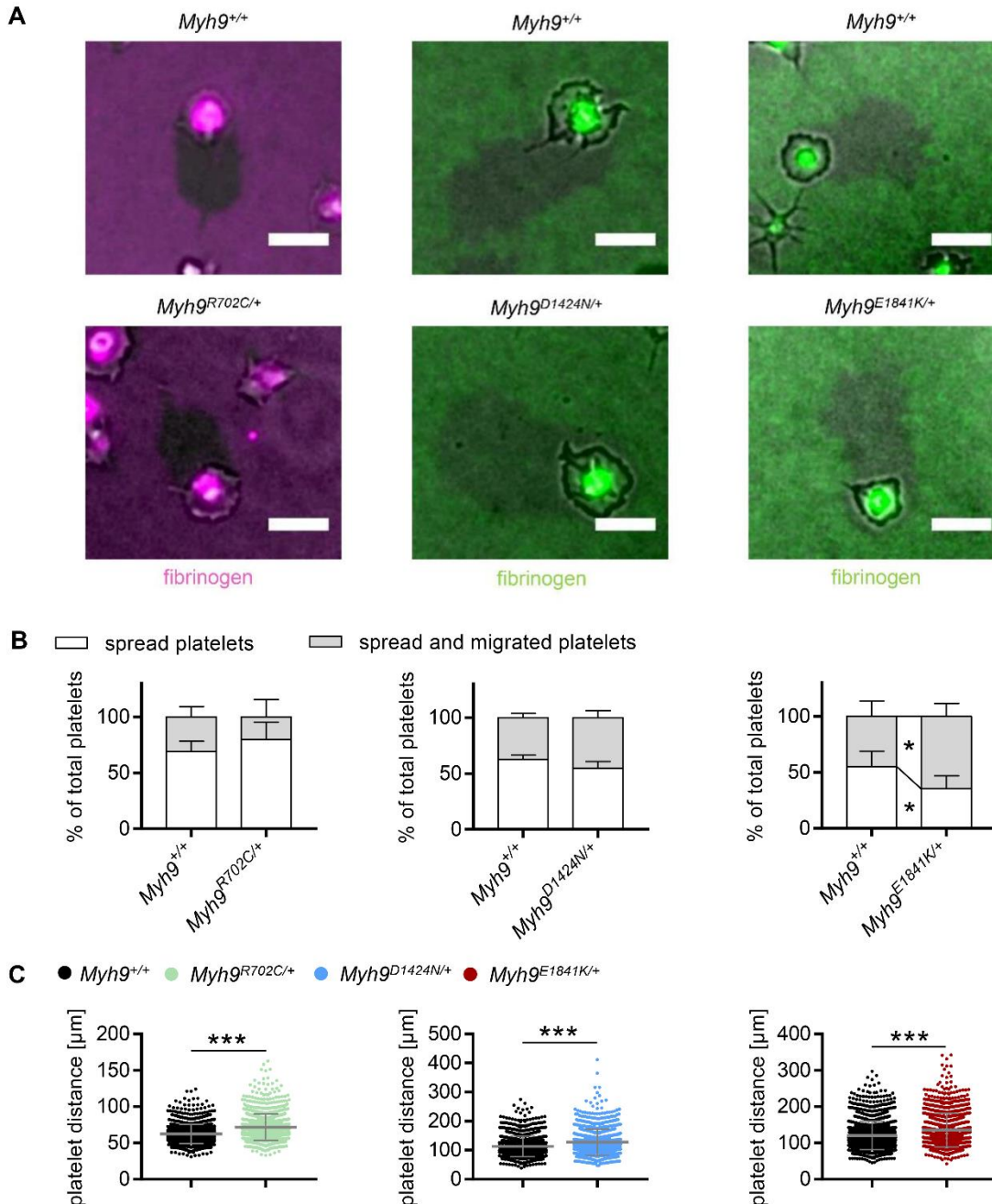


**Figure 31. *Myh9* mutant platelets can migrate and collect fibrinogen.** (A) Representative images of migrated platelets from *Myh9*<sup>+/+</sup> and *Myh9* mutant mice (scale bars 5  $\mu$ m). (B) Platelets of all three mouse lines spread on fibrinogen-coated surface for 3 hours were categorized into groups of spread platelets (white) or spread and migrated platelets (grey) (mean  $\pm$  S.D.; n=4-6). (C) Distance of platelet migration was determined from start of fibrinogen uptake until center of the platelet indicated by green spot of incorporated fibrinogen after three hours. Values are mean  $\pm$  S.D. (*Myh9*<sup>+/+</sup>; n=1569; *Myh9*<sup>R702C/+</sup>; n=1112; *Myh9*<sup>+/+</sup>; n=1152; *Myh9*<sup>D1424N/+</sup>; n=1078; *Myh9*<sup>+/+</sup>; n=1670; *Myh9*<sup>E1841K/+</sup>; n=1147 platelets). Statistics: Mann-Whitney U-test (ns p  $\geq$  0.05; \*0.05 > p  $\geq$  0.01; \*\*0.01 > p  $\geq$  0.001; \*\*\*p < 0.001).

## Results

Increased stiffness of resting *Myh9* mutant platelets as detected with RT-FDC is most likely due to altered biomechanical features (Figure 23B, E). Next, we investigated the deformation of spread platelets. The system of scanning ion conductance microscopy enables non-contact measurements of cells through distance feed-back control via change in ion current flow. Hydrostatic pressure can be applied through the scanning pipette probe to study mechanical properties of cells. In collaboration with the group of Tilman Schaeffer (Eberhard-Karls University of Tübingen), we used SICM to investigate the deformation of spread mutant and control platelets. Spread *Myh9* mutant platelets on fibrinogen were softer as indicated by a decreased Young's modulus except for *Myh9<sup>E1841K/+</sup>* platelets, which displayed comparable stiffness to *Myh9<sup>+/+</sup>* platelets (Figure 32A, B). Area and volume of spread *Myh9<sup>D1424N/+</sup>* and *Myh9<sup>E1841K/+</sup>* mutant platelets were increased (Figure 32C, D). However, aspect ratio and circularity of *Myh9* mutant platelets was comparable to control platelets (Figure 32E, F, G). These data suggest that amino acid exchanges at three different positions in myosin IIA impair the deformability of platelets.

## Results

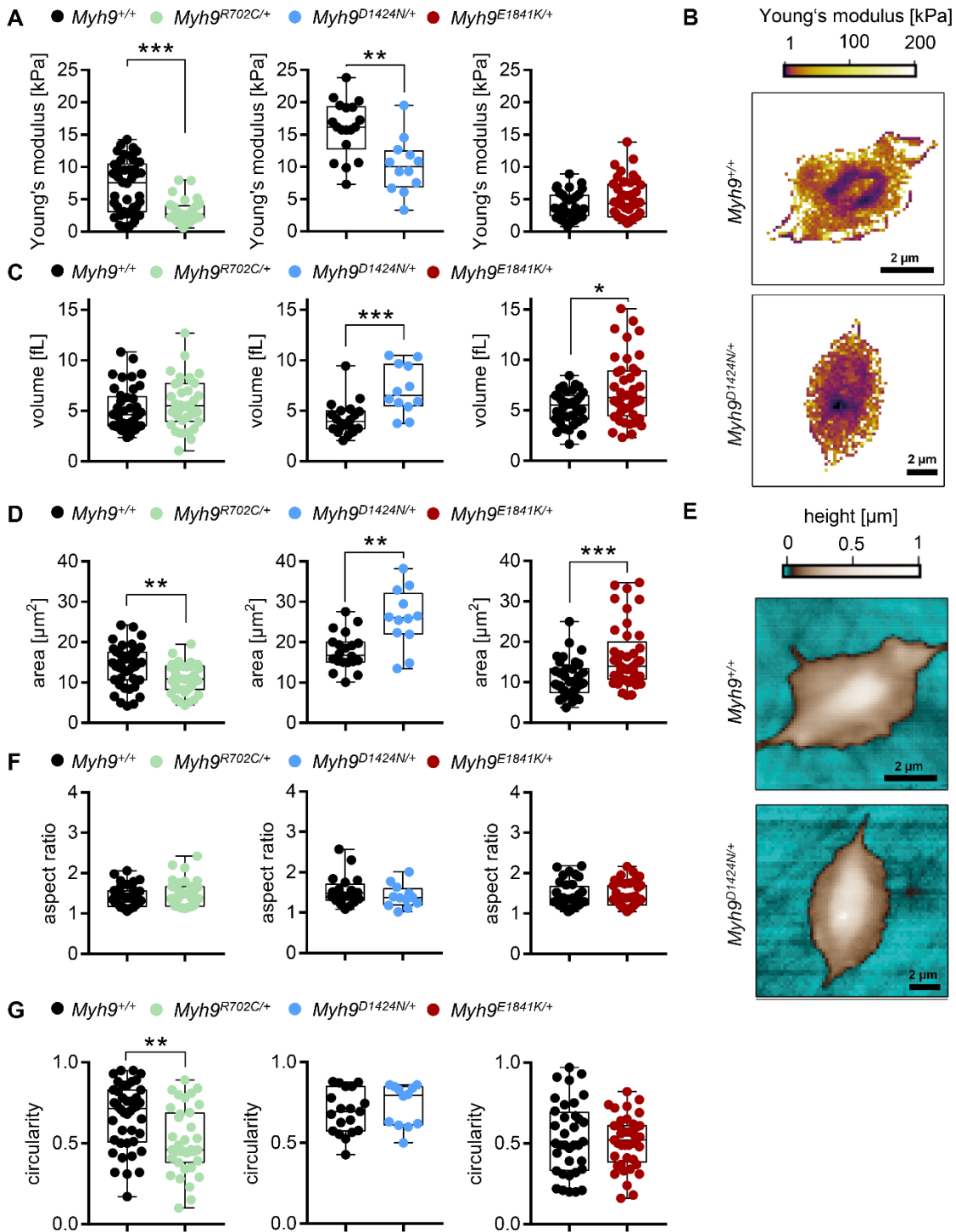


**Figure 32. Spread *Myh9*<sup>R702C/+</sup> and *Myh9*<sup>D1424N/+</sup> platelets are softer.** Washed platelets spread on fibrinogen in the presence of thrombin were analyzed for (A) stiffness, (C) volume, (D) area, (F) aspect ratio and (G) circularity. (A, C, D, F, G) Each symbol represents one platelet (*Myh9*<sup>+/+</sup>: n=42 platelets; *Myh9*<sup>R702C/+</sup>: n=36 platelets; *Myh9*<sup>+/+</sup>: n=20 platelets; *Myh9*<sup>D1424N/+</sup>: n=12 platelets; *Myh9*<sup>+/+</sup>: n=36 platelets; *Myh9*<sup>E1841K/+</sup>: n=41 platelets) and box plots show median ± S.D. Statistics: Mann-Whitney U-test (ns p ≥ 0.05; \*0.05 > p ≥ 0.01; \*\*0.01 > p ≥ 0.001; \*\*\*p < 0.001). Representative images showing (B) Young's modulus or (E) the height of *Myh9*<sup>+/+</sup> and *Myh9*<sup>D1424N/+</sup> platelets (scale bars 2 μm).

## Results

### 5.1.6 Decreased myosin light chain phosphorylation and contractile forces of *Myh9* mutant platelets

Actin and its motor protein myosin IIA form the contractile unit in platelets. The contractile function of myosin IIA is controlled by the phosphorylation of the myosin RLC. After activation, phosphorylation of myosin RLC and the interaction and movement along actin generates contractile forces.<sup>118,119</sup> To assess phosphorylation of MLC2, platelets of wildtype and *Myh9* mutant mice were analyzed under resting and thrombin-activated conditions using ProteinSimple Jess. Expression of total MLC2 in resting and thrombin-activated platelet lysates was comparable between *Myh9*<sup>+/+</sup> and *Myh9* mutant samples. Upon activation MLC2 is known to be phosphorylated at residue serine-19<sup>120,121</sup> and threonine-18.<sup>122</sup> Antibodies against MLC2 phosphorylation at serine-19 (MLC2 p-S19) and threonine-18 (MLC2 p-T18/S19) revealed upregulation of phosphorylation in activated *Myh9*<sup>+/+</sup> platelet lysates by immunoblotting, whereas resting platelet lysates showed nearly no corresponding band at 27 kDa. In resting mutant platelets almost no phosphorylation could be detected as well. Upon activation with thrombin, MLC2 phosphorylation of *Myh9* mutant platelets was upregulated, but not to the same extent as seen for wildtype MLC2 phosphorylation (Figure 33A). Phosphorylation of MLC2 at S19 was reduced to approximately 40% in *Myh9*<sup>R702C/+</sup>, to 56% in *Myh9*<sup>D1424N/+</sup> and to 58% in *Myh9*<sup>E1841K/+</sup> platelet lysates (Figure 33B, left). Usage of an antibody against residue p-T18/S19 showed reduced phosphorylation to 40% in *Myh9*<sup>R702C/+</sup>, to 36% in *Myh9*<sup>D1424N/+</sup> and to 72% in *Myh9*<sup>E1841K/+</sup> platelet lysates (Figure 33B, right). These results suggest impaired contractile properties of platelets with heterozygous point mutations in the *Myh9* gene due to the reduced myosin light chain phosphorylation.

## Results

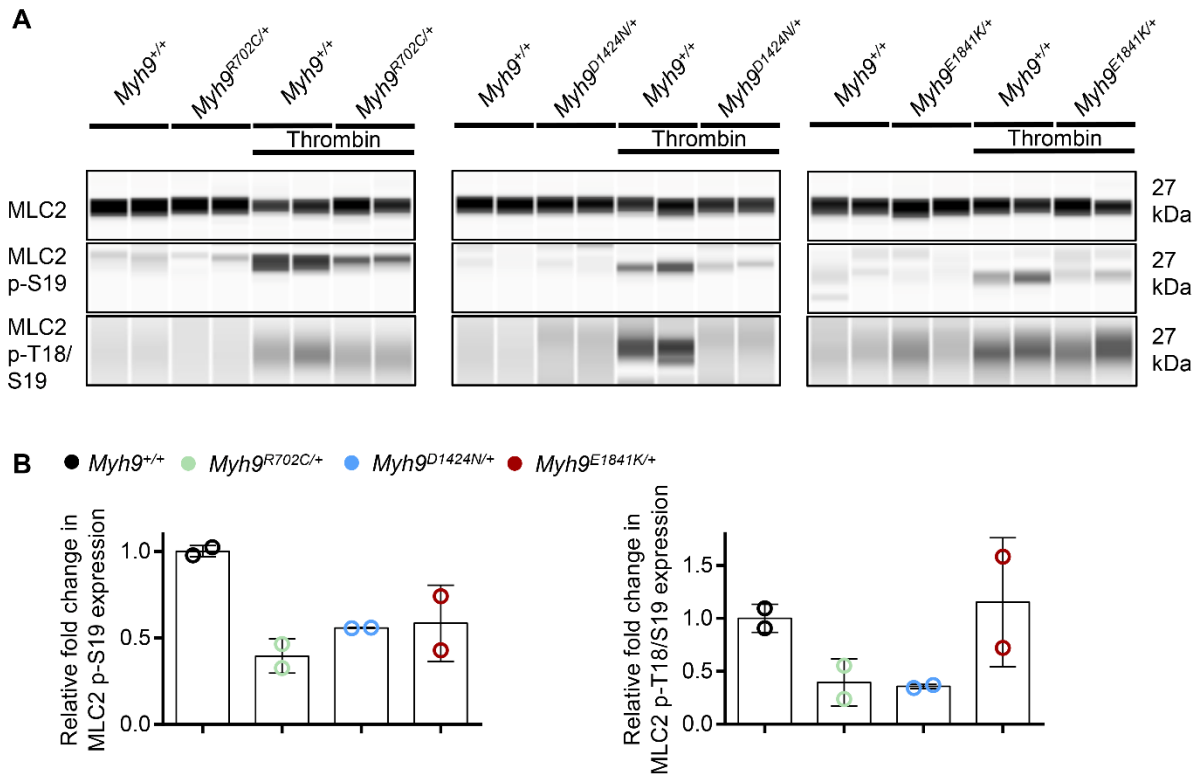
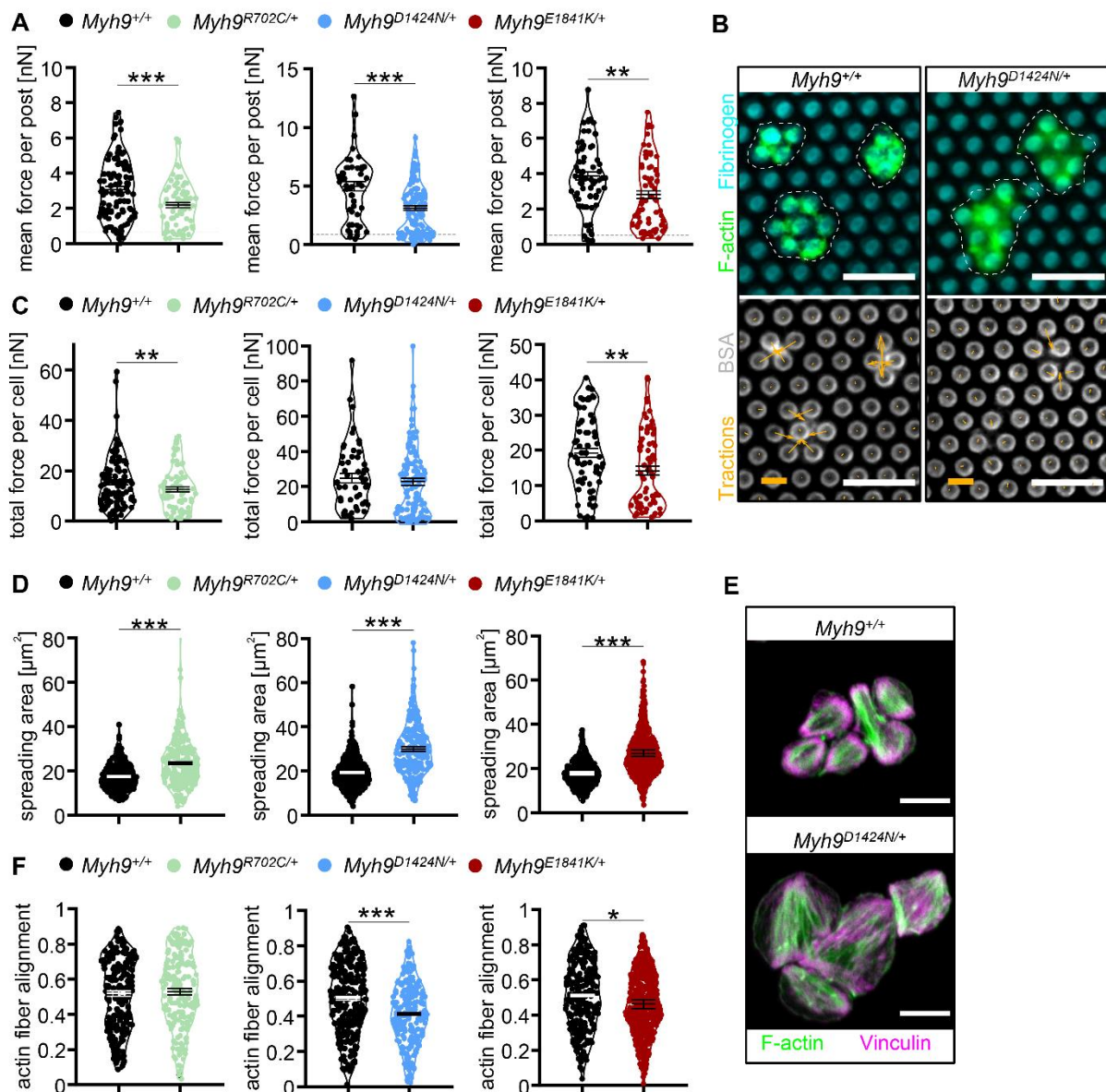


**Figure 33. MLC2 phosphorylation is decreased in *Myh9* mutant platelets.** (A) Expression of total MLC2 and phosphorylated MLC2 at two different phosphorylation sites: p-S19 and p-T18/S19 in resting and thrombin-activated (0.05 U/mL, 1 minute) platelets was determined by using an automated quantitative capillary-based immunoassay platform (ProteinSimple Jess). Representative immunoblot of three independent experiments is shown (n=2). (B) Fold change of pMLC2 p-S19 (left) and pMLC2 p-T18/S19 (right) after activation with thrombin relative to control, which is representative for mouse line D1424N. Each data point indicates one individual platelet lysate sample (n=2; mean  $\pm$  S.D.).

Decreased phosphorylation of MLC2 might impair contractile forces of myosin IIA. Micropost arrays were used to measure cytoskeletal forces of individual platelets transmitted by the actomyosin complex. Platelets adhered to fibrinogen-coated tips and upon shape change, posts were deflected through contractile forces mediated by myosin IIA.<sup>123</sup> All *Myh9* mutant platelets adhered and spread on fibrinogen-coated micropost arrays but pulled at posts to different extents. A reduction for the mean traction force per post was observed by 29% for *Myh9*<sup>R702C/+</sup>, by 38% for *Myh9*<sup>D1424N/+</sup>, and by 28% for *Myh9*<sup>E1841K/+</sup> platelets compared to the respective control (Figure 34A, B lower; arrows indicate traction forces). Considering that one cell covers more than one post, we compared the total force per cell. *Myh9*<sup>R702C/+</sup> and *Myh9*<sup>E1841K/+</sup> platelets generated lower contraction forces per cell compared to respective *Myh9*<sup>+/+</sup> platelets, whereas total force per cell of *Myh9*<sup>D1424N/+</sup> platelets was not significantly different (Figure 34C). The larger spreading area by 55% of *Myh9*<sup>D1424N/+</sup> platelets covered more

## Results

posts, which might compensate for the lower intrinsic contractility, whereas *Myh9<sup>R702C/+</sup>* platelets displayed only a 35% and *Myh9<sup>E1841K/+</sup>* a 51% larger spreading area than respective *Myh9<sup>+/+</sup>* platelets (Figure 34D, 34B upper; dashed white line indicates cell outlines). Confocal images of stained *Myh9<sup>+/+</sup>* and *Myh9<sup>D1424N/+</sup>* platelets show the large spreading area of *Myh9* mutant platelets (Figure 34E). Actin filaments were considerably less bundled in *Myh9<sup>D1424N/+</sup>* and *Myh9<sup>E1841K/+</sup>* platelets and their alignment within single cells was significantly reduced compared to respective *Myh9<sup>+/+</sup>* platelets. However, actin fiber alignment of *Myh9<sup>R702C/+</sup>* platelets was comparable to wildtype control (Figure 34F). These findings strongly suggest a defect in the generation of contractile forces due to mutations in myosin IIA.

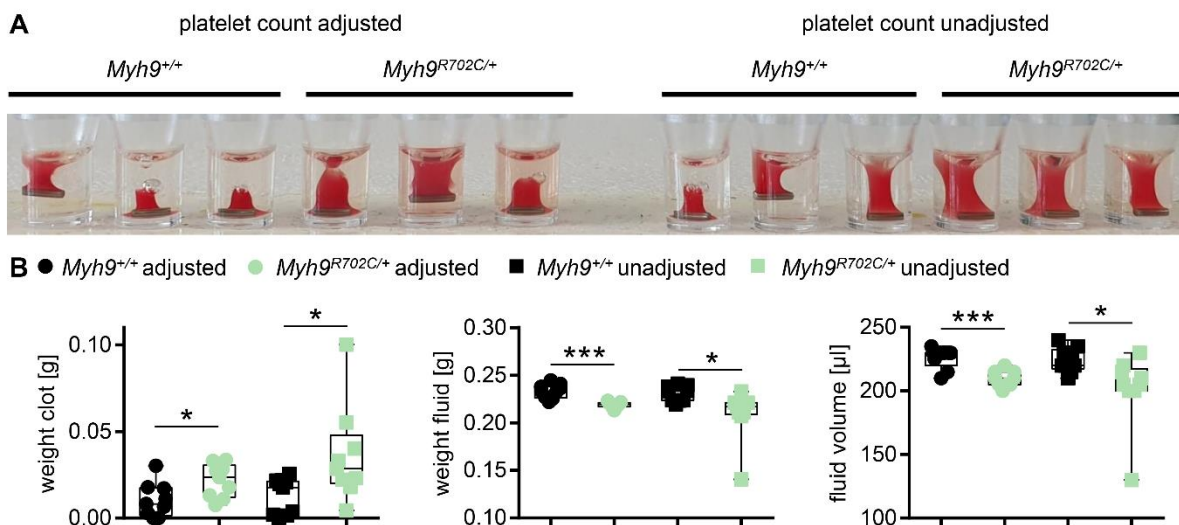




## Results

**Figure 34. Contractile forces of *Myh9* mutant platelets are decreased.** (A) Platelet contractile forces per post, (C) platelet contractile forces with the sum of posts per cell, (D) spreading area and (F) actin fiber alignment of platelets was measured. (A, C, D, F) Values are mean  $\pm$  SEM (*Myh9*<sup>+/+</sup>: n=106; *Myh9*<sup>R702C/+</sup>: n=73; *Myh9*<sup>+/+</sup>: n=51; *Myh9*<sup>D1424N/+</sup>: n=124; *Myh9*<sup>+/+</sup>: n=69; *Myh9*<sup>E1841K/+</sup>: n=74 platelets). Statistics: Mann-Whitney U-test (ns  $p \geq 0.05$ ; \* $0.05 > p \geq 0.01$ ; \*\* $0.01 > p \geq 0.001$ ; \*\*\* $p < 0.001$ ). (B) Representative images of individual platelets (borders of platelets indicated by dashed white line) stained for F-actin (green) on microposts coated with fibrinogen (cyan) on the tips and BSA on laterals (grey). Traction forces of individual platelets pulling on posts are shown in orange (force bars: 10 nN; scale bars: 5  $\mu$ m). (E) Spreading area and actin fiber alignment were assessed by immunostainings of spread platelets on fibrinogen stained for F-actin (phalloidin, green) and vinculin (magenta). Representative images of mouse line D1424N are shown (scale bars 5  $\mu$ m).

Myosin IIA-mediated contractile forces affect compaction and retraction of a clot.<sup>88</sup> Impaired clot contraction was manifested in platelets with heterozygous point mutations in myosin IIA and heterozygous myosin IIA-deficient platelets by a partial failure in clot retraction.<sup>16,83</sup> A total absence of clot retraction was observed in homozygous myosin-deficient platelets.<sup>83</sup> Previously described clot retraction experiments were performed independently of the decreased platelet count in *Myh9* mutant mice. Since the reduced platelet count of the mutant mice might have an effect in this assay, clot retraction in this study was performed with unadjusted and adjusted platelet counts. Clot retraction was significantly impaired in *Myh9* mutant samples compared to controls. Retraction of clots from *Myh9* mutant mice was reduced to a lower extent than controls (Figure 35A, C, E). The heavier non-retracted clots of mutant samples squeezed out less fluid, as quantified by clot weight, as well as weight and volume of residual fluid (Figure 35B, D, F). Even with adjusted platelet count, the extent of clot retraction of *Myh9* mutant samples was reduced (Figure 35). These results support our findings of reduced contractile forces of *Myh9* mutant platelets.



## Results

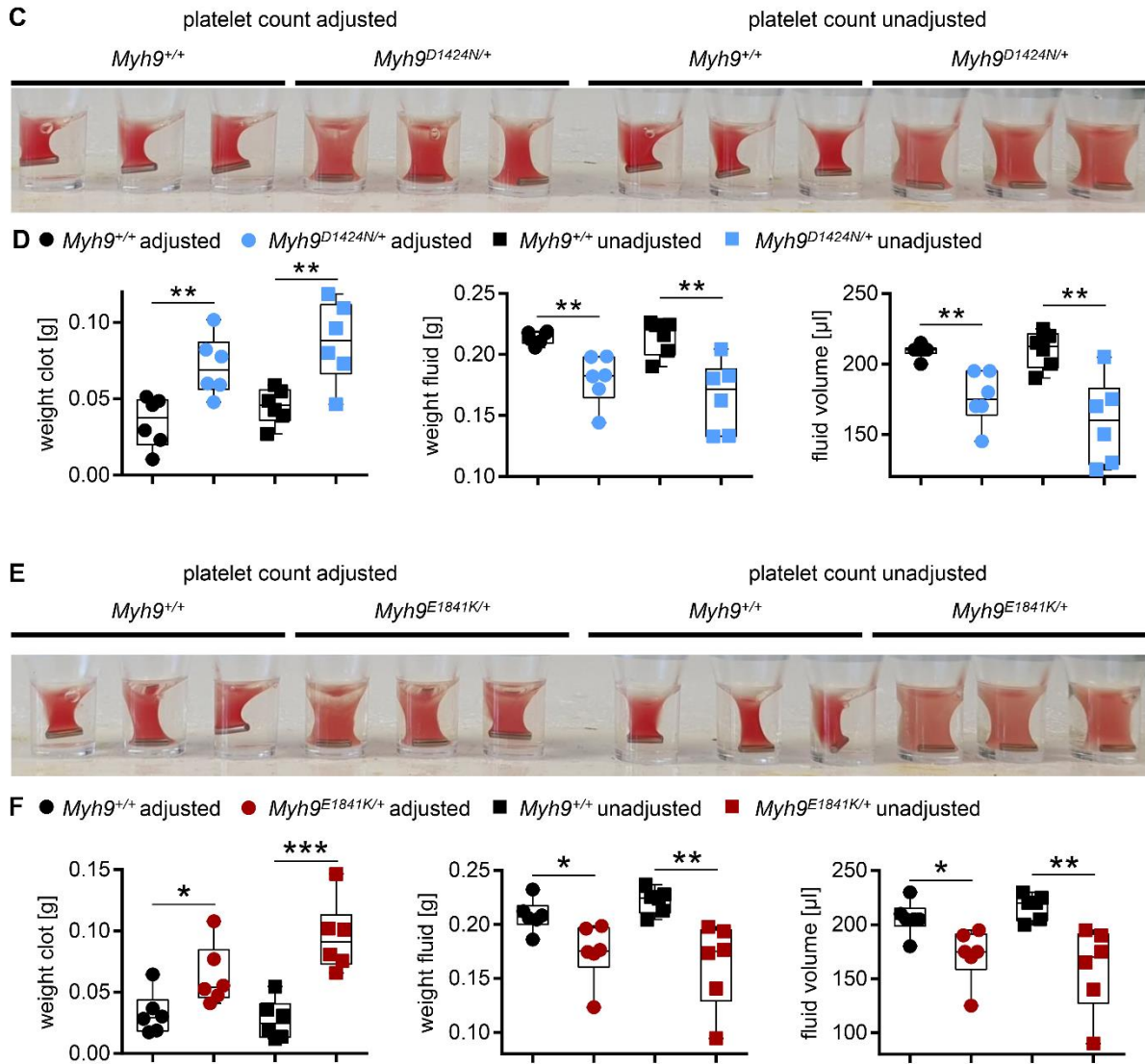


**Figure 35. Extent of clot retraction from *Myh9* mutant samples is reduced.** (A, C, E) Representative images of clot formation from three independent experiments of *Myh9* mutant and control samples at time point 60 minutes are shown (n=3). Platelet count adjusted ( $3 \times 10^5$  platelets/ $\mu\text{L}$ ) conditions are shown on the left and platelet count unadjusted conditions on the right. (B, D, F) Statistical analysis of weight from clot and residual fluid, and of volume from residual fluid are shown in the graphs. Each symbol represents one individual mouse (median  $\pm$  S.D.; Statistics: Multiple comparison using Holm-Sidak \*0.05 > p  $\geq$  0.01; \*\*0.01 > p  $\geq$  0.001; \*\*\*p < 0.001).

## Results

### 5.1.7 Reduced adhesion and interaction forces and decreased thrombus formation of *Myh9* mutant platelets

Stable thrombus formation is not only dependent on contraction forces, but also on the adhesion and interaction forces required to adhere firmly to exposed ECMs. To determine single platelet adhesion and interaction forces we used single platelet force spectroscopy, which allows the measurement of rupture forces from single platelets with minimal platelet activation. A single platelet is picked up by a cantilever coated with low platelet activating collagen (collagen G). The cantilever is brought into contact with HORM collagen and upon cantilever lifting, the deflection of the cantilever is calculated into adhesion force.<sup>124</sup> Adhesion forces of *Myh9* mutant platelets to collagen were reduced by 33% in *Myh9*<sup>R702C/+</sup>, by 69% in *Myh9*<sup>D1424N/+</sup>, and by 42% in *Myh9*<sup>E1841K/+</sup> platelets (Figure 36A). Similarly, interaction forces between two single platelets, one bound to the cantilever, the other adhered to HORM collagen, were reduced by 50% for *Myh9*<sup>R702C/+</sup> platelets, by 39% for *Myh9*<sup>D1424N/+</sup> and by 29% for *Myh9*<sup>E1841K/+</sup> compared to respective *Myh9*<sup>+/+</sup> platelets (Figure 36B). These findings demonstrate, that not only contractile forces of *Myh9* mutant platelets are reduced, but also adhesion and interaction forces are reduced.

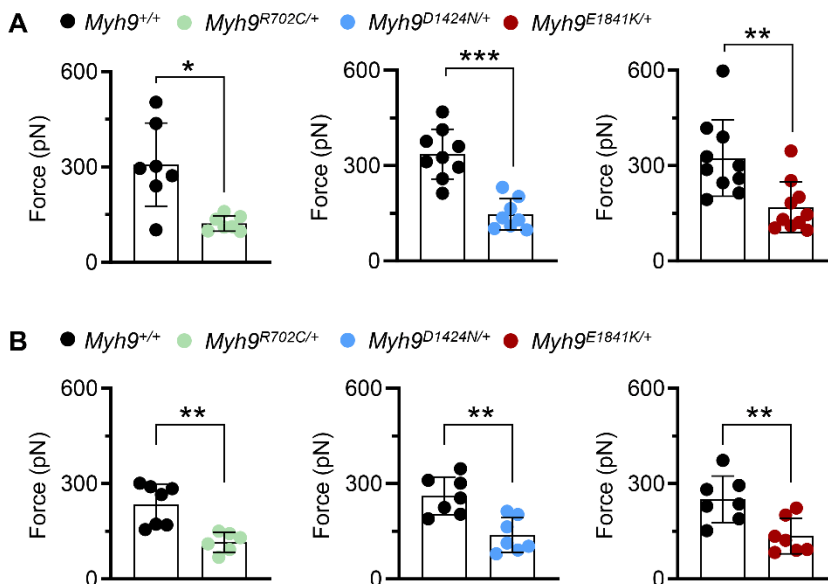
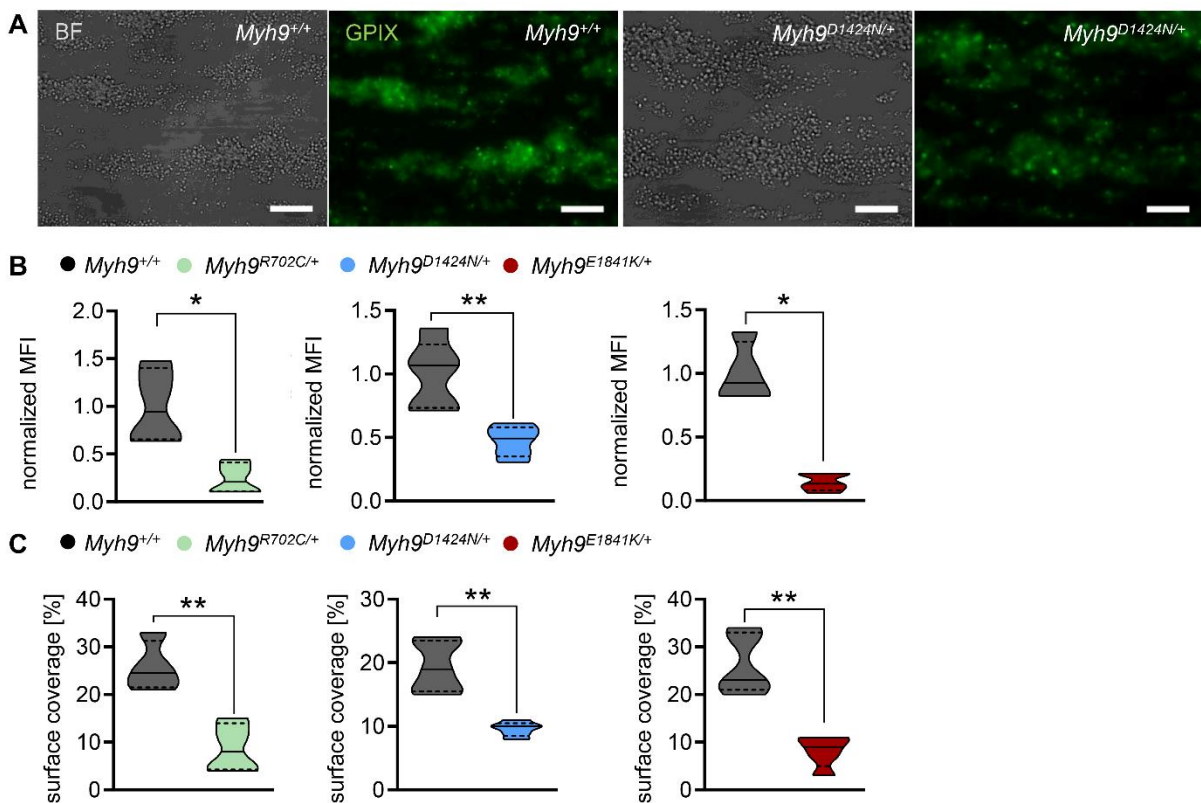


**Figure 36. Lower adhesion and interaction forces of *Myh9* mutant platelets.** SPFS was performed to determine (A) adhesion forces (platelet to collagen) and (B) platelet to platelet interaction forces. Each data point of summary graphs (mean ± S.D.) shows one platelet to collagen (n=7-10) or platelet to platelet (n=7) interaction. Statistics: Mann-Whitney U-test (\*0.05 > p ≥ 0.01; \*\*0.01 > p ≥ 0.001; \*\*\*p < 0.001).

## Results

Next, we were wondering if a stable thrombus can be formed despite of reduced adhesion, interaction, and contraction forces. Therefore, platelet adhesion and thrombus formation under flow conditions were studied. Whole blood was perfused over a collagen-coated surface at shear rates of  $1000\text{ s}^{-1}$ . Control and mutant platelets adhered to collagen and formed thrombi (Figure 37A). However, *Myh9* mutant thrombi were smaller (Figure 37A, B) and surface coverage was reduced on collagen (Figure 37A, C). As the reduced platelet count of *Myh9* mutant mice might have an effect on thrombus formation, the platelet count was adjusted to wildtype platelet count levels. Volume and surface coverage of *Myh9*<sup>R702C/+</sup> and *Myh9*<sup>D1424N/+</sup> thrombi were also significantly reduced under those conditions (Figure 37D-F). Taken together, these results suggest that reduced adhesion (platelet-substrate) and interaction (platelet-platelet) forces lead to reduced thrombus formation of *Myh9*<sup>R702C/+</sup> and *Myh9*<sup>D1424N/+</sup> platelets under shear.



## Results

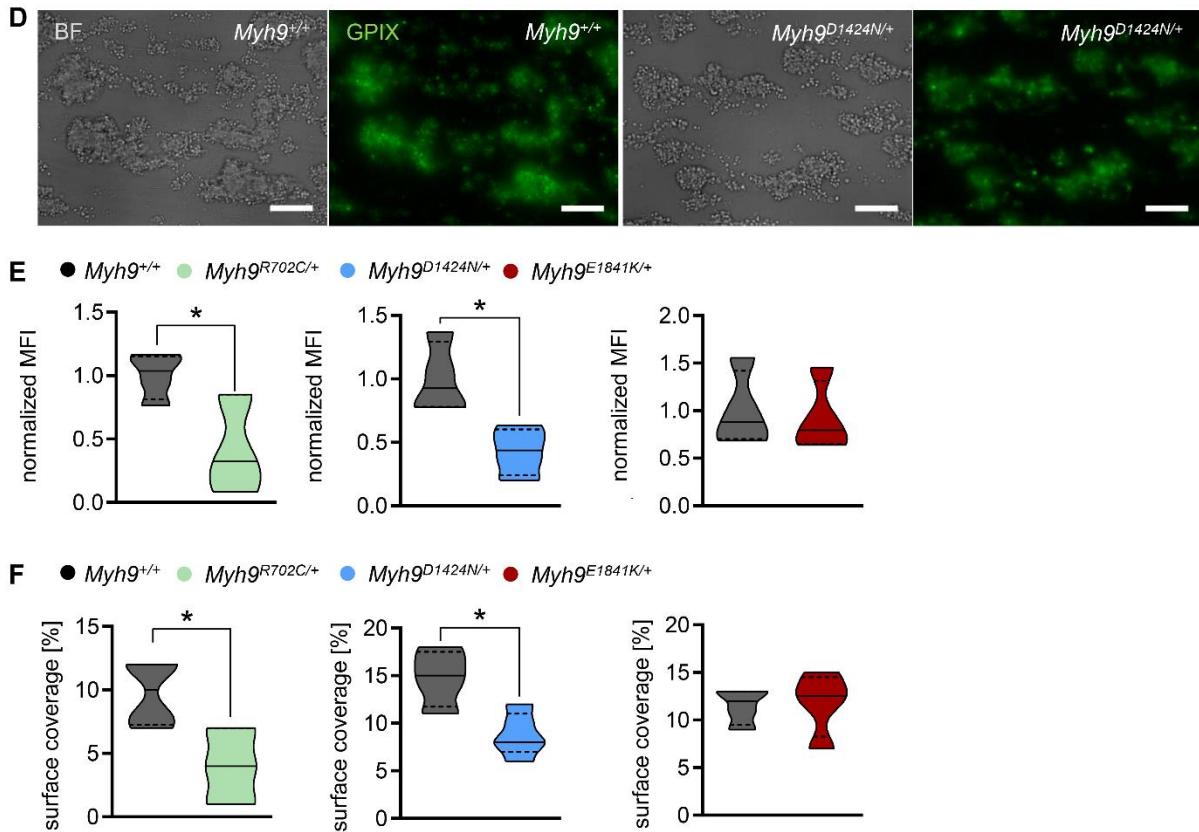


**Figure 37. *Myh9* mutant platelets show reduced thrombus formation under flow.** Platelet adhesion and thrombus formation was assessed under flow (1000/s) when whole blood was perfused over a collagen-coated surface. (A) Representative images of platelet count unadjusted conditions from *Myh9*<sup>D1424N/+</sup> and control platelets taken at the end of perfusion time are shown in brightfield and fluorescence with platelets stained for GPIX (green; scale bars 30  $\mu$ m). Samples of control and *Myh9* mutant platelets with unadjusted platelet count were analyzed for (B) relative normalized fluorescence intensity (MFI) and (C) surface area covered by platelets (%) (mean  $\pm$  S.D.; n=4-5). (D) Representative images of platelet count adjusted conditions from *Myh9*<sup>D1424N/+</sup> and control platelets were analyzed for (E) relative normalized fluorescence intensity (MFI) and (F) surface area covered by platelets (%). Statistics: Mann-Whitney U-test (ns  $p \geq 0.05$ ; \* $0.05 > p \geq 0.01$ ; \*\* $0.01 > p \geq 0.001$ ).

To investigate thrombus stability, colloidal probe spectroscopy was performed on thrombi to determine thrombus stiffness. Thrombi formed under unadjusted platelet count conditions were measured to recapitulate the situation *in vivo*. Thrombi formed by *Myh9* mutant platelets were significantly softer than thrombi formed by wildtype platelets (Figure 38). These results show that the mechanical characteristics of mouse platelets with point mutations are altered. The reduced thrombus formation and increased softness of *Myh9* mutant thrombi are consistent with the reduced adhesion and interaction forces of *Myh9* mutant platelets.

## Results

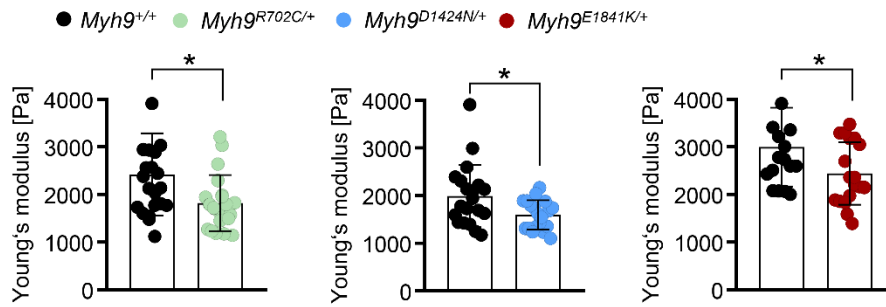


**Figure 38. *Myh9* mutant thrombi are softer as measured by colloidal probe spectroscopy.** Each data point of colloidal probe spectroscopy shows the median Young's modulus of one aggregate of control or *Myh9* mutant sample. Bar plots show mean  $\pm$  S.D. of Young's modulus (n=4-5). Statistics: Mann-Whitney U-test ( $*0.05 > p \geq 0.01$ ).

### 5.1.8 Impaired hemostasis in *Myh9* mutant mice

After we had analyzed *ex vivo* thrombus formation, hemostatic plug formation was studied *in vivo* in order to investigate the influence of the three mutations in myosin IIA on the hemostatic function. Bleeding times in saline after tail tip amputation were prolonged for the *Myh9* mutant mice (Figure 39) consistent with previously published data.<sup>16</sup> This suggests impaired hemostasis in *Myh9* mutant mice due to reduced platelet forces.

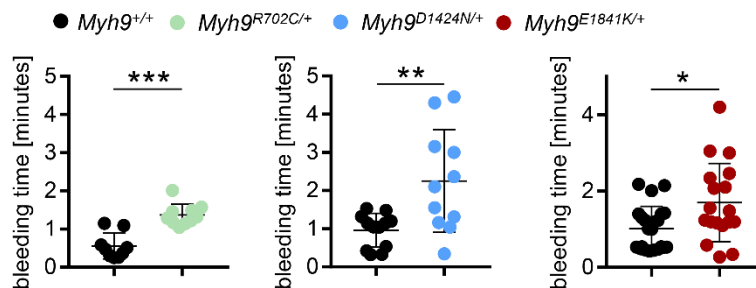


**Figure 39. Mutations in myosin IIA lead to impaired hemostatic function.** A 1 mm segment of the mouse tail tip was cut, and tail was put in saline to observe bleeding until no blood drop was observed. Each symbol represents one individual mouse (mean  $\pm$  S.D.). Statistics: Mann-Whitney U-test ( $*0.05 > p \geq 0.01$ ;  $**0.01 > p \geq 0.001$ ;  $***p < 0.001$ ).

## Results

### 5.2 Analyses of samples from *MYH9*-RD patients

#### 5.2.1 Platelets of *MYH9*-RD patients are stiffer under resting conditions

We received blood from *MYH9*-RD patients with either a point mutation at amino acid position D1424N or E1841K to verify the results obtained from *Myh9* mutant mice. The two patients were invited to the Institute for Immunology and Transfusion Medicine at the University of Greifswald three times each, and blood was taken from healthy donors and the patients (*MYH9* p.D1424N, *MYH9* p.E1841K). Blood cell parameters were analyzed with a hematology analyzer for counts of white and red blood cells, and platelets, as well as other parameters of the red blood cells (hemoglobin and hematocrit) Platelet count of patient blood was strongly decreased to 8 – 26% (Table 4). Other parameters for RBCs and WBCs as well as hemoglobin and hematocrit levels were unaltered.

**Table 4. Blood parameters of *MYH9*-RD patients.** Patient blood with mutations at amino acid position 1424 and 1841 were analyzed for blood cell parameters, measured with a Sysmex Hemato Analyzer poch-100i (n=1). Abbreviations: WBC white blood cell; LYM lymphocyte; MON monocyte; NEUT neutrophils; PLT platelets; RBC red blood cell; HGB hemoglobin; HCT hematocrit. Statistics: Mann-Whitney U-test (ns  $p \geq 0.05$ ; \*\* $0.01 > p \geq 0.001$ ; \*\*\* $p < 0.001$ ).

	control	<i>MYH9</i> p.D1424N	significance	control	<i>MYH9</i> p.E1841K	significance
WBC [10 <sup>3</sup> /μL]	4.7	4.3	ns	5.1	4.0	ns
LYM [10 <sup>3</sup> /μL]	1.9	1.6	ns	2.2	1.6	ns
MON [10 <sup>3</sup> /μL]	0.5	0.6	ns	0.4	0.2	ns
NEUT [10 <sup>3</sup> /μL]	2.3	2.1	ns	2.5	2.2	ns
PLT [10 <sup>3</sup> /μL]	188	15	***	197	51	**
RBC [10 <sup>6</sup> /μL]	3.67	4.64	ns	3.88	4.25	ns
HGB [mmol/L]	7.0	8.4	ns	7.5	7.7	ns
HCT [L/L]	0.323	0.394	ns	0.343	0.372	ns

## Results

The macrothrombocytopenia of *MYH9*-RD patients was confirmed by RT-FDC with a significantly increased platelet size (Figure 40A). In line with the mouse data, RT-FDC revealed patient platelets to be stiffer, as shown by a decreased median deformation (Figure 40B). In the scatter plots, decreased deformation and increased size can be observed by a shift of event density to the lower right (Figure 40C).

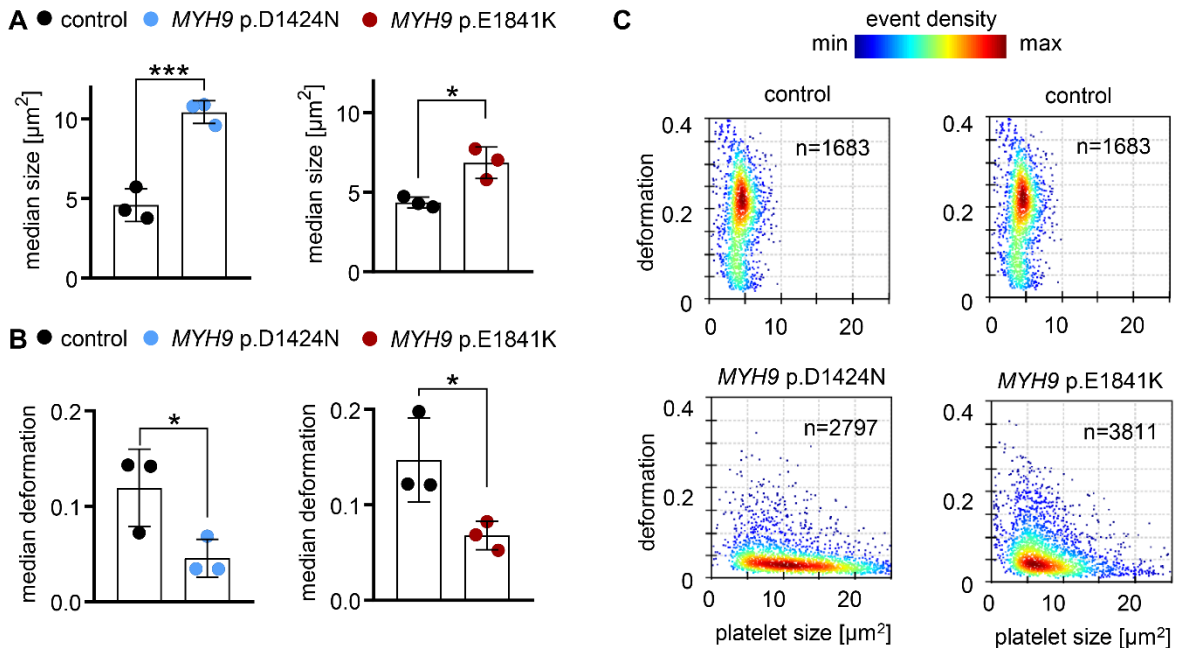


**Figure 40. Platelets of *MYH9*-RD patients show decreased deformability.** RT-FDC measurements show (A) platelet size and (B) deformation of platelets from *MYH9*-RD patients and controls after bleeding into ACD. Summary data points show the median values of individual healthy donors and one *MYH9* p.D1424N or p.E1841K patient on three different days and bar plots show mean  $\pm$  S.D. of platelet deformation and size from non-stimulated platelets. Statistics: Multiple comparison using Holm-Sidak ( $*0.05 > p \geq 0.01$ ;  $***p < 0.001$ ). (C) Representative KDE scatter plots showing the distribution of single platelet deformability in relation to size of platelets from healthy donors and *MYH9*-RD patients (n= number of single platelets).

### 5.2.2 Faster adhesion of *MYH9*-RD patient platelets on fibrinogen

Blood taken from *MYH9*-RD patients and donors in Greifswald was transported to Würzburg and analyzed for spreading behavior. DIC imaging revealed platelets from *MYH9*-RD patients were able to adhere to fibrinogen and change their initially discoid shape. Platelets from *MYH9* p.D1424N patient revealed fast spreading characteristics, with 90% of the platelets reaching full spreading after 15 minutes incubation. Control platelets were much slower in spreading kinetics, which might be explained by the extremely increased size of *MYH9* p.D1424N platelets (Figure 41A; upper). In case of



## Results

the *MYH9* p.E1841K patient more fully spread platelets could be observed compared to control, even if not to the same extent of *MYH9* p.D1424N platelets (Figure 41A; lower). Mutant platelets formed lamellipodia on fibrinogen, as revealed by PREM. Although platelets from myosin IIA knockout mice failed to form F-actin stress fibers,<sup>83</sup> platelets from *MYH9*-RD patients were able to form stress fiber-like structures on fibrinogen after 15 minutes spreading (Figure 41B, arrowhead).

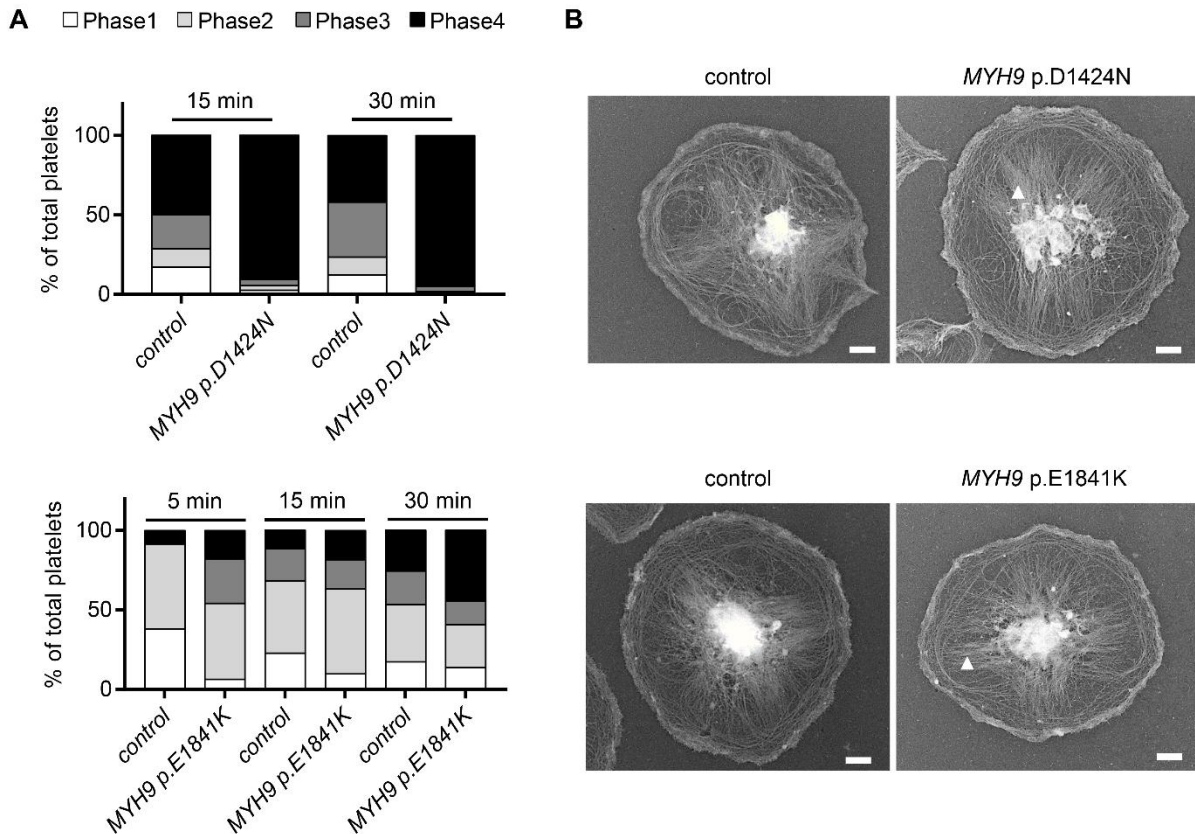


**Figure 41. Faster adhesion and spreading of platelets from *MYH9*-RD patients on fibrinogen.** (A) Washed control and patient platelets were allowed to spread on fibrinogen in the presence of thrombin and fixed at indicated time points (n=1). Platelets were categorized in four different spreading phases. Phase I: resting platelets; Phase II: platelets with filopodia; Phase III: platelet with filopodia and lamellipodia; Phase IV: fully spread platelets with only lamellipodia (“fried-egg-like” shape). No statistics are provided since n=1 each. (B) Representative PREM images of the cytoskeleton ultrastructure of platelets from *MYH9*-RD patients and healthy donors spread on fibrinogen in the presence of thrombin (scale bars 1  $\mu$ m; arrowheads indicate stress fiber-like structures).

## Results

Next, resting platelets on poly-L-lysine were stained with antibodies and analyzed by confocal microscopy. Microtubules were located in a ring structure at the periphery of the cell in control and mutant platelets (Figure 42). The intact microtubule ring structure demonstrates that platelets were not (pre-)activated during transport.

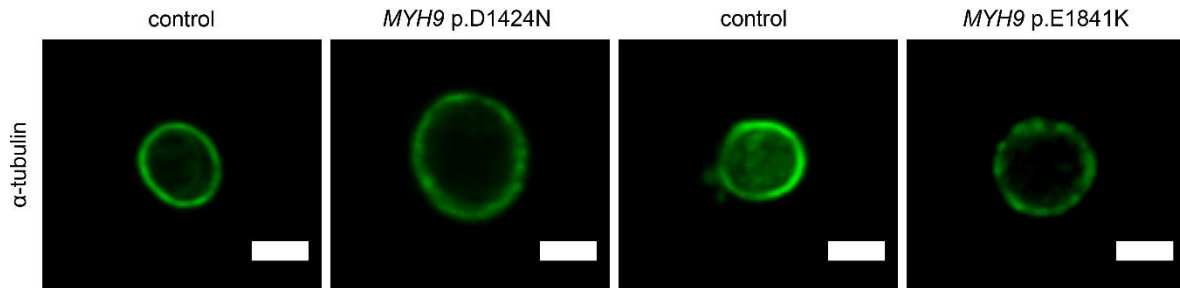
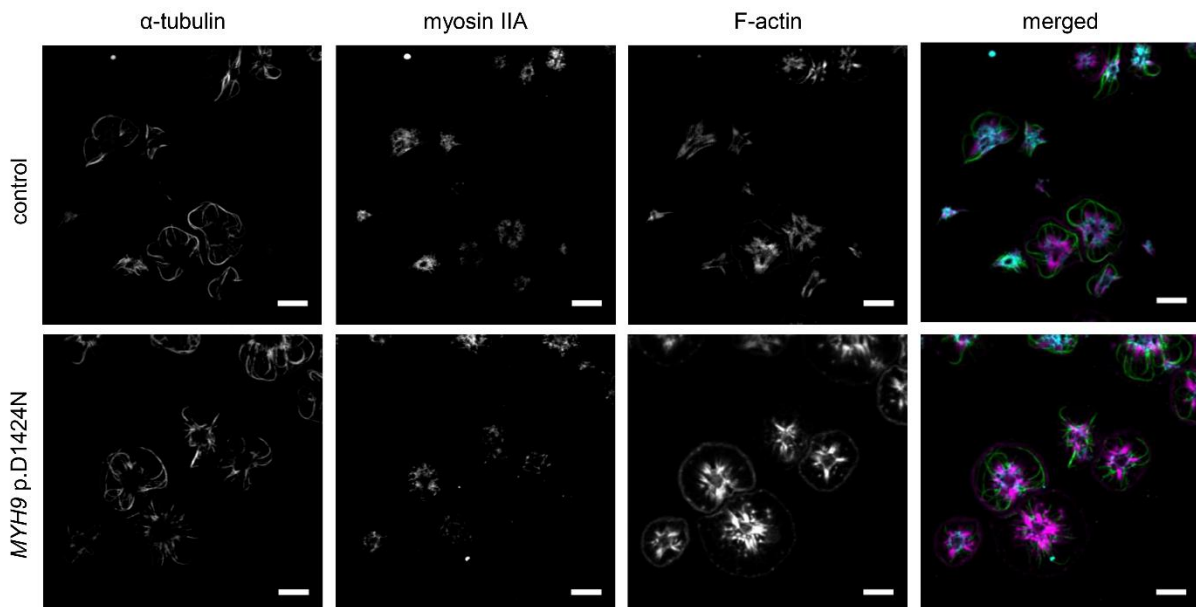


**Figure 42. Marginal band is present in transported control and mutant platelets.** Confocal microscopy images of resting platelets from healthy donor and *MYH9*-RD patient were performed after staining of  $\alpha$ -tubulin (green). Scale bars: 2  $\mu$ m.

The localization of myosin IIA in spread platelets on fibrinogen was investigated and immunostainings revealed a comparable distribution of myosin IIA in patient and control samples.  $\alpha$ -tubulin was rearranged over the whole cell, F-actin was arranged in stress fiber-like structures and an overall comparable distribution of cytoskeletal components in spread mutant platelets on fibrinogen could be observed (Figure 43).



## Results

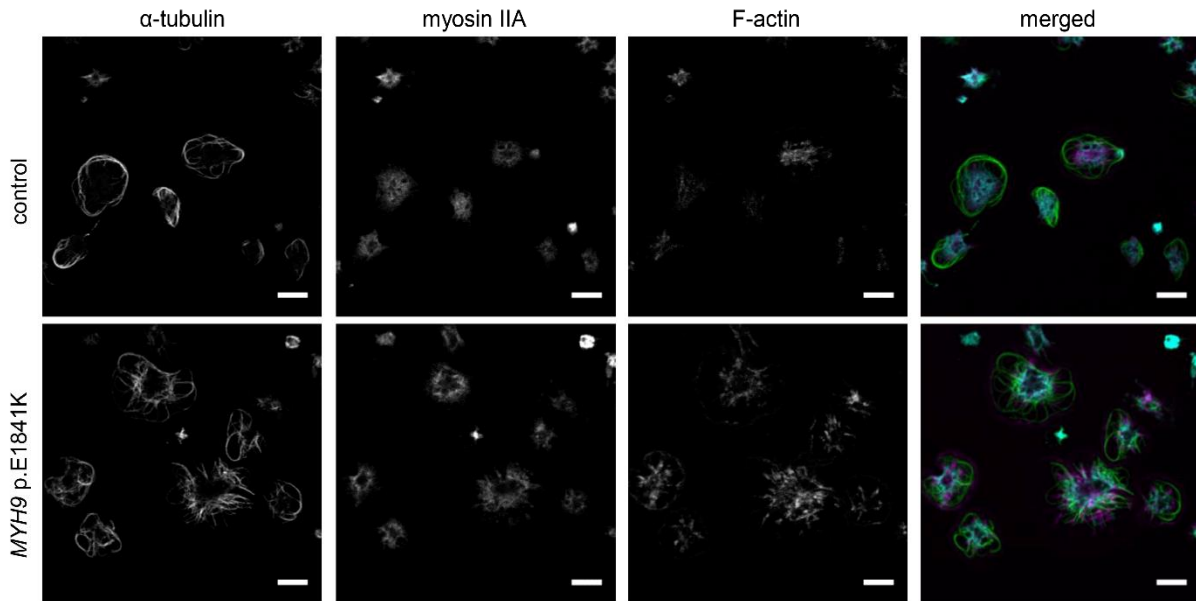


**Figure 43. Platelets of *MYH9*-RD patients can spread on fibrinogen and rearrange F-actin.** Representative confocal microscopy images of spread platelets from healthy donor and *MYH9*-RD patients on fibrinogen in the presence of thrombin are shown (scale bars 5  $\mu$ m). Cytoskeleton components were stained after fixation of 30 minutes spread platelets ( $\alpha$ -tubulin (green), myosin IIA (cyan) and F-actin (phalloidin, magenta)).

### 5.2.3 Impaired thrombus formation of platelets from *MYH9*-RD patients

*Ex vivo* thrombus formation of platelets from mutant mice was impaired even when platelet count had been adjusted before, except for *Myh9*<sup>E1841K/+</sup> samples (Figure 37). Platelet counts of *MYH9*-RD patients were extremely decreased (to 8 – 26% (Table 4)), which makes it impossible to adjust platelet count for the experiments using patient blood. Therefore, a flow chamber assay was performed with unadjusted platelet count, reflecting the situation in the patient. Platelets of *MYH9*-RD patients were able to bind to collagen and form thrombi, but at much lower level than platelets of healthy donors. Area and volume of single thrombi were significantly decreased for patient whole blood (Figure 44A, B). Moreover, determination of the kinetics of thrombus formation over time revealed that mutant platelets covered less area, as observed for healthy donor platelets (Figure 44C, D).

## Results

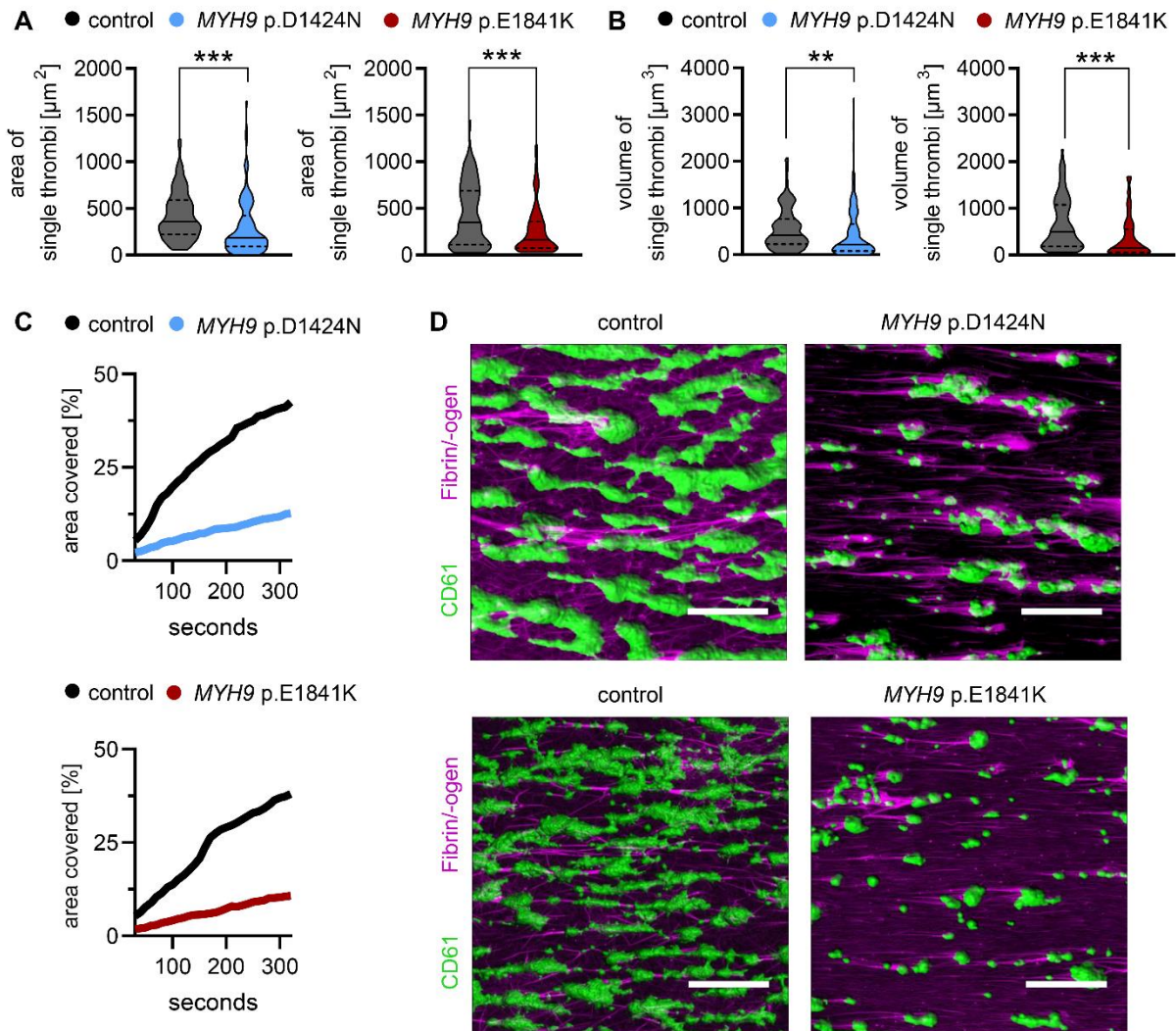


**Figure 44. Thrombi of *MYH9*-RD patient platelets are smaller.** Platelet adhesion and aggregate formation of human patient samples on collagen under flow were assessed using a flow chamber with a shear rate of 1000/s. Platelet count of patient samples were not adjusted. (A) Area and (B) volume of single thrombi are shown as median  $\pm$  quartiles ( $n=100$  single thrombi). Statistics: Mann-Whitney U-test ( $**0.01 > p \geq 0.001$ ;  $***p < 0.001$ ). (C) Area covered over time shows the mean coverage of thrombi from healthy control and patient blood. (D) Representative fluorescent images with platelets in green (CD61) and fibrin-ogen in magenta were taken at the end of the perfusion time (20 minutes). Scale bars: 50  $\mu\text{m}$ .

Next, stiffness of *Myh9* mutant thrombi was measured after the sample run using colloidal probe spectroscopy (atomic force microscopy [AFM]). In agreement to the data obtained from *Myh9*<sup>D1424N/+</sup> mutant mice, *MYH9* p.D1424N thrombi were softer than healthy donor thrombi. In contrast, stiffness of thrombi from the sample of the patient with amino acid exchange E1841K was comparable to control, with only a slight tendency to be softer (Figure 45).

## Results

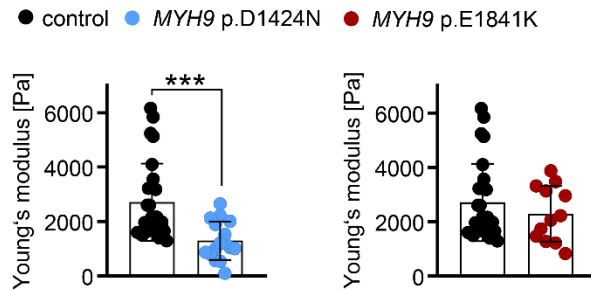


**Figure 45. Thrombi of platelets from the *MYH9* p.D1424N patient are softer.** Colloidal probe spectroscopy was performed with whole blood from healthy donors and *MYH9*-RD patients. Bar plots show mean  $\pm$  S.D. of Young's modulus and each data point represents the median Young's modulus of one aggregate of healthy donor or *MYH9*-RD patient sample. Statistics: Mann-Whitney U-test (ns  $p \geq 0.05$ ; \*\* $0.01 > p \geq 0.001$ ).

Mouse and human data were overall comparable with some exceptions when platelets from mice and patients with the mutation E1841K were used. In more detail this concerns the unaffected thrombus formation of *Myh9*<sup>E1841K/+</sup> platelets under adjusted platelet count conditions and the unaffected thrombus stiffness of *MYH9* p.E1841K patient platelets. Our data suggests that mechanical characteristics measured for mouse platelets largely recapitulate characteristics of human platelets and thus, data received from mice with point mutations in myosin IIA can be transferred to the patient situation.

## Results

### 5.3 Treatment with TXA and magnesium supplementation

#### 5.3.1 TXA improves clot retraction and stabilizes plasminogen-induced fibrinolysis of *Myh9* mutant platelets

Myosin light chain phosphorylation, responsible for generating forces in platelets, was decreased in myosin IIA mutant platelets (Figure 32). Lower adhesion, interaction and traction forces might be responsible for reduced thrombus formation and delayed clot retraction (Figure 34-36). Thrombi composed of platelets with myosin IIA mutations were determined to be softer (Figure 38). Based on these data and the impaired hemostasis in *Myh9* mutant mice, we assumed that thrombi of patients and mutant mice are less compact. Actomyosin contractile machinery mediates the formation of compacted fibrin in a clot, which is reduced in myosin IIA-inhibited cells.<sup>66</sup> It is known that TXA can shorten bleeding time in patients with inherited thrombocytopenia.<sup>57,68,69</sup> TXA blocks the lysine binding site of plasminogen. Plasmin can still be formed but is unable to bind and degrade fibrin.<sup>125,126</sup> For thrombi consisting of myosin IIA mutated platelets, we hypothesized that plasminogen could better fill the gaps between platelets of these less compact clots and solve the clot through increased fibrinolysis. Further, we hypothesized that upon treatment with TXA, plasmin-induced clot lysis decreases, and the clot can be stabilized. To verify this hypothesis, we performed some experiments with TXA treatment and rtPA, that induces clot lysis. TXA had no major impact on clot retraction under standard conditions, most likely because this assay is not supposed to show clot lysis and the mode of TXA action is in prevention of clot lysis (Figure 46A). Treatment of samples with rtPA at the start of experiment showed a concentration-dependent clot lysis for wildtype and mutant samples. A threshold concentration was found, where lysis still occurred (0.0138 nM rtPA; Figure 46B). PRP of *Myh9* mutant and control mice were treated prior to experiment with rtPA and/or TXA in different concentrations. Untreated mutant samples showed a delayed clot retraction as previously shown (Figure 35).<sup>16</sup> Upon rtPA addition clots of either control or mutant samples were lysed. The addition of TXA in concentrations of 10 mM and 100  $\mu$ M inhibited the fibrinolytic effect of rtPA and restored clot retraction. 1  $\mu$ M TXA did not rescue clot retraction and lysis occurred (Figure 46C).

## Results

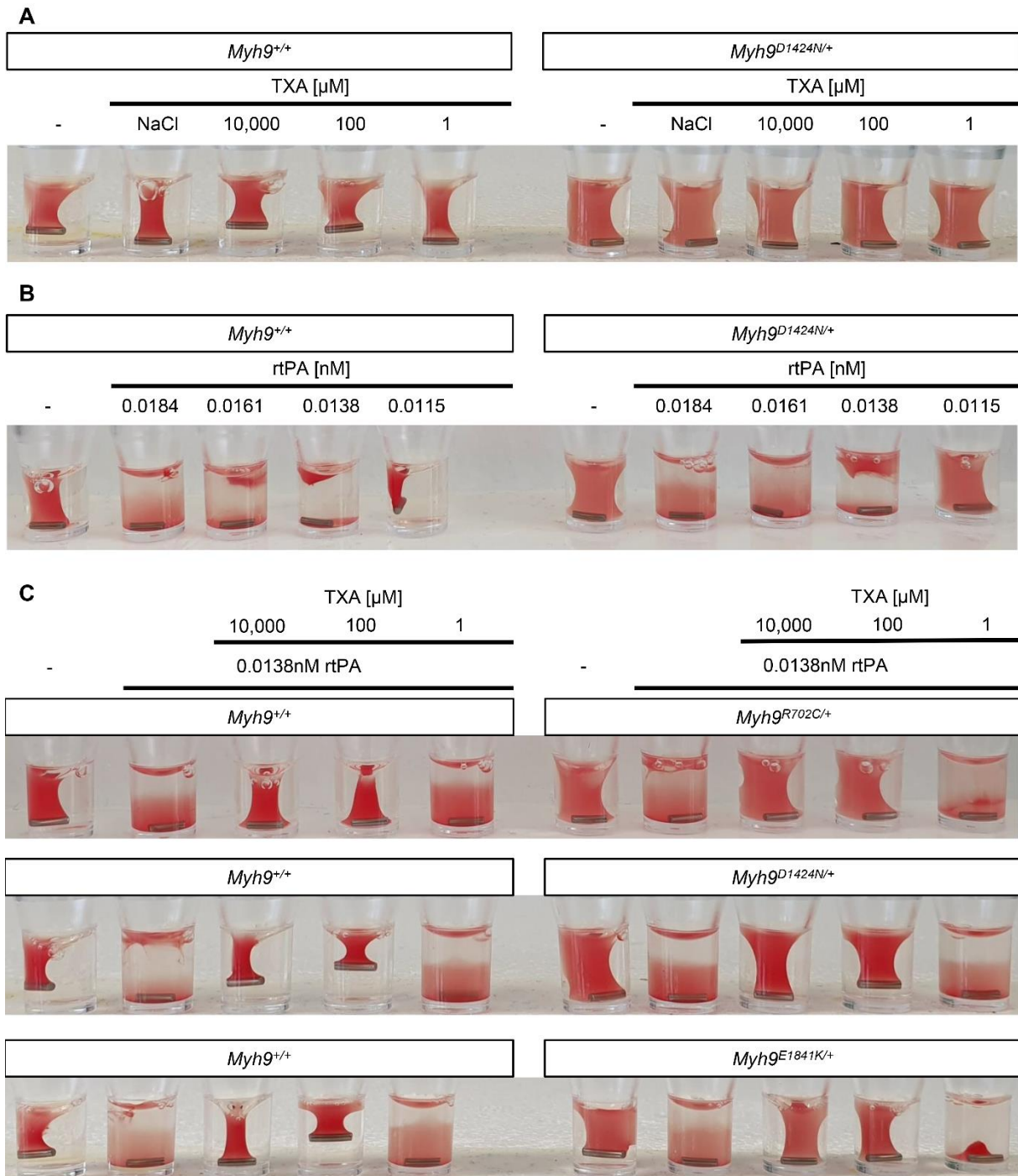


**Figure 46. Inhibition of rtPA-induced clot lysis can be reverted by high concentrations of TXA.** PRP from *Myh9*<sup>+/+</sup> and *Myh9*<sup>D1424N/+</sup> mice was treated with different concentrations of (A) TXA and (B) rtPA. (A) Clot retraction with TXA concentrations of 10 mM, 100  $\mu$ M and 1  $\mu$ M. (B) Identification of threshold concentration of rtPA with different concentrations indicated 0.0138 nM rtPA as threshold concentration with lysis of clots from control and *Myh9* mutant sample. (C) PRP of all three mouse lines was treated with threshold concentration of rtPA and TXA in different concentrations. (A-C) Representative images of three independent experiments are shown.

Quantification of clots and fluid proved clot lysis in rtPA treated samples and when treated with rtPA in combination with 1  $\mu$ M TXA. Addition of high concentrations of TXA

## Results

(10 mM and 100  $\mu$ M) to 0.0138 nM rtPA treated clots restored clot retraction to the extent of untreated samples and improved clot retraction significantly compared to rtPA treated samples (Figure 47).

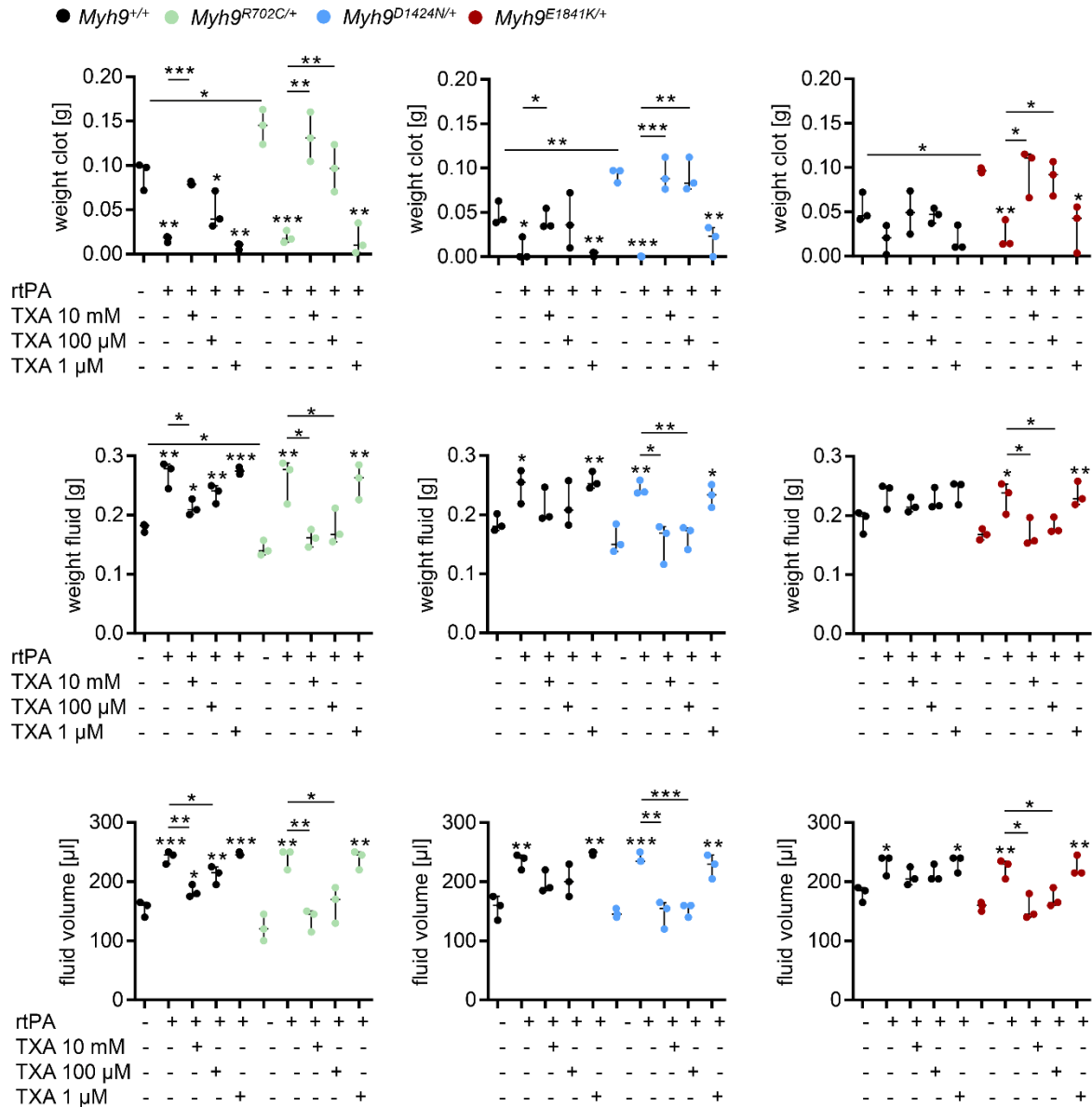


**Figure 47. Clot retraction is improved with high concentrations of TXA.** Clot retraction of PRP treated with 0.0138 nM rtPA and/or TXA in different concentrations was quantified. Weight of clot and fluid, and volume of fluid are given as mean  $\pm$  S.D. (n=3). Statistics: Mann-Whitney U-test (ns  $p \geq 0.05$ ; \* $0.05 > p \geq 0.01$ ; \*\* $0.01 > p \geq 0.001$ ; \*\*\* $p < 0.001$ ). Stars above symbols indicate comparison to untreated control or untreated mutant sample.

Prolonged times of mutant mice *in vivo* was observed in a filter paper model (Figure 48). After intravenous injection of 10  $\mu$ g/g TXA 5 minutes prior to the experiment, bleeding times of *Myh9* mutant mice and corresponding controls were observed.



## Results

Bleeding times of *Myh9*<sup>R702C/+</sup> and *Myh9*<sup>E1841K/+</sup> mutant mice were significantly reduced to bleeding times of wildtype mice (Figure 48). TXA-treated *Myh9*<sup>D1424N/+</sup> mice showed no significant difference in bleeding times. While 43% of untreated and 50% of sodium chloride treated mice showed bleeding times shorter than 10 minutes, 100% of TXA treated *Myh9*<sup>D1424N/+</sup> mice had bleeding times shorter than 10 minutes. In summary, the increased bleeding phenotype and lower extent of clot retraction caused by reduced platelet forces in *Myh9* mutant mice can be rescued with TXA.

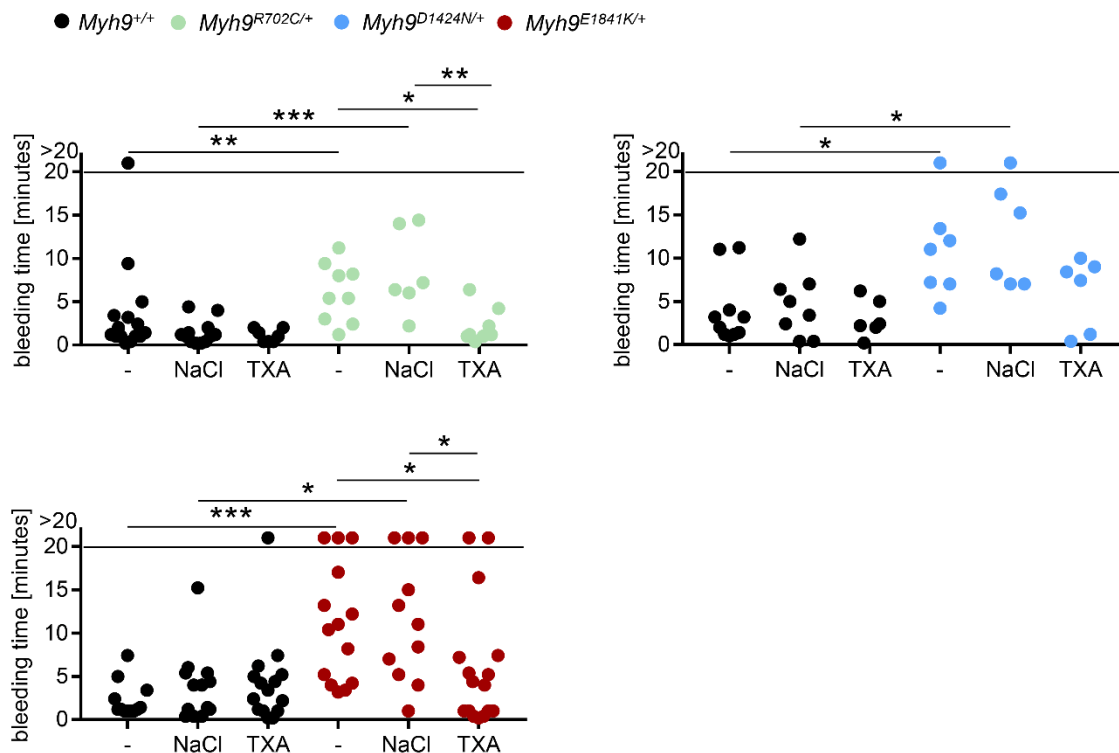


**Figure 48. Hemostasis can be improved by TXA *in vivo*.** Tail bleeding time measurements with filter paper were performed with all three mouse lines under treatment by TXA. A 1 mm segment of the mouse tail tip was cut, and bleeding was observed until no blood drop could be seen on filter paper. Each symbol represents one individual mouse (mean  $\pm$  S.D.). Mann-Whitney-U test was used to analyze data excluding data points exceeding 20 minutes (ns  $p \geq 0.05$ ; \* $0.05 > p \geq 0.01$ ; \*\* $0.01 > p \geq 0.001$ ; \*\*\* $p < 0.001$ ).

To confirm the hypothesis of increased fibrinolysis in less compact *Myh9* mutant clots, we performed an extrinsic tissue factor-activated thromboelastometry assay. The addition of tissue factor to citrated blood enables the acquisition of parameters of the extrinsic coagulation pathway, including information about clot formation and degradation through fibrinolysis. ROTEM verified the results of reduced clot formation and stabilization from blood samples of human patients and *Myh9* mutant mouse blood (Figures 37, 38, 44, 45, 46, 47). Clot time (CT) and clot formation time (CFT) were

## Results

prolonged in blood samples of *MYH9*-RD patients (Figure 49A, B). ROTEM revealed an earlier onset of lysis (LOT) in samples with *MYH9*-RD platelets (Figure 49A, C). The clot with *MYH9*-RD platelets was lysed quicker than control clots upon addition of rtPA in a final concentration of 137 ng/mL. Coincubation of rtPA (137 ng/mL) and TXA (100  $\mu$ M) slowed down the start of lysis, as represented by the time needed to decrease clot firmness by 15% (LOT; Figure 49A, C). Time needed to decrease clot firmness by 90% was prolonged in samples of *MYH9*-RD patients with the addition of TXA as well (LT; Figure 49A, C). Furthermore, the thrombodynamic potential index, representing clot density, was lower in clots of patient samples than controls (control: 52; *MYH9* p.D1424N: 17; *MYH9* p.E1841K: 51). These results support the hypothesis that *Myh9* mutant thrombi are more instable than control thrombi and TXA prevents plasmin-induced clot lysis.

## Results

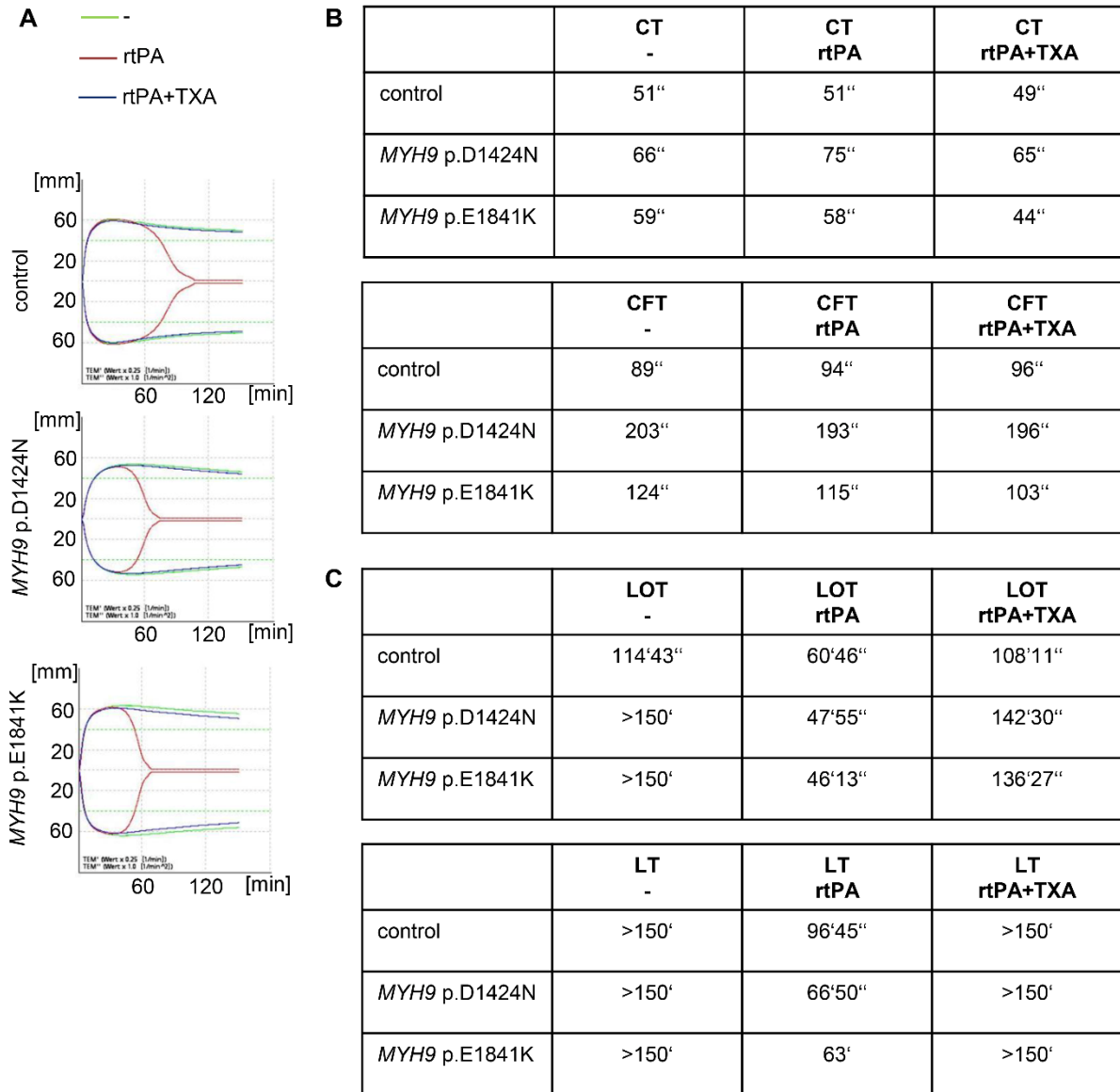


**Figure 49. Lysis of *Myh9* mutant clot is delayed with TXA.** Control and *MYH9*-RD patient blood was analyzed without treatment (green), with rtPA-treatment (red) and with treatment of rtPA and TXA (blue). Curves (A) and respective values of (B) CT and CFT, and (C) LOT and LT are given. Thromboelastometry defines clot time (CT) as the time until 2 mm amplitude is reached, and clot formation time is defined as the time between an amplitude of 2 mm and 20 mm. Lysis onset time (LOT) is defined as the time until clot firmness drops by 15% and lysis time (LT) as the time until clot firmness decreased by 90% (ˆ minutes; ˆˆ seconds).

To investigate whether fibrin formation in the flow chamber assay might be improved in the presence of TXA, we performed flow chamber assays with patient platelets treated with TXA. Whole blood from patients and healthy donors was perfused over a collagen-coated surface. Fibrin in control and mutant samples treated with rtPA, was completely degraded, but was delayed in samples treated with TXA, or a combination of TXA and rtPA (Figure 50A, B). TXA improved not only fibrin formation and

## Results

stabilization, but also delayed the decrease of thrombus volume of control and mutant samples over time (Figure 50B).

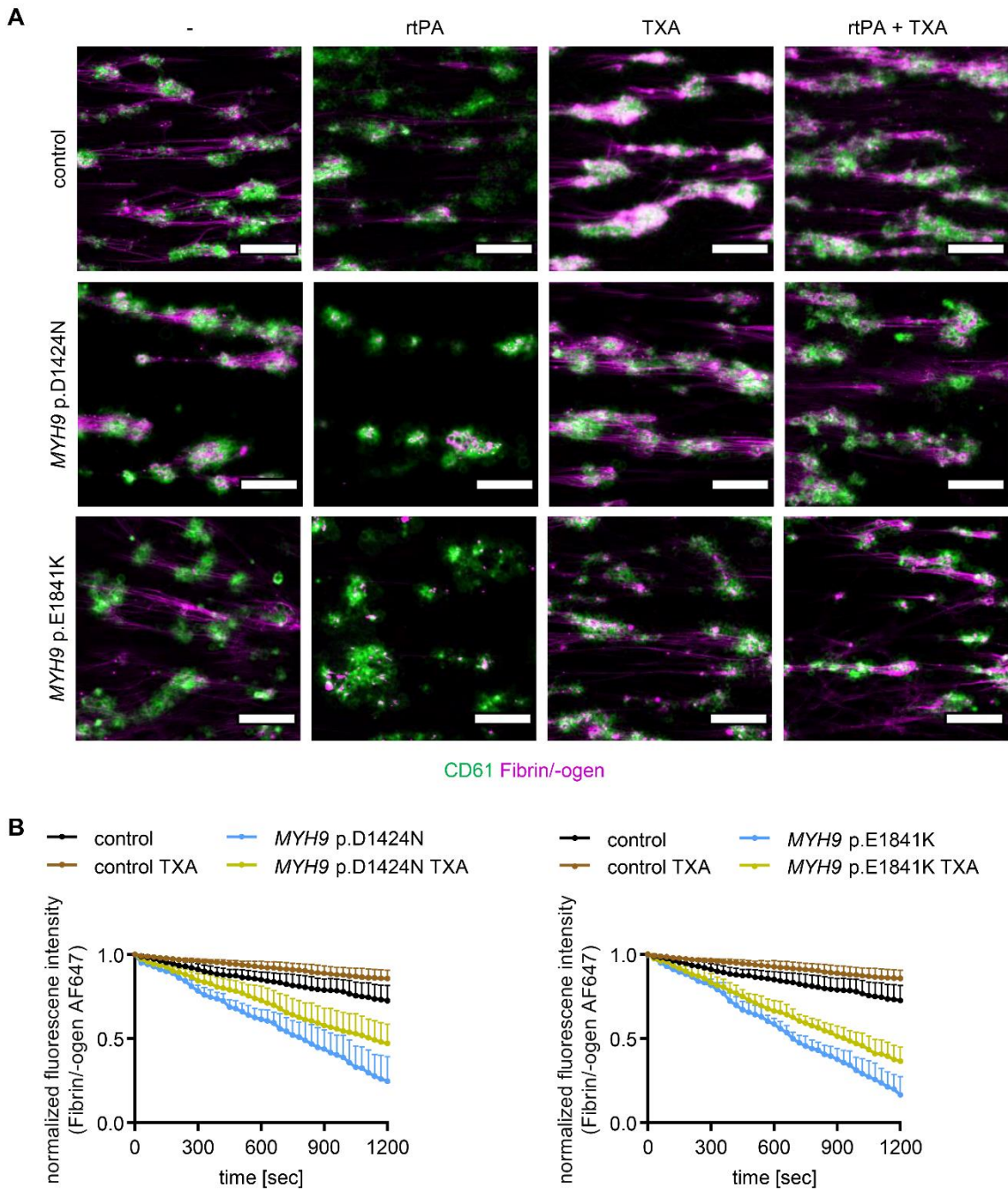


**Figure 50. Fibrinolysis is delayed by TXA.** Flow chamber assay was used to investigate fibrin and aggregate formation under TXA treatment. Whole blood of healthy donor and *MYH9*-RD patient was perfused over a collagen-coated surface at shear rate of 100/s. (A) Representative fluorescence images of thrombi from human platelets (CD61, green) and fibrin (magenta) were taken at 20 minutes. Platelet count was unadjusted and whole blood samples were treated with rtPA or TXA, or a combination of both. Scale bar: 50  $\mu$ m. (B) Fluorescence intensity of labeled fibrin (mean  $\pm$  S.D.) was measured over time in control and *MYH9*-RD patient samples. Untreated versus TXA-treated (100  $\mu$ M) control and patient samples are shown.

## Results

Further, we addressed the question whether TXA treatment has an effect on thrombi stiffness of *MYH9*-RD patient samples using colloidal probe spectroscopy. The combination of rtPA and TXA increased the stiffness of thrombi from *MYH9* p.D1424N samples (Figure 51). Thrombi from the *MYH9* p.E1841K patient did not show stiffening to the same extent as the thrombi of the *MYH9* p.D1424N patient. However, a, yet not significant, tendency of increased stiffness could be observed (Figure 51). Plasmin-induced fibrinolysis can be inhibited by TXA treatment, which also restores clot retraction and improves bleeding time to wildtype levels as shown in Figures 46-48. In line with this, thrombus formation was improved using TXA, and even thrombi of *MYH9* mutant samples were stiffer (Figure 50, 51).

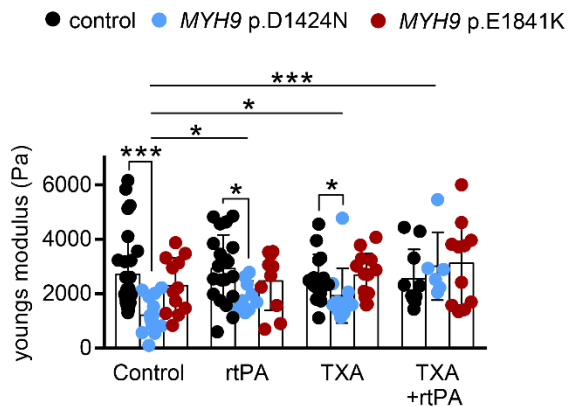


**Figure 51. TXA improves thrombus stiffness of *MYH9* p.D1424N patient sample.** Thrombus stiffness was examined in whole blood of healthy donors and *MYH9*-RD patients using a flow chamber system and colloidal probe spectroscopy (untreated, rtPA-, TXA-treated, or the combination of both). Each data point shows the median Young's modulus of one aggregate formed by platelets of healthy donor or *MYH9*-RD patient and bar plots show mean  $\pm$  S.D. of Young's modulus. Statistics: Mann-Whitney U-test (ns  $p \geq 0.05$ ;  $0.05 > p \geq 0.01$ ;  $***p < 0.001$ ).

## Results

### 5.3.2 Supplementation of magnesium has no effect on thrombocytopenia in *Myh9* mutant mice

Stritt *et al.* provided evidence that proper regulation of magnesium homeostasis in MKs plays a critical role in platelet formation and sizing in human and mice. They suggested magnesium supplementation to be a potential treatment option for patients with increased activity of myosin IIA to manage thrombocytopenia.<sup>127</sup> Increased activity of myosin IIA in MKs was demonstrated by increased contractile forces of MKs from *MYH9*-RD patient D1424N after spreading on fibronectin.<sup>128</sup> To study if a high magnesium diet can increase the platelet count, diet was performed with all three mouse lines for 14 days. Whole blood was analyzed before and 14 days after diet supplementation with magnesium-rich (0.75%)<sup>129</sup> food. The platelet count of *Myh9* mutant mice and *Myh9*<sup>+/+</sup> mice did not increase relative to untreated mice (Figure 52). Hence, magnesium supplementation had no positive effect on platelet production in *Myh9* mutant mice.

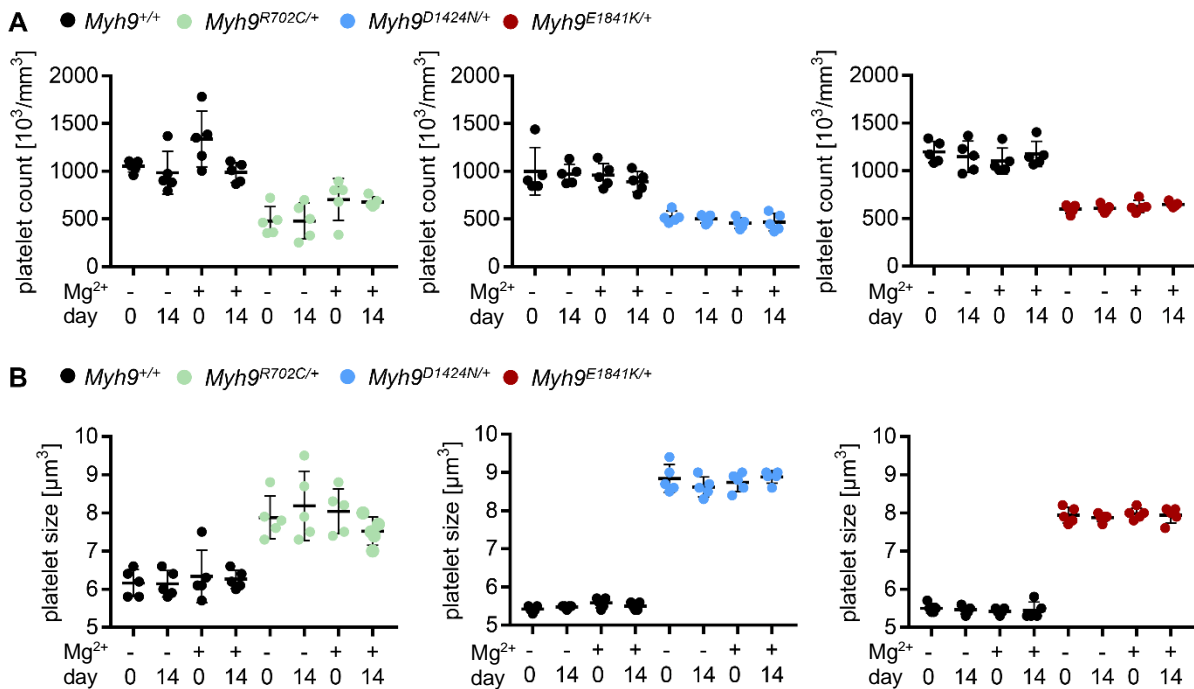


**Figure 52. Unaltered platelet count of control and *Myh9* mutant mice after magnesium supplementation for 14 days.** (A) Platelet count and (B) platelet size of mice with (+) and without (-) high magnesium diet before and 14 days after food supplementation. Statistics: Mann-Whitney U-test (ns  $p \geq 0.05$ ).

### 6 Discussion

*MYH9*-RD is an underestimated disease with a low prevalence, which is expected to be severely higher, since patients carrying this mutation are often misdiagnosed or it remains completely undiscovered.<sup>59,68</sup> To date, there are several mutations in the *MYH9* gene known, of which R702C, D1424N, and E1841K are the three most abundant heterozygous mutations found in humans.<sup>85</sup> Clinical manifestations of *MYH9*-RD are macrothrombocytopenia, bleeding tendency, granulocyte inclusion bodies and other non-hematological manifestations.<sup>57,68</sup> Studies and knowledge of this disease have increased in the last twenty years, due to the use of genetically modified mouse models. Impaired proplatelet formation (PPF) and MK migration was proposed to underlie the production of less and larger platelets.<sup>16,80,83</sup> Since the actomyosin-complex generates contractile forces in platelets, and patients with mutations in myosin IIA have an increased bleeding risk, a better understanding of the underlying mechanisms in clot formation and thrombus stabilization is needed.

We analyzed mouse models with point mutations in the *Myh9* gene for their basic biological platelet functions. Results obtained in these mouse models were verified with human samples from *MYH9*-RD patients and more insights regarding the beneficial effect of TXA were found. The three mouse models, each with a point-mutation, recapitulated the clinical manifestations observed in *MYH9*-RD patients, such as macrothrombocytopenia (Figure 18) and bleeding tendency (Figure 39, 48). Giant platelets of *Myh9* mutant mice showed increased expression of GPs on the surface and increased agonist-induced activation, whereas platelets with similar size from control and mutant mice showed overall comparable GP expression and activation (Table 2, Figure 20, 21). Mutant platelets aggregated and changed their shape upon activation (Figure 22, Table 3). Flow cytometric analysis showed that F-actin content in resting platelets of *Myh9* mutant mice is dependent on the platelet size (Figure 28), which might affect stiffness of resting *Myh9* mutant platelets as revealed with RT-FDC (Figure 23). However, the G- to F-actin ratio was unaltered (Figure 27). Ultrastructure of cytoskeletal components in resting (Figure 25, 26) and spread platelets (Figure 29, 30) were overall normal in terms of distribution and ability to form F-actin structures, whereas impaired assembly of F-actin upon activation might result in softer platelets of *Myh9*<sup>D1424N/+</sup> mice (Figure 28, 32).

## Discussion

Expression of myosin heavy and light chain were unaltered, but phosphorylation of MLC2 was significantly decreased in *Myh9* mutant platelets (Figure 33), which might impair contractile force generation. In accordance with this, contraction forces of *Myh9* mutant platelets were decreased, as well as adhesion and interaction forces (Figure 34-36), which might affect hemostasis as indicated by a delayed clot retraction and an unstable thrombus formation (Figure 35, 37). The obtained results were verified with blood samples from *MYH9*-RD patients and recapitulated initial experiments, like less deformable resting mutant platelets (Figure 40), ability to form lamellipodia, change their shape upon activation (Figure 41-43), and the reduced thrombus formation and stiffness of patient platelets (Figure 44, 45). TXA, an antifibrinolytic agent given to patients with *MYH9*-RD, stabilized thrombus formation and inhibited plasminogen-induced fibrinolysis (Figure 46-51). Hemostasis of *Myh9* mutant mice was improved by TXA (Figure 48). An increased count of MKs in the BM indicates the adaption of the BM to the decreased platelet count in circulation. However, magnesium supplementation had no positive effect on platelet formation (Figure 52).

### 6.1 Genotype-phenotype relationship

In patients with *MYH9*-RD a relationship of the localization of the mutation and the risk of hematological and non-hematological manifestations was observed. Patients with mutations in exon 16 have a higher risk of bleeding, renal and hearing impairment.<sup>68,85</sup> Hereby, the most affected amino acid is at position 702 causing larger platelets and lower platelet count.<sup>59</sup> Conformational changes in the head domain by a mutation at position 702 leads to a reduction of ATPase activity to 25% in platelets and an impaired actin-binding in HEK cells.<sup>72,73</sup> Patients with mutations in the tail domain have a lower risk of clinical manifestations at a young age. Patients with mutations in exon 30 at amino acid position 1424 have a high risk for cataracts and sensorineural hearing loss at a late-onset age.<sup>59,68</sup> Taken together, the further the position of the mutation is away from the head domain, the milder is the phenotype.<sup>59,68,70,85</sup>

Mutant mice of mouse line R702C showed impairment of the eyes upon birth (our findings and <sup>16</sup>). The eyes of those mice were closed and ulcerated, which, however, had no impact on mouse behaviour. *Myh9*<sup>D1424N/+</sup> mice showed the highest increase of platelet size by 54% (*Myh9*<sup>R702C/+</sup> by 27%; *Myh9*<sup>E1841K/+</sup> by 39%) and decrease of



## Discussion

platelet count of around 58% (*Myh9*<sup>R702C/+</sup>: 54%; *Myh9*<sup>E1841K/+</sup>: 38%) (Figure 18A, B). Mutant mice of mouse line E1841K showed the mildest platelet phenotype. F-actin assembly of *Myh9*<sup>E1841K/+</sup> platelets was unaltered upon stimulation with different agonists and spread platelets had comparable Young's modulus compared to wildtype platelets, indicating comparable stiffness. Thrombus formation on collagen *ex vivo* was impaired when platelet count was unadjusted, whereas platelet count adjusted conditions led to thrombus formation comparable to controls. Thrombi formed by human platelets of *MYH9* p.E1841K patients were comparable to healthy platelet-derived thrombi regarding stiffness. Consistent with the literature, the mutation affecting amino acid exchange E1841K showed the mildest platelet phenotype in mice. However, the exchange D1424N showed a more severe platelet phenotype in mice than the exchange R702C, which shows the most affected phenotype in human patients. These findings show that the position of the mutation (genotype) differently affects non-hematological, but similarly affects hematological manifestations (phenotype) in mice.

### 6.2 Correlation of men and mice

*MYH9* mutant platelets can aggregate, but fail to undergo shape change in aggregometry in response to collagen, ADP, and TRAP1.<sup>79</sup> Myosin IIA-deficient mouse platelets are also able to aggregate, but fail to undergo shape change, whereas in our studies heterozygous mutant mouse platelets can aggregate and undergo shape change.<sup>83</sup> Unfortunately, we did not measure aggregation and shape change of the human samples. Thus, the difference in the ability to undergo shape change between patient platelets and platelets with heterozygous point mutations or heterozygous deficiency of myosin IIA in mice remains unclear. We cannot exclude a more severe defect in cytoskeletal rearrangement of patients' platelets than observed in the mouse models. Nevertheless, in patient samples of *MYH9*-RD it was shown that mutations in the *MYH9* gene have an influence on shape change and therefore shows, that myosin IIA plays a crucial role in platelet shape change.

Canobbio and colleagues showed impaired cytoskeletal reorganization upon platelet activation of human samples with D1424N and E1841K mutations.<sup>79</sup> This is due to an increased amount of polymerized actin cytoskeleton in resting platelets of *MYH9*-RD

## Discussion

patients, which cannot reorganize upon activation to the same extent as platelets from healthy humans.<sup>79</sup> We provide data on myosin IIA mutant mice showing elevated F-actin content in resting platelets and impaired F-actin assembly upon activation of *Myh9*<sup>D1424N/+</sup> mutant platelets. Upon gating in flow cytometry on a population of mutant and wildtype platelets with a similar size, we measured unaltered F-actin content, but still decreased F-actin assembly upon activation of *Myh9*<sup>D1424N/+</sup> platelets. We can conclude that in the myosin IIA mutant mouse models, the reduced F-actin assembly upon stimulation with different agonists is rather not related to enhanced cytoskeletal organization since G-/F-actin ratio is unaltered. The impaired F-actin assembly in *Myh9*<sup>D1424N/+</sup> mutant platelets might be an effect of myosin IIA involvement in actin cytoskeleton dynamics. This assumption is also supported by reduced actin polymerization found in myosin IIA-deficient platelets upon activation with thrombin.<sup>80</sup>

The cytoskeletal components, actin (total) and  $\alpha$ -tubulin, are reported to be at a normal level in mutant platelets of *MYH9*-RD patients as demonstrated by densitometric analysis of immunoblots.<sup>130</sup> Expression of myosin IIA was decreased in *MYH9* p.D1424N patient platelets as revealed by immunoblotting.<sup>130,131</sup> In contrast, in this study immunoblotting and a capillary-based immunoassay approach revealed no changes in myosin IIA expression in platelets of *Myh9* mutant mice (Figure 17). Myosin IIA in human platelets is localized in a speckled or punctuated pattern around the granulomere in the periphery of the spread cell.<sup>132</sup> Spinler and colleagues showed that the localization of myosin IIA in spread mutant platelets of the *MYH9* p.D1424N patient was altered and peripheral myosin IIA localization was not detectable.<sup>131</sup> In contrast to Spinler *et al.* there was no obvious, visible difference in myosin IIA localization in spread mutant platelets in this study. Myosin IIA of mutant platelets of mouse line R702C was detected via GFP-labeling of myosin IIA. The fluorescence signal of GFP-labeled myosin IIA compared to antibody-stained myosin IIA (mouse line D1424N, E1841K, wildtype of mouse line R702C) was less, but localization of myosin IIA was observed around the granulomere in some platelets. The formation of filopodia and lamellipodia of mutant mice and patients' platelets were comparable to controls (Figure 29, 41). In our study, increased platelet spreading kinetics within the first 15 minutes might be the result of the enlarged platelet size of mutants, and therefore, an earlier adhesion to the activating surface. In contrast, a previous study showed reduced lamellipodia formation and less spread *Myh9*<sup>D1424N/+</sup> platelets, whereas *Myh9*<sup>R702C/+</sup>

## Discussion

and *Myh9*<sup>E1841K/+</sup> platelets showed normal spreading behaviour.<sup>76</sup> In summary, we found a normal cytoskeletal distribution and organization in resting and spread *Myh9* mutant platelets of all three mouse lines and human patients as shown with several imaging techniques. These data show that mutations in the gene encoding for the heavy chain of myosin IIA have no impact on distribution and a minor impact on organization of the platelet cytoskeleton.

### 6.3 Impact of myosin IIA mutations on hemostasis and thrombosis

Previous publication<sup>16</sup> and our data (Figure 39, 48) showed that bleeding times in *Myh9* mutant mice were prolonged, which confirms the bleeding tendency observed in *MYH9*-RD patients. Thrombus formation is a multi-step process of platelet adhesion, activation, and aggregation to prevent blood loss (Figure 4). Flow chamber experiments with knockout or inhibited myosin IIA platelets showed few layers of loosely packed platelets, which had no contracted bodies, and forces of a contracting thrombus were shown to be reduced in viscoelastic approaches.<sup>83,133</sup> Stability of thrombi upon myosin IIA deficiency was reduced with large emboli detaching from the thrombus.<sup>83</sup> In our study, we could confirm these data by showing reduced thrombus formation (Figure 37, 44) and stability (Figure 38, 45, 49, 50) independent of platelet count at least for the mouse lines R702C and D1424N and human samples from the *MYH9* p.D1424N patient.

Many factors contribute to the hemostatic and thrombotic function of platelets, like adhesion and activation of platelets via glycoproteins on the surface. Altered platelet count or changes in platelet deformation can influence thrombus formation or stability. Possible factors are discussed in the following section.

Previously, it was demonstrated that unexpectedly low platelet counts sufficiently maintain hemostatic function, when platelets are fully functional in mice.<sup>134</sup> The platelet count of *Myh9* mutant mice and *MYH9*-RD patients seems to be sufficient to maintain hemostasis unless the platelet function in biomechanics would be unaltered. Despite the sufficiently high number of platelets in *Myh9* mutant mice, hemostasis was impaired. Experiments performed with adjusted platelet count (Thrombus formation

## Discussion

[Figure 37] and clot retraction [Figure 35]) indicated no beneficial effect of increasing the platelet count, suggesting an altered function of *Myh9* mutant platelets.

Next, the platelet receptor GPIb mediates initial platelet adhesion to the site of vascular injury, subsequently GPVI triggers intracellular activation of platelets, integrin receptors undergo conformational change to enable firm platelet adhesion and thrombus growth. Actin cytoskeletal structures undergo rapid rearrangements to form filopodial extensions and stress fiber-like structures, which together with the motor protein myosin IIA exert contractile forces (Figure 7).<sup>40,135,136</sup> The mechanical extrusion of procoagulant platelets (phosphatidylserine-rich membrane surface) through contraction of the thrombus enhances cell-based thrombin generation, which facilitates blood coagulation.<sup>29,137</sup> Thrombin converts fibrinogen to fibrin to cover the thrombus and determine its mechanical integrity.<sup>138</sup> DiPumpo *et al.* reported defective expression of the GPIb-V-IX complex in platelets of some, but not all, *MYH9*-RD patients with other mutations as analyzed in the mouse models used in this thesis.<sup>139</sup> Blebbistatin-treated platelets showed normal GPIb $\alpha$  and GPIIb (integrin  $\alpha$ Ib) expression. Similarly, myosin IIA-deficient platelets showed no defect in the expression of GPIb $\alpha$ , GPIb $\beta$ , and GPV.<sup>83,140</sup> In this study, GP expression was increased on large *Myh9* mutant platelets. Upon comparison of populations of similar-sized mutant and control platelets, GP expression on the surface of mutant platelets was still increased, but to a lower level (Table 2). Most notably, the expression of the GPIb-V-IX complex level was elevated on mutant platelets of mice (Table 2). Unfortunately, we did not measure the GP expression of *MYH9* mutant platelets from patients. Nevertheless, we conclude that the investigated *Myh9* mutations have only a minor effect on glycoprotein expression of mouse platelets. Additionally, flow cytometric analysis revealed overall comparable  $\alpha$ Ib $\beta$ 3 activation and P-selectin exposure of *Myh9* mutant and wildtype platelets when platelet populations of similar size were compared (Figure 21). Therefore, myosin IIA mutations do not influence platelet adhesion and intracellular activation through surface receptors.

Last, an increase in platelet size changes the microcirculatory bloodstream, from smaller-sized platelets flowing near the vessel wall, to giant platelets localized more within the middle of the flowing bloodstream, which are therefore less available for subendothelial interaction.<sup>68</sup> Margination, the relocation of leucocytes from flowing

## Discussion

blood to the vessel wall, depends on size and stiffness of cells.<sup>141</sup> Owing to the high stiffness of platelets (0.1 – 0.2; Figure 23B, E) compared to red blood cells (0.3; Figure 24B), and small size, platelets travel near the vessel wall similar to white blood cells.<sup>142</sup> The collision of a soft and a stiff cell leads to deformation of the soft and displacement of the stiffer cell.<sup>141</sup> Since *Myh9* mutant platelets are stiffer than controls (Figure 23), those platelets might be localized more in the middle of the blood stream and might be less available for the interaction with damaged endothelium. Interestingly, *Myh9* mutations had no impact on deformation of red blood cells (Table 1, 4, Figure 24, and <sup>112</sup>), implicating a specific impact of *Myh9* mutations on platelets. Viscoelastic material properties and the contractile prestress of cells are controlled by the actomyosin activity.<sup>143</sup> Myosin inhibition in adherent<sup>143-148</sup> cells showed softening of cells. Softer cells had a higher fluidity and lower net contractile moment, indicating less prestress of softer cells.<sup>143</sup> Concluding these data, it is shown that mutations in myosin IIA lead to softening of platelets (Figure 32) through reduced myosin IIA activity, leading to lower net contractile moment,<sup>143</sup> and decreased F-actin assembly after stimulation (Figure 28). The altered deformability of *Myh9* mutant platelets (rest: decrease; spread: increase) might be the outcome of altered F-actin content and assembly of *Myh9* mutant platelets, influencing microcirculation and thrombus formation.

In summary these data show that platelet count, glycoprotein expression and platelet activation in *Myh9* mutant mice and *MYH9*-RD patients have no or minor effects on altered hemostasis. The changes in deformability are highly dependent on the cytoskeletal mechanics and might impair thrombus formation. Therefore, we addressed the relevance of the biomechanical function of platelets in *MYH9*-related bleeding diathesis.

### 6.4 Myosin IIA-mediated contraction forces in *Myh9* mutant platelets

Phosphorylation of the myosin light chain in platelets is a crucial step for the generation of contractile forces. It was shown that MKs from *Myh9*<sup>D1424N/+</sup> mice have higher levels of phosphorylated RLC compared to wildtype MKs.<sup>76</sup> The authors suggested increased contractility of *Myh9*<sup>D1424N/+</sup> MKs.<sup>76</sup> In contrast, we detected reduced phosphorylation of MLC2 in mutant platelets after activation with thrombin (Figure 33). In the view of reduced contractile forces, the result of decreased MLC phosphorylation fits better to

## Discussion

the phenotype observed in platelets of *Myh9* mutant mice. We were wondered about the reduced light chain phosphorylation in these mouse models with mutations in the heavy chain and raised two possible hypotheses responsible for this result: (1) impaired interaction of myosin light and heavy chain, or (2) failure of myofilament assembly of the two heavy chains. To verify the first hypothesis, we performed pull-down assays. Preliminary data from pull-down assays (data not shown) showed that the interactions between the myosin heavy and the light chain of *Myh9* mutant platelets is unaltered. As the myosin RLC is rather instable in the absence of the HC, this could result in degradation of the MLC2.<sup>83,149,150</sup> However, MLC2 expression was unaltered in *Myh9* mutant platelets. These results rule out an impaired interaction of the heavy and light chain as a cause for reduced MLC2 phosphorylation. In the literature, a defect in myosin IIA filament assembly is described in *Myh9* mutant mice,<sup>76</sup> supporting the second hypothesis. The phosphorylation of the HC at serine 1943 (pS1943) suppresses contractility in platelets, by blockage of myofilament assembly.<sup>131</sup> Pal *et al.* reported that heterozygous point-mutated MKs of mouse line R702C showed elevated HC phosphorylation.<sup>76</sup> Platelets from patient *MYH9* p.D1424N have reduced myosin IIA expression, but comparable phosphorylation level of S1943, resulting in a higher ratio of phosphorylated to total protein myosin IIA in the patient sample.<sup>131</sup> Furthermore, they report on impaired myosin IIA filament assembly or stability in MKs and platelets from R702C mice, which is in accordance with findings in other publications.<sup>76,131,151</sup> These data suggest impaired myosin IIA filament assembly in *Myh9* mutant platelets which leads to conformational changes and strongly affects MLC phosphorylation. Thus, the reduction of phosphorylated RLC in *Myh9* mutant platelets might impair contractile function of myosin IIA.

As shown by others<sup>16</sup> and in this study, clot retraction of *Myh9* mutant samples is delayed independently of platelet count. In contrast, myosin IIA knockout mouse lines have a completely abolished clot retraction, showing the importance of the myosin IIA contractile machinery in platelet contraction.<sup>83,152</sup> We could show that adhesion forces to collagen, platelet-platelet interaction forces, and contractile forces were reduced in *Myh9* mutant mouse platelets (Figure 34, 36). Hematopoietic cells express only one isotype of myosin II, myosin IIA, which cannot be compensated by other myosin II isoforms.<sup>70</sup> Heterodimers of myosin IIA consisting of one mutant and one wildtype myosin IIA might be formed by only 20 – 25% of total myosin IIA in *Myh9*<sup>R702C/+</sup>

## Discussion

platelets.<sup>16</sup> This indicates that there are still some dimers of wildtype myosin IIA, which can contribute to contractile forces. This is contrary to knockout *Myh9* mouse models, where presumably no or very weak platelet contractile forces can be generated. In our studies, micropost array experiments revealed reduced traction forces per post, but comparable total contractile forces generated per platelet of *Myh9*<sup>D1424N/+</sup> mice as compared to their corresponding controls (Figure 34A, C). These results might be explained by the enlarged size of *Myh9*<sup>D1424N/+</sup> platelets by 54% compared to corresponding controls combined with the increased number of surface receptors on large platelets. Considering a clot with the same number of sparsely incorporated platelets per volume, the total force seems more important for clot compaction. As in a platelet-rich thrombus, contractility per unit volume is the relevant parameter, forces per post have to be considered preferable, especially because *Myh9* mutant platelets are larger in size and thus, take up more volume. These results show that *Myh9* mutant platelets have reduced contractile forces on fibrinogen, reduced adhesion and interaction forces and a delayed clot retraction. In conclusion, mutations in the gene *Myh9* impair the contractile feature of myosin IIA in platelets and therefore, might influence thrombus stability.

Platelets sense the mechanical properties of their microenvironment via integrin  $\alpha\text{IIb}\beta\text{3}$  and upon contractile pulling forces, mediated through actomyosin complex, overcome matrix stability, platelets start to pile-up the weakened ligands and migrate towards regions of higher matrix densities (haptotaxis).<sup>27,153,154</sup> Branched actin networks forming two-dimensional, sheet-like lamellipodia through Arp2/3-dependent actin nucleation is required for directional migration.<sup>153</sup> Premature lamellipodia-like extensions formed by *Cyfip*-deficient platelets are adequate to promote platelet migration *in vitro*.<sup>153</sup> In the context of acute hemostatic clot formation, platelet haptotaxis is not required, but in bacterial inflammation migrating platelets prevent bleedings and bacterial invasion without the need of forming an occlusive thrombus.<sup>153,154</sup> It was shown that the typical shape of a migrating platelet is a half-moon shape.<sup>27,153</sup> Since *Cyfip*-deficient platelets cannot form a half-moon shape but are still able to migrate,<sup>153</sup> one can conclude that *Myh9* mutant platelets seem to have no impaired Arp2/3-dependent actin nucleation even if wildtype and mutant platelets do not form half-moon shapes (Figure 31A). *Myh9* mutant platelets can form lamellipodia on a fibrinogen-coated surface (Figure 29, 30) and the expression and

## Discussion

activation of integrin  $\alpha\text{IIb}\beta\text{3}$  is unaltered (Table 2, Figure 21; except for low doses of thrombin). It was demonstrated that myosin IIA inhibited platelets were able to spread on a fibrinogen-coated surface, but the myosin IIA inhibitor, blebbistatin, dose-dependently prevented migration.<sup>27</sup> Platelets deficient of myosin IIA revealed a similar migration defect *in vitro* and *in vivo*.<sup>27,83</sup> In our study, contractile forces of *Myh9* mutant platelets are decreased but still sufficient to overcome matrix stability in order to migrate (Figure 31). Probably the increased platelet size of *Myh9* mutant platelets enables them to migrate longer distances.

### 6.5 The fibrinolytic system

Kim and colleagues found that adherent platelets spreading over a single fibrin fiber stretch their filopodia along the fiber axis.<sup>66</sup> As soon as the filopodium begins to contract, the attached fiber is bent sharply and moves toward the main body of the cell. The fiber becomes deformed to a kink and gets incorporated with a bundle of compacted fibrin fibers. Another platelet's filopodium bound to the same fiber pulls on it in a hand-over-hand motion to form bundles and clusters of fibrin and platelets. Continuous clot contraction is dependent on filopodia extension and retraction, whereas inhibition of myosin II activity leads to reduced fibrin compaction. This indicates that formation of compacted fibrin in a clot is highly mediated by the platelet actomyosin contractile machinery. Clot compaction through platelet myosin activity leads to shrinkage of clot volume, which can be reduced via blebbistatin treatment.<sup>66</sup> Platelet contraction and fibrin network remodeling are key features in the entire process of clot contraction.<sup>66,155,156</sup> Paradoxically, clot shrinkage of fully functional platelets is facilitated by limited fibrinolysis (induced by 0.5 nM rtPA), and prevented by 10 mM TXA.<sup>88</sup> We demonstrate that heterozygous mutations in the *Myh9* gene lead to less compaction of the clot through reduction of contractile forces (Figure 34, 46, 47). Since a consequence of clot retraction is the inhibition of clot lysis and decreased binding of tissue-type plasminogen,<sup>157</sup> we hypothesized that a less compact clot might be more vulnerable to fibrinolysis. TXA, in turn, might stabilize the clot through prevention of plasmin-induced clot instability and fibrinolysis. Indeed, the addition of TXA reversed the prolonged bleeding times in mutant mice and restored hemostatic function (Figure 48). Plasmin-induced clot lysis *in vitro* was accelerated in human blood samples of



## Discussion

*MYH9*-RD patients as shown with thromboelastometry (Figure 49), strengthening the hypothesis, that less compact clots are more vulnerable to plasmin/-ogen-induced fibrinolysis than firm clots of wildtype platelets. Plasmin-induced clot lysis of mouse and human clots consisting of *Myh9* mutant platelets was prevented by TXA addition at a final concentration of 100  $\mu$ M (Figure 46), which is expected to inhibit fibrinolysis.<sup>100</sup> The final concentration of 10 mM TXA prevented plasmin-induced fibrinolysis as well (Figure 46C), but alone had no effect on clot retraction (Figure 46A), which in contrast to the results of TXA-treated human PRP by Samson *et al.*<sup>88</sup> One might assume that clot shrinkage was facilitated by limited fibrinolysis of wildtype clots treated with 0.0115 nM rtPA (Figure 46B), as shown previously in human PRP clots with 0.5 nM rtPA.<sup>88</sup> Clot retraction of *Myh9* mutant samples was unaffected with 0.0115 nM rtPA, which might be explained by the reduced contractile function of those platelets, which might benefit insufficiently from limited fibrinolysis (Figure 46B). Samson and colleagues used rtPA from a different company and PRP from human donors,<sup>88</sup> which might explain the differences in fibrinolysis-inducing concentration of rtPA. These findings suggest that reduced forces of *Myh9* mutant platelets contribute to insufficient hemostatic plug compaction, including a more vulnerable fibrin network to lysis, which can be overcome by TXA-mediated clot stabilization.

### 6.6 Proplatelet formation

Macrothrombocytopenia observed in *Myh9* mutant mice and *MYH9*-RD patients can originate from different defects. One reason could be a defect in differentiation of mutant MKs, another could be a migration defect of MKs towards the sinusoids, or maybe a defect in proplatelet formation.<sup>16,76,128,131</sup>

The defect in forming normal platelets was shown to not originate from a defect in MK differentiation since MK ploidy was normal, but rather from a defect in proplatelet formation.<sup>76</sup> MKs derived from BM of mutant mice and *MYH9*-RD patients formed fewer proplatelets with thicker stalks as well as shorter, less branched proplatelets and fewer but larger buds.<sup>16</sup> The large perimeter of platelets corresponding to preplatelet perimeter and the increased presence of the rough endoplasmic reticulum point to a defect in terminal platelet processing of *MYH9* mutant platelets.<sup>131</sup> It was demonstrated that platelets are generated but cannot undergo fission due to decreased myosin IIA

## Discussion

activity mediated by increased S1943-phosphorylation. Shear stress usually reduces pS1943 in platelets released into the blood flow to obtain a contractile phenotype in platelets. The contractile platelet phenotype was reduced in *MYH9* p.D1424N mutant platelets, as shear stress cannot reduce pS1943 to the same extent as in control platelets to promote myofilament assembly.<sup>131</sup> Another publication showed altered traction forces of MKs on fibronectin.<sup>128</sup> After 1 and 2 hours of spreading, traction forces of *MYH9*-RD derived MKs (D1424N) were comparable to control, but after 12 hours of MK spreading a strong MK-fibronectin interaction was measured.<sup>128</sup> Higher number of focal adhesion sites of *Myh9*<sup>D1424N/+</sup> MKs suppressed chemotaxis by increased adhesion.<sup>76</sup> The increase of MK count was suggested to compensate for the low platelet count in the blood circuit (Figure 19 and <sup>76</sup>), but as less MKs were in direct contact to sinusoids, this was suggested by the authors to influence platelet release into the blood flow.<sup>76</sup> In our studies, we did not quantify distance of MKs to sinusoids, but at least no ectopic release was observed, showing that proplatelets are not released into BM but into the sinusoids (Figure 19). In conclusion, we suggest that the macrothrombocytopenia observed in *MYH9*-RD patients and *Myh9* mutant mice originate most likely from a defect in proplatelet formation through missing fission of proplatelets.

Since cytoskeletal alterations play a key role in platelet biogenesis, it was suggested to manage thrombocytopenia in *MYH9*-RD patients with the supplementation of magnesium.<sup>127</sup> Magnesium inhibits myosin IIA activity by regulating ADP release and its affinity to actin filaments.<sup>127,158</sup> Therefore, MKs with increased activity of myosin IIA might be treated with magnesium to decrease myosin IIA activity and manage thrombocytopenia.<sup>127</sup> This conclusion is based on a publication showing increased contractile forces of MKs from *MYH9* p.D1424N patient after spreading.<sup>128</sup> In contrast, we were able to show that contractile forces are reduced in *Myh9* mutant platelets (Figure 34). Supplementation of magnesium did not increase the platelet count in *Myh9* mutant mice (Figure 52). The failure of MKs from *MYH9*-RD patients in division of proplatelets to smaller platelets<sup>131</sup> points to an inhibitory effect of myosin IIA function by heterozygous mutations, which cannot be rescued by magnesium, which inhibits myosin IIA activity probably even more. One can conclude that magnesium supplementation might be beneficial to manage thrombocytopenia in individuals with increased myosin IIA activity, but rather not in patients with *MYH9*-RD.

## Concluding Remarks

### 7 Concluding Remarks

In summary, the work presented here shows studies on mouse platelets with heterozygous mutations in the *Myh9* gene and on human platelets of *MYH9*-RD patients. Given the central role of myosin IIA in force generation, biophysical mechanisms of clot formation and thrombus stabilization were investigated. In addition, platelets of *Myh9* mutant mice and *MYH9*-RD patients were treated with tranexamic acid to improve clot stabilization and overcome decreased contractile forces. The major findings are:

1. *Myh9* mutant mice display macrothrombocytopenia and a bleeding tendency recapitulating clinical features of *MYH9*-RD patients.
2. The basic platelet functions of *Myh9* mutant mice were overall comparable in terms of activation, aggregation and shape change.
3. Phosphorylation of the myosin light chain 2, which is responsible for the generation of contractile forces in platelets, was reduced in *Myh9* mutant platelets.
4. Reduced contractile forces impair clot retraction and stable thrombus formation of mutant platelets from mice and *MYH9*-RD patients and are less influenced by a reduced platelet count.
5. The mutations R702C, D1424N, and E1841K have an overall similar impact on the biophysical platelet function, with the mutation E1841K having a lower impact on thrombus formation and stiffness.
6. Inhibition of fibrinolysis with TXA improves the hemostatic function in *Myh9* mutant mice.
7. Magnesium supplementation has no effect on thrombocytopenia of *Myh9* mutant mice.

With this work, we show that increased bleeding tendency, impaired thrombus formation and clot retraction can be linked to reduced myosin IIA mediated force generation in platelets and interfering with the fibrinolytic system improves hemostatic function in *Myh9* mutant mice.

### 8 Outlook

Studies regarding biomechanical features of platelets and MKs in health and disease will provide a better understanding, e.g., on how platelets and MKs alter their cytoskeleton in response to environmental changes, and how stiffness of cells impairs cell function. The knowledge about these fundamental biomechanical processes could provide new therapeutic opportunities and provides deeper insights on how drugs may change mechanical properties of cells. We are currently planning to perform RT-FDC with MKs from *Myh9* mutant mice to investigate how MK stiffness might influence proplatelet formation. Furthermore, studies showed the importance of environmental stiffness for MK differentiation and proplatelet formation, wherein the absence of myosin IIA resulted in abnormal cell deformation of MKs and a severely decreased proplatelet formation.<sup>159</sup> To mimic BM stiffness, methylcellulose reflects a three dimensional medium in terms of stiffness and might contribute to simulate a more *in vivo* like environment in *in vitro* studies. Further studies with methylcellulose are conceivable to investigate the cytoskeleton together with its biomechanical contribution to cell stiffness, and the guided MK migration along rigidity gradients.<sup>159,160</sup>

Neither in human samples, nor in *Myh9* mutant mouse samples alterations in other blood parameters were found. Furthermore, deformability of red blood cells determined by ektacytometry<sup>112</sup> and RT-FDC (our findings) was unaltered. Nevertheless, myosin IIA is also expressed in other cell types. In the constitutive knock-in mouse model used in this study, heterozygous mutations of myosin IIA are also expressed in other cell types, which define the phenotype of *Myh9* mutant mice and *MYH9*-RD patients. Bilateral cataracts, hearing loss, and kidney abnormalities were found in human patients and mutant mice.<sup>16,68</sup> The impact of mutations on other cells remains unclear, like the contribution of myosin IIA-dependent mechanical properties of endothelial and vascular smooth muscle cells to the bleeding diathesis. Previous work showed that myosin II in an endothelial cell line from bovine pulmonary artery regulates cell tension, which is abrogated by blebbistatin. Goeckeler *et al.* also showed, that blebbistatin treatment of endothelial cells leads to disappearance of stress fiber-like structures, pointing to a role of myosin II in the maintenance of endothelial integrity.<sup>161</sup> Thus, further studies have to be conducted to address the role of myosin IIA mutations in

## Outlook

endothelial cells and whether this contribute to bleeding diathesis in myosin IIA mutant mouse lines and human patients.

It was also previously described that myosin-deficient mouse platelets and MKs cannot form stress fiber-like structures upon spreading.<sup>83,162</sup> To get deeper insights into stress fiber-like structure formation and cytoskeleton rearrangement in myosin IIA mutant platelets and megakaryocytes, micropatterns would give the advantage to let cells spread on different surfaces on a spatially restricted area, forcing the cell to stretch along patterns. The big advantage of micropattern arrays is the possible quantification of morphodynamic changes in cells, using live cell imaging and the ability of a controlled way to analyse changes in cytoskeletal rearrangements. In addition, micropattern arrays with a gradient could be used to study platelet migration towards substance gradients, which provides a powerful platform for advanced analysis of platelet movement *in vitro*, with the ability to add bacteria for the investigation of mechano-scavenger abilities in connection to the role of platelets in immune responses.<sup>27,153</sup> Since myosin IIA deficient platelets were unable to migrate,<sup>27</sup> but point mutated myosin IIA platelets were able to migrate in our *in vitro* studies, further investigations on point mutated platelets are required.

TXA targets the last steps of thrombus stabilization through inhibition of plasmin-induced fibrinolysis. Reduced platelet force generation of *Myh9* mutant mice and *MYH9*-RD patients leads to impaired thrombus formation and increased bleeding tendency, which can be improved by TXA through interfering with the fibrinolytic system. Another possible methodology to stabilize the fibrin network and prevent excessive bleeding was published by Kearney *et al.* The publication showed for the first time non-antibody fibrinogen-specific proteins, termed Affimers, which bind to fibrinogen in close proximity to plasminogen binding sites and thus interfere with the mechanism of fibrinolysis.<sup>163</sup> The stabilization of the fibrin network by Affimers with the potential to reduce the bleeding risk represents a possible target to improve hemostasis in *MYH9*-RD patients. Nevertheless, other therapeutical targets in earlier steps of platelet adhesion and thrombus formation are demanded to improve clinical outcome of patients with bleeding risks. A possible, but not yet approved, mechanism would include the arginylation of platelets and MKs through arginyl-transfer RNA protein transferase (ATE) participating in stress responses. Deficiency of ATE in mice

## Outlook

resulted in decreased arginylation in platelets and MKs.<sup>164</sup> It was observed that mice lacking ATE1 showed enhanced clot retraction of platelets and increased thrombus formation *in vivo*. Since phosphorylation of MLC on Ser19 was enhanced in ATE1 deficient platelets, this effect might cause enhanced myosin IIA contractility. This demonstrates that arginylation is involved in phosphorylation-dependent protein regulation and myosin function in platelets by changing myosin conformation and/or binding of the enzymatic machinery.<sup>164</sup> *Myh9* mutant platelets showed reduced phosphorylation of the MLC2 upon thrombin stimulation (Figure 33). This raises the question, if defects in contractile force generation of platelets from mice with point mutations in myosin IIA can be reversed by loss of ATE1.

## References

### 9 References

1. Noetzli LJ, French SL, Machlus KR. New Insights Into the Differentiation of Megakaryocytes From Hematopoietic Progenitors. *Arterioscler Thromb Vasc Biol.* 2019;39(7):1288-1300.
2. Machlus KR, Thon JN, Italiano JE, Jr. Interpreting the developmental dance of the megakaryocyte: a review of the cellular and molecular processes mediating platelet formation. *Br J Haematol.* 2014;165(2):227-236.
3. Ebbe S. Biology of megakaryocytes. *Prog Hemost Thromb.* 1976;3:211-229.
4. Gurney AL, Carver-Moore K, de Sauvage FJ, Moore MW. Thrombocytopenia in c-mpl-deficient mice. *Science.* 1994;265(5177):1445-1447.
5. Blair P, Flaumenhaft R. Platelet alpha-granules: basic biology and clinical correlates. *Blood Rev.* 2009;23(4):177-189.
6. Behnke O. An electron microscope study of the megakaryocyte of the rat bone marrow. I. The development of the demarcation membrane system and the platelet surface coat. *J Ultrastruct Res.* 1968;24(5):412-433.
7. Radley JM, Haller CJ. The demarcation membrane system of the megakaryocyte: a misnomer? *Blood.* 1982;60(1):213-219.
8. Thon JN, Italiano JE. Platelets: production, morphology and ultrastructure. *Handb Exp Pharmacol.* 2012(210):3-22.
9. Bender M, Thon JN, Ehrlicher AJ, et al. Microtubule sliding drives proplatelet elongation and is dependent on cytoplasmic dynein. *Blood.* 2015;125(5):860-868.
10. Schwer HD, Lecine P, Tiwari S, Italiano JE, Jr., Hartwig JH, Shivdasani RA. A lineage-restricted and divergent beta-tubulin isoform is essential for the biogenesis, structure and function of blood platelets. *Curr Biol.* 2001;11(8):579-586.
11. Kunishima S, Kobayashi R, Itoh TJ, Hamaguchi M, Saito H. Mutation of the beta1-tubulin gene associated with congenital macrothrombocytopenia affecting microtubule assembly. *Blood.* 2009;113(2):458-461.
12. Thon JN, Montalvo A, Patel-Hett S, et al. Cytoskeletal mechanics of proplatelet maturation and platelet release. *J Cell Biol.* 2010;191(4):861-874.
13. Bender M, Eckly A, Hartwig JH, et al. ADF/n-cofilin-dependent actin turnover determines platelet formation and sizing. *Blood.* 2010;116(10):1767-1775.
14. Italiano JE, Jr., Lecine P, Shivdasani RA, Hartwig JH. Blood platelets are assembled principally at the ends of proplatelet processes produced by differentiated megakaryocytes. *J Cell Biol.* 1999;147(6):1299-1312.
15. Patel SR, Richardson JL, Schulze H, et al. Differential roles of microtubule assembly and sliding in proplatelet formation by megakaryocytes. *Blood.* 2005;106(13):4076-4085.
16. Zhang Y, Conti MA, Malide D, et al. Mouse models of MYH9-related disease: mutations in nonmuscle myosin II-A. *Blood.* 2012;119(1):238-250.
17. Schmitt A, Guichard J, Masse JM, Debili N, Cramer EM. Of mice and men: comparison of the ultrastructure of megakaryocytes and platelets. *Exp Hematol.* 2001;29(11):1295-1302.
18. Aurbach K, Spindler M, Haining EJ, Bender M, Pleines I. Blood collection, platelet isolation and measurement of platelet count and size in mice—a practical guide. *Platelets.* 2019;30(6):698-707.
19. Escolar G, White JG. The platelet open canalicular system: a final common pathway. *Blood Cells.* 1991;17(3):467-485; discussion 486-495.
20. Gerrard JM, White JG, Peterson DA. The platelet dense tubular system: its relationship to prostaglandin synthesis and calcium flux. *Thromb Haemost.* 1978;40(2):224-231.
21. Essex DW, Wu Y. Multiple protein disulfide isomerases support thrombosis. *Curr Opin Hematol.* 2018;25(5):395-402.
22. Breton-Gorius J, Guichard J. Ultrastructural localization of peroxidase activity in human platelets and megakaryocytes. *Am J Pathol.* 1972;66(2):277-293.

## References

23. Shin EK, Park H, Noh JY, Lim KM, Chung JH. Platelet Shape Changes and Cytoskeleton Dynamics as Novel Therapeutic Targets for Anti-Thrombotic Drugs. *Biomol Ther (Seoul)*. 2017;25(3):223-230.
24. Daniel JL, Molish IR, Rigmaiden M, Stewart G. Evidence for a role of myosin phosphorylation in the initiation of the platelet shape change response. *J Biol Chem*. 1984;259(15):9826-9831.
25. Mattila PK, Lappalainen P. Filopodia: molecular architecture and cellular functions. *Nat Rev Mol Cell Biol*. 2008;9(6):446-454.
26. Schurr Y, Sperr A, Volz J, et al. Platelet lamellipodium formation is not required for thrombus formation and stability. *Blood*. 2019;134(25):2318-2329.
27. Gaertner F, Ahmad Z, Rosenberger G, et al. Migrating Platelets Are Mechano-scavengers that Collect and Bundle Bacteria. *Cell*. 2017;171(6):1368-1382 e1323.
28. Thomas SG. The Structure of Resting and Activated Platelets. In: Michelson AD, ed. *Platelets*: Elsevier Inc.; 2019:47-77.
29. Hou Y, Carrim N, Wang Y, Gallant RC, Marshall A, Ni H. Platelets in hemostasis and thrombosis: Novel mechanisms of fibrinogen-independent platelet aggregation and fibronectin-mediated protein wave of hemostasis. *J Biomed Res*. 2015;29.
30. Radomski MW, Palmer RM, Moncada S. The anti-aggregating properties of vascular endothelium: interactions between prostacyclin and nitric oxide. *Br J Pharmacol*. 1987;92(3):639-646.
31. Meng R, Wu J, Harper DC, et al. Defective release of alpha granule and lysosome contents from platelets in mouse Hermansky-Pudlak syndrome models. *Blood*. 2015;125(10):1623-1632.
32. Sharda A, Flaumenhaft R. The life cycle of platelet granules. *F1000Res*. 2018;7:236.
33. Nieswandt B, Pleines I, Bender M. Platelet adhesion and activation mechanisms in arterial thrombosis and ischaemic stroke. *J Thromb Haemost*. 2011;9 Suppl 1:92-104.
34. Versteeg HH, Heemskerk JW, Levi M, Reitsma PH. New fundamentals in hemostasis. *Physiol Rev*. 2013;93(1):327-358.
35. Patel-Hett S, Richardson JL, Schulze H, et al. Visualization of microtubule growth in living platelets reveals a dynamic marginal band with multiple microtubules. *Blood*. 2008;111(9):4605-4616.
36. Italiano JE, Jr., Bergmeier W, Tiwari S, et al. Mechanisms and implications of platelet discoid shape. *Blood*. 2003;101(12):4789-4796.
37. Condeelis PS, Caceres A. Microtubule assembly, organization and dynamics in axons and dendrites. *Nat Rev Neurosci*. 2009;10(5):319-332.
38. Chang L, Goldman RD. Intermediate filaments mediate cytoskeletal crosstalk. *Nat Rev Mol Cell Biol*. 2004;5(8):601-613.
39. Cerecedo D, Martinez-Vieyra I, Mondragon R, Mondragon M, Gonzalez S, Galvan IJ. Haemostatic role of intermediate filaments in adhered platelets: importance of the membranous system stability. *J Cell Biochem*. 2013;114(9):2050-2060.
40. Bender M, Palankar R. Platelet Shape Changes during Thrombus Formation: Role of Actin-Based Protrusions. *Hamostaseologie*. 2021;41(1):14-21.
41. Bearer EL, Prakash JM, Li Z. Actin dynamics in platelets. *Int Rev Cytol*. 2002;217:137-182.
42. Gunning PW, Ghoshdastider U, Whitaker S, Popp D, Robinson RC. The evolution of compositionally and functionally distinct actin filaments. *J Cell Sci*. 2015;128(11):2009-2019.
43. Herman IM. Actin isoforms. *Curr Opin Cell Biol*. 1993;5(1):48-55.
44. Pollard TD, Goldman RD. *The Cytoskeleton*: Cold Spring Laboratory Press; 2017.
45. Mannherz HG. The Actin Cytoskeleton and Bacterial Infection. In: Ahmed R, Akira S, Casadevall A, et al., eds. *Current Topics in Microbiology and Immunology*. Vol. 399: Springer; 2017.
46. Kabsch W, Mannherz HG, Suck D, Pai EF, Holmes KC. Atomic structure of the actin:DNase I complex. *Nature*. 1990;347(6288):37-44.



## References

47. Hohmann T, Dehghani F. The Cytoskeleton-A Complex Interacting Meshwork. *Cells*. 2019;8(4).
48. Hartwig JH, DeSisto M. The cytoskeleton of the resting human blood platelet: structure of the membrane skeleton and its attachment to actin filaments. *J Cell Biol*. 1991;112(3):407-425.
49. Hartwig JH. Mechanisms of actin rearrangements mediating platelet activation. *J Cell Biol*. 1992;118(6):1421-1442.
50. Jennings LK, Fox JE, Edwards HH, Phillips DR. Changes in the cytoskeletal structure of human platelets following thrombin activation. *J Biol Chem*. 1981;256(13):6927-6932.
51. Pellegrin S, Mellor H. Actin stress fibres. *J Cell Sci*. 2007;120(Pt 20):3491-3499.
52. Oakes PW, Beckham Y, Stricker J, Gardel ML. Tension is required but not sufficient for focal adhesion maturation without a stress fiber template. *J Cell Biol*. 2012;196(3):363-374.
53. Calaminus SD, Auger JM, McCarty OJ, Wakelam MJ, Machesky LM, Watson SP. MyosinIIa contractility is required for maintenance of platelet structure during spreading on collagen and contributes to thrombus stability. *J Thromb Haemost*. 2007;5(10):2136-2145.
54. Odrionitz F, Kollmar M. Drawing the tree of eukaryotic life based on the analysis of 2,269 manually annotated myosins from 328 species. *Genome Biol*. 2007;8(9):R196.
55. Ronen D, Ravid S. Myosin II tailpiece determines its paracrystal structure, filament assembly properties, and cellular localization. *J Biol Chem*. 2009;284(37):24948-24957.
56. Fernandez-Prado R, Carriazo-Julio SM, Torra R, Ortiz A, Perez-Gomez MV. MYH9-related disease: it does exist, may be more frequent than you think and requires specific therapy. *Clinical Kidney Journal* 2019:488-493.
57. Althaus K, Greinacher A. MYH-9 Related Platelet Disorders: Strategies for Management and Diagnosis. *Transfus Med Hemother*. 2010;37(5):260-267.
58. Badirou I, Pan J, Souquere S, et al. Distinct localizations and roles of non-muscle myosin II during proplatelet formation and platelet release. *J Thromb Haemost*. 2015;13(5):851-859.
59. Pecci A, Ma X, Savoia A, Adelstein RS. MYH9: Structure, functions and role of non-muscle myosin IIA in human disease. *Gene*. 2018;664:152-167.
60. Chin VT, Nagrial AM, Chou A, et al. Rho-associated kinase signalling and the cancer microenvironment: novel biological implications and therapeutic opportunities. *Expert Rev Mol Med*. 2015;17:e17.
61. Getz TM, Dangelmaier CA, Jin J, Daniel JL, Kunapuli SP. Differential phosphorylation of myosin light chain (Thr)18 and (Ser)19 and functional implications in platelets. *J Thromb Haemost*. 2010;8(10):2283-2293.
62. Coureux PD, Sweeney HL, Houdusse A. Three myosin V structures delineate essential features of chemo-mechanical transduction. *EMBO J*. 2004;23(23):4527-4537.
63. Straight AF, Cheung A, Limouze J, et al. Dissecting temporal and spatial control of cytokinesis with a myosin II Inhibitor. *Science*. 2003;299(5613):1743-1747.
64. Kovacs M, Toth J, Hetenyi C, Malnasi-Csizmadia A, Sellers JR. Mechanism of blebbistatin inhibition of myosin II. *J Biol Chem*. 2004;279(34):35557-35563.
65. Ramamurthy B, Yengo CM, Straight AF, Mitchison TJ, Sweeney HL. Kinetic mechanism of blebbistatin inhibition of nonmuscle myosin IIb. *Biochemistry*. 2004;43(46):14832-14839.
66. Kim OV, Litvinov RI, Alber MS, Weisel JW. Quantitative structural mechanobiology of platelet-driven blood clot contraction. *Nat Commun*. 2017;8(1):1274.
67. Bloemink MJ, Geeves MA. Shaking the myosin family tree: biochemical kinetics defines four types of myosin motor. *Semin Cell Dev Biol*. 2011;22(9):961-967.
68. Althaus K, Greinacher A. MYH9-related platelet disorders. *Semin Thromb Hemost*. 2009;35(2):189-203.
69. Althaus K, Najm J, Greinacher A. MYH9 related platelet disorders - often unknown and misdiagnosed. *Klin Padiatr*. 2011;223(3):120-125.
70. Kunishima S, Saito H. Advances in the understanding of MYH9 disorders. *Curr Opin Hematol*. 2010;17(5):405-410.

## References

71. Pecci A, Panza E, Pujol-Moix N, et al. Position of nonmuscle myosin heavy chain IIA (NMMHC-IIA) mutations predicts the natural history of MYH9-related disease. *Hum Mutat.* 2008;29(3):409-417.
72. Heath KE, Campos-Barros A, Toren A, et al. Nonmuscle myosin heavy chain IIA mutations define a spectrum of autosomal dominant macrothrombocytopenias: May-Hegglin anomaly and Fechtner, Sebastian, Epstein, and Alport-like syndromes. *Am J Hum Genet.* 2001;69(5):1033-1045.
73. Hu A, Wang F, Sellers JR. Mutations in human nonmuscle myosin IIA found in patients with May-Hegglin anomaly and Fechtner syndrome result in impaired enzymatic function. *J Biol Chem.* 2002;277(48):46512-46517.
74. Heynen MJ, Blockmans D, Verwilghen RL, Vermeylen J. Congenital macrothrombocytopenia, leucocyte inclusions, deafness and proteinuria: functional and electron microscopic observations on platelets and megakaryocytes. *Br J Haematol.* 1988;70(4):441-448.
75. Pecci A, Malara A, Badalucco S, et al. Megakaryocytes of patients with MYH9-related thrombocytopenia present an altered proplatelet formation. *Thromb Haemost.* 2009;102(1):90-96.
76. Pal K, Nowak R, Billington N, et al. Megakaryocyte migration defects due to nonmuscle myosin IIA mutations underlie thrombocytopenia in MYH9-related disease. *Blood.* 2020;135(21):1887-1898.
77. Noris P, Spedini P, Belletti S, Magrini U, Balduini CL. Thrombocytopenia, giant platelets, and leukocyte inclusion bodies (May-Hegglin anomaly): clinical and laboratory findings. *Am J Med.* 1998;104(4):355-360.
78. Lusher JM, Barnhart MI. Congenital disorders affecting platelets. *Semin Thromb Hemost.* 1977;4(2):123-186.
79. Canobbio I, Noris P, Pecci A, Balduini A, Balduini CL, Torti M. Altered cytoskeleton organization in platelets from patients with MYH9-related disease. *J Thromb Haemost.* 2005;3(5):1026-1035.
80. Pertuy F, Eckly A, Weber J, et al. Myosin IIA is critical for organelle distribution and F-actin organization in megakaryocytes and platelets. *Blood.* 2014;123(8):1261-1269.
81. Bastida JM, Gonzalez-Porras JR, Rivera J, Lozano ML. Role of Thrombopoietin Receptor Agonists in Inherited Thrombocytopenia. *Int J Mol Sci.* 2021;22(9).
82. Balduini CL, Noris P, Belletti S, Spedini P, Gamba G. In vitro and in vivo effects of desmopressin on platelet function. *Haematologica.* 1999;84(10):891-896.
83. Leon C, Eckly A, Hechler B, et al. Megakaryocyte-restricted MYH9 inactivation dramatically affects hemostasis while preserving platelet aggregation and secretion. *Blood.* 2007;110(9):3183-3191.
84. Eckly A, Rinckel JY, Laeuffer P, et al. Proplatelet formation deficit and megakaryocyte death contribute to thrombocytopenia in Myh9 knockout mice. *J Thromb Haemost.* 2010;8(10):2243-2251.
85. Balduini CL, Pecci A, Savoia A. Recent advances in the understanding and management of MYH9-related inherited thrombocytopenias. *Br J Haematol.* 2011;154(2):161-174.
86. Kopp JB. Glomerular pathology in autosomal dominant MYH9 spectrum disorders: what are the clues telling us about disease mechanism? *Kidney Int.* 2010;78(2):130-133.
87. Dunn CJ, Goa KL. Tranexamic acid: a review of its use in surgery and other indications. *Drugs.* 1999;57(6):1005-1032.
88. Samson AL, Alwis I, Maclean JAA, et al. Endogenous fibrinolysis facilitates clot retraction in vivo. *Blood.* 2017;130(23):2453-2462.
89. Nieswandt B, Bergmeier W, Rackebrandt K, Gessner JE, Zirngibl H. Identification of critical antigen-specific mechanisms in the development of immune thrombocytopenic purpura in mice. *Blood.* 2000;96(7):2520-2527.

## References

90. Bergmeier W, Rackebrandt K, Schroder W, Zirngibl H, Nieswandt B. Structural and functional characterization of the mouse von Willebrand factor receptor GPIb-IX with novel monoclonal antibodies. *Blood*. 2000;95(3):886-893.
91. Nieswandt B, Bergmeier W, Schulte V, Rackebrandt K, Gessner JE, Zirngibl H. Expression and function of the mouse collagen receptor glycoprotein VI is strictly dependent on its association with the FcRgamma chain. *J Biol Chem*. 2000;275(31):23998-24002.
92. Nieswandt B, Brakebusch C, Bergmeier W, et al. Glycoprotein VI but not alpha2beta1 integrin is essential for platelet interaction with collagen. *EMBO J*. 2001;20(9):2120-2130.
93. Bergmeier W, Schulte V, Brockhoff G, Bier U, Zirngibl H, Nieswandt B. Flow cytometric detection of activated mouse integrin alphaIIb beta3 with a novel monoclonal antibody. *Cytometry*. 2002;48(2):80-86.
94. Stritt S, Wolf K, Lorenz V, et al. Rap1-GTP-interacting adaptor molecule (RIAM) is dispensable for platelet integrin activation and function in mice. *Blood*. 2015;125(2):219-222.
95. May F, Hagedorn I, Pleines I, et al. CLEC-2 is an essential platelet-activating receptor in hemostasis and thrombosis. *Blood*. 2009;114(16):3464-3472.
96. Schurr Y, Spindler M, Kurz H, Bender M. The cytoskeletal crosslinking protein MACF1 is dispensable for thrombus formation and hemostasis. *Sci Rep*. 2019;9(1):7726.
97. Herfs L, Swieringa F, Jooss N, et al. Multiparameter microfluidics assay of thrombus formation reveals increased sensitivity to contraction and antiplatelet agents at physiological temperature. *Thromb Res*. 2021;203:46-56.
98. Mangin PH, Gardiner EE, Nesbitt WS, et al. In vitro flow based systems to study platelet function and thrombus formation: Recommendations for standardization: Communication from the SSC on Biorheology of the ISTH. *J Thromb Haemost*. 2020;18(3):748-752.
99. Kuiper GJ, Kleinegris MC, van Oerle R, et al. Validation of a modified thromboelastometry approach to detect changes in fibrinolytic activity. *Thromb J*. 2016;14:1.
100. Picetti R, Shakur-Still H, Medcalf RL, Standing JF, Roberts I. What concentration of tranexamic acid is needed to inhibit fibrinolysis? A systematic review of pharmacodynamics studies. *Blood Coagul Fibrinolysis*. 2019;30(1):1-10.
101. Laemmli UK. Cleavage of structural proteins during the assembly of the head of bacteriophage T4. *Nature*. 1970;227(5259):680-685.
102. Heib T, Hermanns HM, Manukjan G, et al. RhoA/Cdc42 signaling drives cytoplasmic maturation but not endomitosis in megakaryocytes. *Cell Rep*. 2021;35(6):109102.
103. Kawamoto T. Use of a new adhesive film for the preparation of multi-purpose fresh-frozen sections from hard tissues, whole-animals, insects and plants. *Arch Histol Cytol*. 2003;66(2):123-143.
104. Otto O, Rosendahl P, Mietke A, et al. Real-time deformability cytometry: on-the-fly cell mechanical phenotyping. *Nat Methods*. 2015;12(3):199-202, 194 p following 202.
105. Rosendahl P, Plak K, Jacobi A, et al. Real-time fluorescence and deformability cytometry. *Nat Methods*. 2018;15(5):355-358.
106. Urbanska M, Rosendahl P, Krater M, Guck J. High-throughput single-cell mechanical phenotyping with real-time deformability cytometry. *Methods Cell Biol*. 2018;147:175-198.
107. Weber A, Iturri J, Benitez R, Toca-Herrera JL. Measuring biomaterials mechanics with atomic force microscopy. 1. Influence of the loading rate and applied force (pyramidal tips). *Microsc Res Tech*. 2019;82(9):1392-1400.
108. Glaubitz M, Medvedev N, Pussak D, et al. A novel contact model for AFM indentation experiments on soft spherical cell-like particles. *Soft Matter*. 2014;10(35):6732-6741.
109. Schoen I, Hu W, Klotzsch E, Vogel V. Probing cellular traction forces by micropillar arrays: contribution of substrate warping to pillar deflection. *Nano Lett*. 2010;10(5):1823-1830.
110. Seifert J, Rheinlaender J, Lang F, Gawaz M, Schaffer TE. Thrombin-induced cytoskeleton dynamics in spread human platelets observed with fast scanning ion conductance microscopy. *Sci Rep*. 2017;7(1):4810.
111. Rheinlaender J, Vogel S, Seifert J, et al. Imaging the elastic modulus of human platelets during thrombin-induced activation using scanning ion conductance microscopy. *Thromb Haemost*. 2015;113(2):305-311.

## References

112. Smith AS, Pal K, Nowak RB, et al. MYH9-related disease mutations cause abnormal red blood cell morphology through increased myosin-actin binding at the membrane. *Am J Hematol.* 2019;94(6):667-677.
113. Sachs L, Wesche J, Lenkeit L, et al. Ex vivo anticoagulants affect human blood platelet biomechanics with implications for high-throughput functional mechanophenotyping. *Commun Biol.* 2022;5(1):86.
114. Byrnes JR, Wolberg AS. Red blood cells in thrombosis. *Blood.* 2017;130(16):1795-1799.
115. Painter RG, Ginsberg MH. Centripetal myosin redistribution in thrombin-stimulated platelets. Relationship to platelet Factor 4 secretion. *Exp Cell Res.* 1984;155(1):198-212.
116. Sixma JJ, van den Berg A, Jockusch BM, Hartwig J. Immunoelectron microscopic localization of actin, alpha-actinin, actin-binding protein and myosin in resting and activated human blood platelets. *Eur J Cell Biol.* 1989;48(2):271-281.
117. Park K, Mao FW, Park H. The minimum surface fibrinogen concentration necessary for platelet activation on dimethyldichlorosilane-coated glass. *J Biomed Mater Res.* 1991;25(3):407-420.
118. Scholey JM, Taylor KA, Kendrick-Jones J. Regulation of non-muscle myosin assembly by calmodulin-dependent light chain kinase. *Nature.* 1980;287(5779):233-235.
119. Sellers JR, Spudich JA, Sheetz MP. Light chain phosphorylation regulates the movement of smooth muscle myosin on actin filaments. *J Cell Biol.* 1985;101(5 Pt 1):1897-1902.
120. Jakes R, Northrop F, Kendrick-Jones J. Calcium binding regions of myosin 'regulatory' light chains. *FEBS Lett.* 1976;70(1):229-234.
121. Pearson RB, Jakes R, John M, Kendrick-Jones J, Kemp BE. Phosphorylation site sequence of smooth muscle myosin light chain (Mr = 20 000). *FEBS Lett.* 1984;168(1):108-112.
122. Ikebe M, Hartshorne DJ, Elzinga M. Identification, phosphorylation, and dephosphorylation of a second site for myosin light chain kinase on the 20,000-dalton light chain of smooth muscle myosin. *J Biol Chem.* 1986;261(1):36-39.
123. Palankar R, Glaubitz M, Martens U, et al. 3D Micropillars Guide the Mechanobiology of Human Induced Pluripotent Stem Cell-Derived Cardiomyocytes. *Adv Healthc Mater.* 2016;5(3):335-341.
124. Nguyen TH, Palankar R, Bui VC, Medvedev N, Greinacher A, Delcea M. Rupture Forces among Human Blood Platelets at different Degrees of Activation. *Sci Rep.* 2016;6:25402.
125. Hoylaerts M, Lijnen HR, Collen D. Studies on the mechanism of the antifibrinolytic action of tranexamic acid. *Biochim Biophys Acta.* 1981;673(1):75-85.
126. Mannucci PM. Hemostatic drugs. *N Engl J Med.* 1998;339(4):245-253.
127. Stritt S, Nurden P, Favier R, et al. Defects in TRPM7 channel function deregulate thrombopoiesis through altered cellular Mg(2+) homeostasis and cytoskeletal architecture. *Nat Commun.* 2016;7:11097.
128. Chen Y, Boukour S, Milloud R, et al. The abnormal proplatelet formation in MYH9-related macrothrombocytopenia results from an increased actomyosin contractility and is rescued by myosin IIA inhibition. *J Thromb Haemost.* 2013;11(12):2163-2175.
129. Sontia B, Montezano AC, Paravicini T, Tabet F, Touyz RM. Downregulation of renal TRPM7 and increased inflammation and fibrosis in aldosterone-infused mice: effects of magnesium. *Hypertension.* 2008;51(4):915-921.
130. Deutsch S, Rideau A, Bochaton-Piallat ML, et al. Asp1424Asn MYH9 mutation results in an unstable protein responsible for the phenotypes in May-Hegglin anomaly/Fechtner syndrome. *Blood.* 2003;102(2):529-534.
131. Spinler KR, Shin JW, Lambert MP, Discher DE. Myosin-II repression favors pre/proplatelets but shear activation generates platelets and fails in macrothrombocytopenia. *Blood.* 2015;125(3):525-533.

## References

132. Takubo T, Hino M, Suzuki K, Tatsumi N. Localization of myosin, actin, alpha-actinin, tropomyosin and vinculin in surface-activated, spreading human platelets. *Biotech Histochem.* 1998;73(6):310-315.
133. Ting LH, Fegghi S, Taparia N, et al. Contractile forces in platelet aggregates under microfluidic shear gradients reflect platelet inhibition and bleeding risk. *Nat Commun.* 2019;10(1):1204.
134. Morowski M, Vogtle T, Kraft P, Kleinschnitz C, Stoll G, Nieswandt B. Only severe thrombocytopenia results in bleeding and defective thrombus formation in mice. *Blood.* 2013;121(24):4938-4947.
135. Sorrentino S, Conesa JJ, Cuervo A, et al. Structural analysis of receptors and actin polarity in platelet protrusions. *Proc Natl Acad Sci U S A.* 2021;118(37).
136. Fegghi S, Munday AD, Tooley WW, et al. Glycoprotein Ib-IX-V Complex Transmits Cytoskeletal Forces That Enhance Platelet Adhesion. *Biophys J.* 2016;111(3):601-608.
137. Nechipurenko DY, Receveur N, Yakimenko AO, et al. Clot Contraction Drives the Translocation of Procoagulant Platelets to Thrombus Surface. *Arterioscler Thromb Vasc Biol.* 2019;39(1):37-47.
138. Ni R, Neves MAD, Wu C, et al. Activated thrombin-activatable fibrinolysis inhibitor (TAFIa) attenuates fibrin-dependent plasmin generation on thrombin-activated platelets. *J Thromb Haemost.* 2020;18(9):2364-2376.
139. Di Pumpo M, Noris P, Pecci A, et al. Defective expression of GPIb/IX/V complex in platelets from patients with May-Hegglin anomaly and Sebastian syndrome. *Haematologica.* 2002;87(9):943-947.
140. Shin JW, Swift J, Spinler KR, Discher DE. Myosin-II inhibition and soft 2D matrix maximize multinucleation and cellular projections typical of platelet-producing megakaryocytes. *Proc Natl Acad Sci U S A.* 2011;108(28):11458-11463.
141. Qiu Y, Myers DR, Lam WA. The biophysics and mechanics of blood from a materials perspective. *Nat Rev Mater.* 2019;4(5):294-311.
142. Walton BL, Lehmann M, Skorczewski T, et al. Elevated hematocrit enhances platelet accumulation following vascular injury. *Blood.* 2017;129(18):2537-2546.
143. Schierbaum N, Rheinlaender J, Schaffer TE. Combined atomic force microscopy (AFM) and traction force microscopy (TFM) reveals a correlation between viscoelastic material properties and contractile prestress of living cells. *Soft Matter.* 2019;15(8):1721-1729.
144. Martens JC, Radmacher M. Softening of the actin cytoskeleton by inhibition of myosin II. *Pflugers Arch.* 2008;456(1):95-100.
145. Schafer A, Radmacher M. Influence of myosin II activity on stiffness of fibroblast cells. *Acta Biomater.* 2005;1(3):273-280.
146. Balland M, Richert A, Gallet F. The dissipative contribution of myosin II in the cytoskeleton dynamics of myoblasts. *Eur Biophys J.* 2005;34(3):255-261.
147. MacKay JL, Keung AJ, Kumar S. A genetic strategy for the dynamic and graded control of cell mechanics, motility, and matrix remodeling. *Biophys J.* 2012;102(3):434-442.
148. Nijenhuis N, Zhao X, Carisey A, Ballestrem C, Derby B. Combining AFM and acoustic probes to reveal changes in the elastic stiffness tensor of living cells. *Biophys J.* 2014;107(7):1502-1512.
149. Franke JD, Boury AL, Gerald NJ, Kiehart DP. Native nonmuscle myosin II stability and light chain binding in *Drosophila melanogaster*. *Cell Motil Cytoskeleton.* 2006;63(10):604-622.
150. Weissenbruch K, Grewe J, Hippler M, et al. Distinct roles of nonmuscle myosin II isoforms for establishing tension and elasticity during cell morphodynamics. *Elife.* 2021;10.
151. Franke JD, Dong F, Rickoll WL, Kelley MJ, Kiehart DP. Rod mutations associated with MYH9-related disorders disrupt nonmuscle myosin-IIA assembly. *Blood.* 2005;105(1):161-169.
152. Johnson GJ, Leis LA, Krumwiede MD, White JG. The critical role of myosin IIA in platelet internal contraction. *J Thromb Haemost.* 2007;5(7):1516-1529.
153. Nicolai L, Schiefelbein K, Lipsky S, et al. Vascular surveillance by haptotactic blood platelets in inflammation and infection. *Nat Commun.* 2020;11(1):5778.

## References

154. Petito E, Momi S, Gresele P. The Migration of Platelets and their Interaction with Other Migrating Cells. In: Gresele P, Kleiman N, Lopez J, Page C, eds. *Platelets in Thrombotic and Non-Thrombotic Disorders*: Springer; 2017:337-351.
155. Lam WA, Chaudhuri O, Crow A, et al. Mechanics and contraction dynamics of single platelets and implications for clot stiffening. *Nat Mater*. 2011;10(1):61-66.
156. Tutwiler V, Singh J, Litvinov RI, Bassani JL, Purohit PK, Weisel JW. Rupture of blood clots: Mechanics and pathophysiology. *Sci Adv*. 2020;6(35):eabc0496.
157. Kunitada S, FitzGerald GA, Fitzgerald DJ. Inhibition of clot lysis and decreased binding of tissue-type plasminogen activator as a consequence of clot retraction. *Blood*. 1992;79(6):1420-1427.
158. Swenson AM, Trivedi DV, Rauscher AA, et al. Magnesium modulates actin binding and ADP release in myosin motors. *J Biol Chem*. 2014;289(34):23977-23991.
159. Aguilar A, Pertuy F, Eckly A, et al. Importance of environmental stiffness for megakaryocyte differentiation and proplatelet formation. *Blood*. 2016;128(16):2022-2032.
160. Mitrossilis D, Fouchard J, Guiroy A, et al. Single-cell response to stiffness exhibits muscle-like behavior. *Proc Natl Acad Sci U S A*. 2009;106(43):18243-18248.
161. Goeckeler ZM, Bridgman PC, Wysolmerski RB. Nonmuscle myosin II is responsible for maintaining endothelial cell basal tone and stress fiber integrity. *Am J Physiol Cell Physiol*. 2008;295(4):C994-1006.
162. Eckly A, Strassel C, Freund M, et al. Abnormal megakaryocyte morphology and proplatelet formation in mice with megakaryocyte-restricted MYH9 inactivation. *Blood*. 2009;113(14):3182-3189.
163. Kearney KJ, Pechlivani N, King R, et al. Affimer proteins as a tool to modulate fibrinolysis, stabilize the blood clot, and reduce bleeding complications. *Blood*. 2019;133(11):1233-1244.
164. Lian L, Suzuki A, Hayes V, et al. Loss of ATE1-mediated arginylation leads to impaired platelet myosin phosphorylation, clot retraction, and in vivo thrombosis formation. *Haematologica*. 2014;99(3):554-560.

### 10 Appendix

#### 10.1 Abbreviations

ACD	Acid-Citrate-Dextrose
ADP	Adenosine diphosphate
AFM	Atomic force microscopy
APC	Allophycocyanin
APS	Ammonium peroxidsulfate
ATP	Adenosine-triphosphate
BM	Bone marrow
BSA	Bovine serum albumin
CKII	Casein kinase II
cDNA	Complementary DNA
CFT	Clot formation time
CLEC2	C-type lectin-like receptor 2
c-Mpl	Cellular myeloproliferative leukemia protein
CRP	Collagen-related peptide
CT	Clotting time
CVX	Convulxin
DAPI	4',6-Diamidino-2-phenylindol
DIC	Differential interference contrast
DTS	Dense tubular system
DMS	Demarcation membrane system
DNA	Deoxyribonucleic acid
dNTP	Desoxynukleosidtriphosphate
ECL	Enhanced chemiluminescence
ECM	Extracellular matrix

## Appendix

EDTA	Ethylenediaminetetraacetic acid
EGTA	Ethylene glycol-bis(2-aminoethylether)-N,N,N',N'-tetraacetic acid
EOS	Eosinophils
EXTEM	Extrinsic tissue-factor activated thromboelastometry
FA	Focal adhesion
F-actin	Filamentous actin
FITC	Fluorescein isothiocyanate
FSC	Forward scatter
G-actin	Globular actin
GAPDH	Glycerinaldehyd-3-phosphat-dehydrogenase
GP	Glycoprotein
GFP	Green fluorescent protein
GRA	Granulocyte
GTPases	Guanosine triphosphatases
HC	Heavy chain
HCT	Hematocrit
HEPES	4-(2-hydroxyethyl)-1-piperazineethanesulfonic acid
HGB	Hemoglobin
HMDS	Hexamethyldisilazane
HRP	Horseradish peroxidase
HSCs	Hematopoietic stem cells
IgG	Immunoglobulin G
ITAM	Immunoreceptor tyrosine-based activation motif
ITP	Immune thrombocytopenia
KDE	Kernel density estimate
LOT	Lysis onset time



## Appendix

LT	Lysis time
LYM	Lymphocyte
Max. Agg.	Maximum aggregation
Max. Grad.	Maximum gradient
MFI	Mean fluorescence intensity
mRNA	Messenger ribonucleic acid
MK	Megakaryocyte
MLC	Myosin light chain
MLCK	Myosin light chain kinase
MON	Monocyte
<i>MYH9</i> -RD	<i>MYH9</i> -related disease
MYPT1	Myosin phosphatase 1
N	Nucleus
Neo	Neomycin
NEUT	Neutrophils
NIR	Near-infrared
PAGE	Polyacrylamide gel electrophoresis
PBS	Phosphate buffered saline
PCR	Polymerase chain reaction
PE	Phycoerythrin
PF4	Platelet factor 4
PFA	Paraformaldehyde
PGI <sub>2</sub>	Prostaglandin
P <sub>i</sub>	Phosphate
PIPES	Piperazine-N,N'-bis(2-ethanesulfonic acid)
PKC	Protein kinase C

## Appendix

PLL	Poly-L-lysine
PLT	Platelets
PR	Postrigor
PREM	Platinum replica electron microscopy
PRP	Platelet-rich plasma
PVDF	Polyvinylidene difluoride
RBC	Red blood cell
RC	Rhodocytin
RLC	Regulatory light chain
ROTEM	Rotational thromboelastometry
RT	Room temperature
RT-FDC	Real-time fluorescence deformability cytometry
rtPA	Recombinant tissue plasminogen activator
Rock	Rho-associated, coiled-coil containing protein kinase
S-19	Serine 19
SDS	Sodium dodecyl sulfate
SICM	Scanning ion conductance microscopy
SPFS	Single platelet force spectroscopy
SSC	Sideward scatter
T-18	Threonine 18
TAE	Tris-Acetate-EDTA
Taq	Thermus aquaticus
TBS	Tris-Buffered Saline
TEM	Transmission electron microscopy
TEMED	Tetramethylethylenediamine
TPO	Thrombopoietin

## Appendix

TXA	Tranexamic acid
TRAP1	TNF Receptor Associated Protein 1
TRPM7	Transient receptor potential melastatin 7
vWF	von Willebrand factor
WBC	White blood cell

## Appendix

### 10.2 Acknowledgment

The work presented here was performed at the Department of Experimental Biomedicine I, University Hospital / University Würzburg, in the group of Dr. Markus Bender. During the period of my PhD studies (2018 – 2022) many people helped and supported me on my way. I would like to thank the following people:

*Dr. Markus Bender* for giving me the chance to perform my PhD work in his laboratory and for his constant support and trust. Thank you for your time and nerves. I really enjoyed my work in your group and the team spirit you spread.

*Prof. Dr. Andreas Greinacher* for being a member of my thesis committee and a great collaboration partner. I am grateful for the time you spend in our monthly meetings to discuss problems and giving advice.

*Prof. Dr. Thomas Dandekar* for being a member of my thesis committee. Thank you for your supportive discussions.

*My office (Markus Spindler, Kristina Mott, and Yvonne Schurr)* for supporting me in theoretical or practical questions. Thank you for the fun and crazy conversations and for being my work family.

*All present and past members* of the lab, including bachelor (*Kim Ulbrich, Tamara Nahm, Yannick Throm*) and master students (*Katharina Ermer*), and technicians (*Nadine Winter, Daniela Naumann*), for their experimental support, useful discussions, and pleasant atmosphere in the lab.

*All external collaborators* in Greifswald, Tübingen and Munich who contributed to this work. Especially *Laura Sachs* and *Raghavendra Palankar* who contributed a lot to this study.

*All proof-readers* of this thesis.

*My close friends, family and my partner André* for their support and patience with me.

## Appendix

### 10.3 Publications

#### 10.3.1 Original Article

##### **Deletion of Grin1 in mouse megakaryocytes reveals NMDA receptor role in platelet function and proplatelet formation**

James I. Hearn, Taryn N. Green, Colin L. Hisey, Markus Bender, Emma C Josefsson, Nicholas Knowlton, **Juliane Baumann**, Raewyn C Poulsen, Stefan K Bohlander, Maggie L. Kalev-Zylinska. *Blood*. 2022.

##### **Reduced platelet forces underlie impaired hemostasis in mouse models of MYH9-related disease.**

**Juliane Baumann** and Laura Sachs, Otto Oliver, Ingmar Schoen, Peter Nestler, Carlo Zaninetti, Martin Kenny, Ruth Kranz, Hendrik von Eysmond, Johanna Rodriguez, Tilman E. Schäffer, Zoltan Nagy, Andreas Greinacher, Raghavendra Palankar and Markus Bender. *Science Advances*. 2022.

#### 10.3.2 Oral Presentation

##### **“Low adhesion and interaction forces of Myh9 mutant platelets lead to impaired clot retraction and unstable thrombus formation.”**

65<sup>th</sup> Meeting of the Society of Thrombosis and Haemostasis Research (GTH), February 2021, online

#### 10.3.3 Poster

##### **“The Role of the Platelet Cytoskeleton in Platelet Mechanics.”**

14<sup>th</sup> International EUREKA Symposium GSLS, October 2019, Würzburg, Germany

##### **“Biomechanical analysis of Myh9 mutant platelets reveals lower platelet interaction forces and unstable thrombi.”**

15<sup>th</sup> International EUREKA Symposium GSLS, October 2020, online

##### **“Reduced platelet forces underlie increased bleeding in MYH9-related disease.”**

16<sup>th</sup> International EUREKA Symposium GSLS, October 2021, online

## Appendix

**“Low adhesion and interaction forces of *Myh9* mutant platelets lead to impaired clot retraction and unstable thrombus formation.”**

XXIX<sup>th</sup> The International Society on Thrombosis and Haemostasis (ISTH), July 2021, online

## Appendix

### 10.4 Curriculum vitae

## Appendix

### 10.5 Affidavit

I hereby confirm that my thesis entitled “*Studies on the influence of mutations in the Myh9 gene on platelet function*” is the result of my own work. I did not receive any help or support from commercial consultants. All sources and/or materials applied are listed and specified in the thesis.

Furthermore, I confirm that this thesis has not yet been submitted as part of another examination process neither in identical nor in similar form.

Würzburg, June 2022

---

Juliane Baumann

### Eidesstaatliche Erklärung

Hiermit erkläre ich an Eides statt, die Dissertation “*Studien zum Einfluss von Mutationen im Myh9 Gen auf die Thrombozytenfunktion*” eigenständig, d.h. insbesondere selbstständig und ohne Hilfe eines kommerziellen Promotionsberaters, angefertigt und keine anderen als die von mir angegebenen Quellen und Hilfsmittel verwendet zu haben.

Ich erkläre außerdem, dass die Dissertation weder in gleicher noch in ähnlicher Form bereits in einem anderen Prüfungsverfahren vorgelegen hat.

Würzburg, Juni 2022

---

Juliane Baumann